Buckling behaviour of cold-formed steel lipped channel sections with edge-stiffened web holes under eccentric compression loading

Xianglun Xi

A thesis submitted in fulfilment of the requirements

for the degree of Master of Engineering

Supervised by

Dr Zhiyuan (Arthur) Fang and Prof James Lim

School of Engineering

The University of Waikato

New Zealand

THE UNIVERSITY OF
WAIKATO
Te Whare Wānanga o Waikato

2024

Abstract

Cold-formed steel (CFS) channel sections with web holes are being increasingly popular as vertical load-carrying members. Traditional unstiffened web holes can significantly reduce the compression capacity, which limits their size and spacing. Recently, edge-stiffened web holes have gained popularity, particularly in New Zealand. These channels often experience eccentric compression loading due to combined lateral and gravity loads when used as vertical members. However, there's a lack of studies on how CFS channel sections with these web holes perform under such conditions.

This research focuses on numerically studying the structural behavior of CFS channel sections with plain webs, unstiffened web holes, and edge-stiffened web holes under eccentric compression loading along both major and minor axes. Finite element (FE) models were developed to simulate these sections, considering material nonlinearity and initial imperfections. The FE analysis results closely matched experimental results in terms of compressive strength and failure modes.

The study also investigates how factors like section lengths, thickness, hole size, spacing, and load eccentricities influence the compressive capacity of these perforated channel sections.

To account for the effects of the aforementioned design variables on the capacity of these CFS channel members, a combined approach leverages the parametrization of Ansys and the superior solver of Abaqus to conduct a comprehensive parametric study, including a total of 3078 FE models. Based on the FEA results from the parametric study, it appears that the direction of eccentricity (i.e., $e_x < 0$) emerges as the critical factor affecting the capacity of CFS channel sections with unstiffened or edge-stiffened web holes. Specifically, for $e_x < 0$, the compression capacity of the channel section with unstiffened web holes reduced by up to 20.55%, compared to a plain channel section; conversely, the channel section having edge-

stiffened web holes had a maximum increase of 20.10%, compared to the same channel with unstiffened web holes. However, when $e_x > 0$, the influence of different web openings became less significantly.

Finally, based on the FE results of the parametric study, an assessment of current design rules, including American Iron and Steel Institute (AISI-S100) and Australian/New Zealand Standard (AS/NZS-4600), was conducted. The assessment shows the design capacities under eccentric loading predicted by the interaction equation are conservative by 16%-33% on average for plain channels and unstiffened web hole channels. Consequently, new reduction factor interaction equations were proposed for predicting the eccentric compressive capacity of CFS channel sections with different web openings, and a reliability analysis was conducted to ensure the proposed equations could be reliable.

Keywords: Cold-formed stainless steel; Channel sections; Eccentric compression; Edge-stiffened web holes; Finite element analysis; Initial imperfection.

Preface

This thesis is submitted to the University of Waikato, New Zealand, in fulfilment of the requirement for the master's degree in civil engineering. The work contained in this thesis has not been previously submitted for a degree or diploma at any other higher educational institution. To the best of my knowledge and belief, the thesis contains no material previously published or written by another person except where due reference is made.

Acknowledgements

I extend profound gratitude to Dr. Zhiyuan (Arthur) Fang, my primary supervisor, along with Dr. Krishanu Roy and Professor James B.P. Lim, my esteemed co-supervisors. Their steadfast support and sage guidance were pivotal in navigating the intricate terrain of research, culminating in the successful submission of my journal papers and fostering my evolution into an autonomous researcher.

I reserve special appreciation for Shubham Tiwari and Kushal Gosh, whose unwavering encouragement bolstered my resolve at every turn. My sincerest thanks also extend to the supportive community in New Zealand, whose encouragement and insights contributed significantly to the refinement of my thesis.

To my cherished comrades in New Zealand—Wei Wang, Dinesh Lakshmanan Chandramohan, Gagan Sengundham Dinesh, and Vivekanandan Sivaji I offer heartfelt gratitude for their enduring camaraderie and support throughout the journey. Additionally, I acknowledge the University of Waikato, School of Engineering, for their provision of cutting-edge computing resources and invaluable research assistance.

Lastly, I express profound appreciation to my family—my father, Jianhong Xi; my mother, Qinghua Zhang; and my wife, Ying Ao—for their unwavering belief in my aspirations and unwavering support, which served as the bedrock of my academic pursuit. Their boundless encouragement and sacrifice have been the driving force behind my academic achievements.

Notation	
a	Diameter of circular web holes;
h	Depth of the flat portion of web;
Le	Total length of the CFS channel section;
L	Total length of the CFS channel section;
n	Number of web holes;
q	Length of edge-stiffener;
s	Web hole spacing;
E	Young's modulus of elasticity;
σ	Engineering stress
σ_u	Ultimate tensile strength
σ_{true}	True stress
σ_e	Measured engineering stress;
ε	Engineering strain;
ε_e	Measured engineering stress;
b_f	Overall flange width of section;
b_l	Overall lip width of section;
t	Thickness of the channel section;
CFS	Cold formed steel;
FE	Finite element;

Notation	
K	Effective length factor;
M_{bx}, M_{by}	Nominal member moment capacities about the x- and y-axes, respectively;
M_{nx}, M_{ny}	Nominal member moment capacities about the x- and y-axes, respectively;
M_x, M_y	Applied bending moments on the x-and y-axes, respectively;
M^*_x, M^*_y	Applied bending moments on the x-and y-axes, respectively;
P	Applied axial compression;
N^*	Applied axial compression;
P_n	Nominal capacity of a member in compression;
P_{Code}	Capacity of beam-columns predicted by the codes' interaction equation;
P_{EF}	Predicted capacity of beam-columns obtained through FE models;
P_{prop}	Capacity of beam-columns predicted by proposed interaction equation;
P_{Test}	Capacity of beam-columns obtained from the reference experiments;
r	Radius of gyration;
R	Radius of round corners;
r_y	Radius of gyration about the minor-axis
ø	Resistance factor;
a/h	Ration of hole depth to web depth
COV	Coefficient of variation;
d	Overall web depth of section;

Notation	
DSM	Direct strength method;
FEA	Finite element analysis;
f_{ol}	Elastic local buckling stress;
f_{od}	Elastic distortional stress;
f_y	Yield stress
f_u	Ultimate stress

Table of Contents

List of Figures

List of Tables

Chapter 1: Introduction

1.1 General

Cold-formed steel (CFS) channels are increasingly favoured as primary load-bearing members in low- to mid-rise buildings due to their high strength-to-weight ratio, ease of construction, manufacturing flexibility, recyclability, and sustainability [1, 2, 3]. These channels often feature web openings to accommodate services installation, which can significantly affect their load-carrying capacity. Figure 1.1 (a) illustrates typical CFS channels with unstiffened web holes, while Figure 1.1 (b) depicts a newer generation of CFS channel with edge-stiffened web holes, which has gained popularity in New Zealand [4, 5, 6].

Research by Chen et al. [4, 5] and Fang et al. [6] has shown that edge-stiffened web holes (Figure 1.1 (c)), where there is a continuous stiffener around the perimeter of circular web openings, can enhance the structural capacity of CFS channels compared to unstiffened holes, particularly under axial compression. However, current design standards lack specific guidelines for the combined loading conditions that CFS channels with either type of web hole (unstiffened or edge-stiffened) may encounter in practical applications.

Figures 1.2 and 1.3 illustrate examples of CFS channel sections with unstiffened and edge-stiffened web openings, respectively, used in multi-storey buildings. These sections demonstrate the adaptation of CFS technology to meet varied construction needs while leveraging advancements in structural design to optimize performance and efficiency.

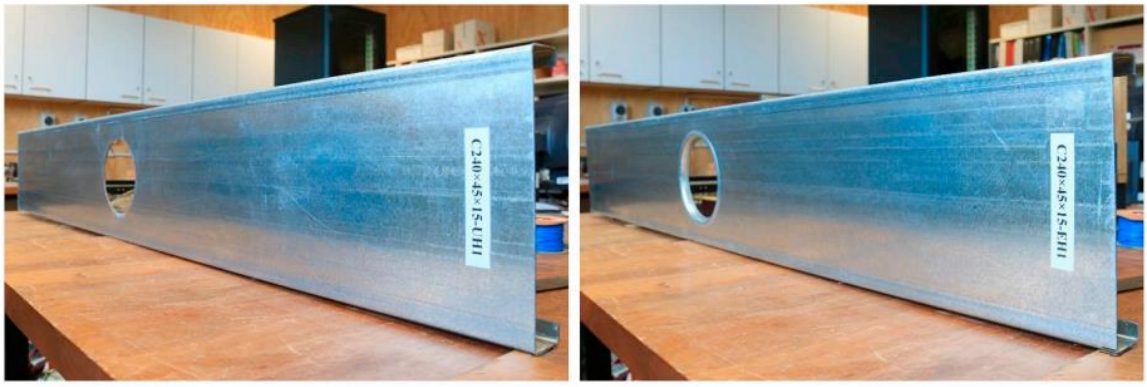

(a) Section with unstiffened web openings [4] (b) Section with edge-stiffened web openings [4]

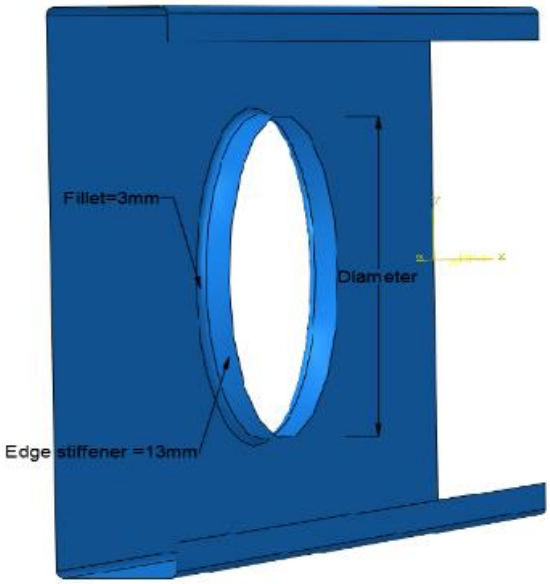

(c) Edge-stiffened web openings detail

Figure 1.1 CFS channel sections

Figure 1.2 CFS used in multi-storey buildings [42]

Figure 1.3 CFS channels with edge-stiffened web holes used in buildings [43]

In multi-storey buildings, many primary load-bearing CFS channel sections serve as beam-column elements due to their exposure to combined axial compression and bending actions [7]. In stud-wall systems, illustrated in Figure 1.4, this combined loading typically arises from eccentric compression loads (Figure 1.4(a)), often due to end connection details or shifts in the effective centroid caused by cross-sectional instabilities like wall studs in ledger framing systems [8, 9]. Additionally, CFS members may experience transverse loads (Figure 1.4(b)) along with axial compression, such as those found in perimeter stud walls [7]. In moment-resisting frames using CFS columns, simultaneous axial compression and bending actions are common (Figure 1.4(c)) [10, 11].

Numerous studies have investigated the structural performance of CFS beam-column members under various load combinations. For instance, Torabian et al. [12, 13] examined 55 lipped channel and 43 Z-shaped warping-restrained CFS beam-columns subjected to axial compression and bi-axial bending. Their experimental findings demonstrated that the simple linear interaction approach recommended by AISI S100 (2012) [14] generally provides conservative strength predictions for beam-column members. Similarly, Li et al. [15] conducted experimental and numerical studies on 57 eccentrically compressed beam-columns, reaching a comparable conclusion regarding the predictive accuracy of design approaches.

These studies underscore the importance of accurately modeling and predicting the behavior of CFS beam-columns under combined loading scenarios, highlighting the need for refined design methodologies to ensure structural reliability and safety in diverse construction applications.

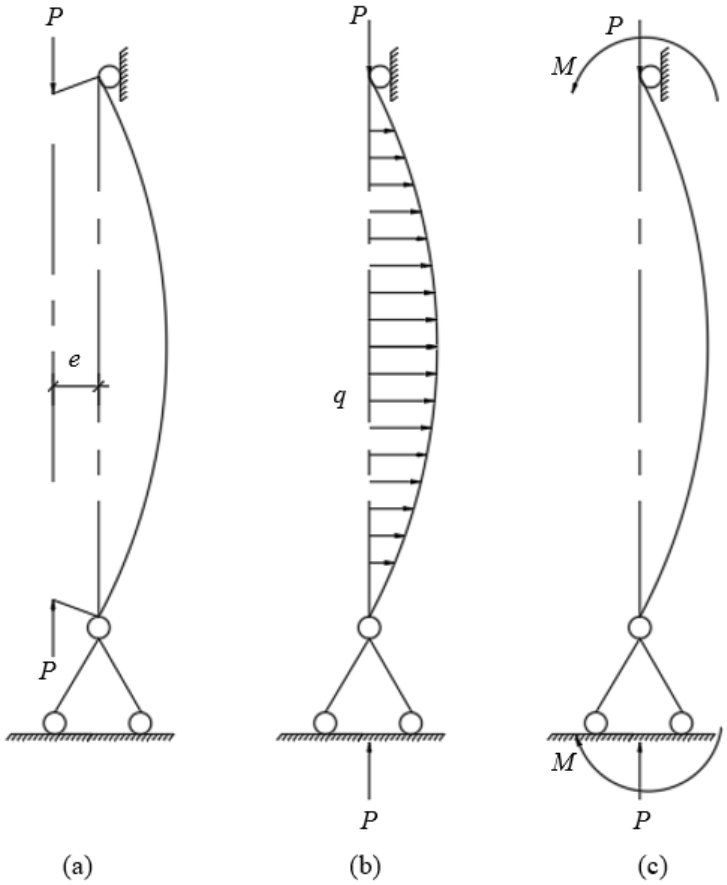

Figure 1.4 Beam-column member subjected to (a) eccentric axial load; (b) combined axial compression and transverse load; and (c) combined axial compression and bending.

1.2 CFS channel section subjected to eccentric compression

Cheng et al. [16] presented an analytical study on the flexural and lateral-torsional buckling of CFS lipped channel sections subjected to combined axial compression and bending about their major and minor axes. It was shown that the bending moment decreased the critical compressive load when CFS sections were subjected to combined compression and major-axis bending. On the other hand, for a section subjected to combined compression and minor-axis bending, the influence of the bending moment on the critical compression load was found to be dependent on the direction of the applied moment. When the minor-axis bending moment compressed the lips, the critical value of the compressive load was reduced; however, the direction of the bending moment compressing the web had almost no effect on the critical value

of the compression load unless the applied moment was close to the design flexural capacity of the member.

Ma et al. [17] conducted an experimental investigation on 51 short high-strength CFS elements with square and rectangular hollow sections subjected to combined compression and bending with varying eccentricities. The results indicated that the interaction equations proposed by American [18], European [19], and Australian design provisions [20] generally provided conservative predictions, ranging from 13% to 21% on average. In another study, Li and Young [21] assessed the interaction equations for the CFS built-up open sections under different eccentric loads through experimental investigations. They concluded that current CFS design standards (i.e., AISI S100 [22], AS/NZS 4600 [23], EN 1993-1-1 [19], and ANSI/AISC 360 [24]) generally underestimate the strength of such sections. In a subsequent study [25], they modified the interaction equation for the design of beam-columns with built-up sections.

In a more recent study, Hasanali et al. [26] evaluated the accuracy of available methods for estimating the load-carrying capacity of CFS warping-restrained beam-column members. Their comprehensive parametric study using experimentally validated finite element (FE) models showed that the Direct Strength Method (DSM) produced the most conservative predictions, up to 55% compared to other methods. Errors associated with warping-restrained boundary condition effects, buckling load calculations, and the AISI linear interaction equation contributed to this discrepancy. Additionally, Hasanali et al. [27] conducted a parametric study on CFS channel sections under various combinations of compression and bending about major and minor axes. They identified element and web slenderness ratios, as well as the magnitude and direction of eccentricity, as key factors influencing behaviour. Based on their findings, they proposed a new design interaction equation aimed at improving code strength prediction accuracy.

1.3 CFS channel section with edge-stiffened web holes subjected to axial compression

Obviously, compared to unstiffened web holes, edge-stiffened web holes can increase the compression capacity of CFS channels. In terms of the effects of edge-stiffened web holes, extensive research has been conducted both experimentally and numerically. Chen et al. [4, 5] investigated the effects of opening spacing and column length on the compression resistance of channel sections. Their results show that the compression resistance capacity of channel sections with edge-stiffened web holes increased by as much as 22%, whereas the same section with unstiffened web holes experienced a 20% reduction in compression resistance compared to a plain channel section. To address this, more reasonable interaction equations are proposed, wherein an enhancement factor is applied to the original equations. The enhancement factor was determined using a bivariate linear regression analysis. These proposed design equations closely predict the enhanced axial capacity of CFS channels with edge-stiffened holes.

1.4 Research gap found in literature review

It appears that there has been considerable research conducted on CFS channel sections subjected to various loading conditions, including axial compression, and CFS channel sections with different web openings under axial compression. However, in engineering practice, the web holes will always be included in column members for installation convenience. Therefore, there is a notable gap in the literature regarding CFS channel sections with unstiffened or edge-stiffened web holes subjected to eccentric compression.

Eccentric compression, particularly in the context of CFS channel sections with web openings, presents unique challenges and behaviours that warrant further investigation. The interaction between eccentric loading and the presence of unstiffened or edge-stiffened web holes can significantly influence the structural response and ultimate capacity of these sections.

Given the importance of understanding the behaviour of CFS channel sections in practical engineering applications, further research focusing on eccentric compression and its effects on sections with web openings is warranted. Such studies could provide valuable insights into the behaviour, strength, and failure mechanisms of these sections, ultimately informing the development of more accurate design guidelines and recommendations for structural engineers working with CFS components.

1.5 Aim and scope of this research

By addressing this gap in the existing body of research, future studies will enhance our understanding of CFS channel sections under eccentric compression. This contribution has the potential to advance structural engineering practices in the field of CFS construction.

In terms of the design standards, the American Iron and Steel Institute (AISI) [22], the Australian and New Zealand Standards (AS/NZS) [23] and EC3 [29-31] do not offer any guidance or rules for predicting the capacity of CFS channel sections with edge-stiffened/unstiffened web openings in combined loading conditions. The accuracy of the current design standards in predicting the strength of CFS beam-columns was evaluated in this study using experimental data for combined loading cases obtained from the literature. To this end, detailed nonlinear FE models of CFS beam-column members under various load combinations were developed, taking into account material nonlinearity and geometric imperfections, and then validated against the results of experimental tests.

The validated models were then utilised for a comprehensive parametric study comprising 3078 FE models, spanning various design parameters, such as length (i.e., 1.0, 2.0, 2.5 m), thickness (i.e., 1, 2, 3 mm), and cross-sectional dimensions, as well as the diameters and the number of holes in edge-stiffened/unstiffened web holes under nine different load eccentricities. Finally, the parametric study results were used to develop more accurate interaction equations for the

design of CFS beam-column members, while its accuracy for practical applications was demonstrated by conducting a reliability analysis.

Chapter 2: Summary of experiments by Torabian et. al. [32] and Chen et. al [4]

Torabian et al. [32] conducted experimental tests to investigate the structural behaviour of CFS-lipped plain channel sections under eccentric compression (Figure 2.1), including: (i) compression and a negative minor-axis bending moment (-38.1mm $\leq e_x < 0$); (ii) compression and a positive minor-axis bending moment ($0 < e_x \leq$ 38.1mm); (iii) compression and a major-axis bending moment (-190.5mm $\leq e_y < 0$); and (iv) compression and bi-axial bending moments (-15.53mm $\leq e_x \leq$ 15.53mm and -127mm $\leq e_y \leq$ -17.78mm). In the investigation [32], the proposed equations on the compressive strength for each limit state were developed. In the current study, 12 of the test results from Torabian et al. [32] were used for FE validation.

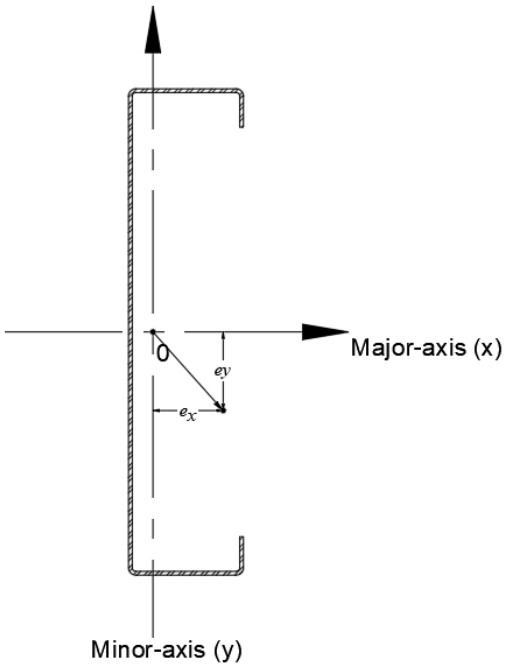

Figure 2.1 Definition of x- and y- axis

Chen et al. [4] conducted experimental tests to investigate the axial strength of CFS-lipped channel sections, including 10 channel sections with edge-stiffened web holes. In the tests, 26 axial compression tests and 49 finite element analysis results are reported on the compression

resistance of CFS channel sections with both edge-stiffened and unstiffened web openings. For comparison, channel sections without web openings were also tested. For all specimens, initial imperfections were measured using a laser scanner. A nonlinear elasto-plastic finite element model was also developed, and the results showed reasonable agreement with the test results. In the current study, the similar numerical modelling methods from Chen et al. [4] for edge-stiffened web holes were employed, and the corresponding test results were used to validate the FE models, as shown in Chapter 3.

Chapter 3: Finite element analysis

3.1 General

It has been previously demonstrated that FE analysis using ABAQUS software and ANSYS software can be used as efficient and reliable tools to predict the structural performance of thin-walled CFS elements and connections under various loading conditions. In the current study, the test results conducted by Torabian et al. [32] and Chen et al. [4] on CFS channel sections under eccentric compression and CFS channel sections with edge-stiffened web holes under axial compression (i.e., beam-columns), respectively, were utilised to validate the developed FE model.

3.2 New methodology application in FE analysis

Figures 3.1-3.4 illustrate the procedure for integrating Ansys and Abaqus to perform finite element (FE) analysis modelling. This combined approach leverages the strengths of both software platforms (the parametrization of Ansys [44] and the superior solver of Abaqus [45]) to achieve a comprehensive analysis of structural behaviour.

In Figure 3.1, the initial step of model creation is depicted, where the geometry and boundary conditions are defined using Ansys. This stage involves setting up the structural model, applying loads, specifying material properties and defining the initial geometry imperfections.

Figure 3.2 demonstrates the process of exporting the model from Ansys to Abaqus. This step involves converting the Ansys models into input (.inp) files compatible with Abaqus, ensuring seamless transfer of geometry, mesh, and boundary conditions.

Figure 3.3 illustrates the continuation of the analysis within Abaqus, where multiple input (.inp) files for Abaqus are generated from the precious step of joining the files. At this stage, a large number of FE models can be automatically executed in Abaqus software by running a Windows

batch file. This approach streamlines the process of running multiple FE models, saving time and effort for engineers and analysts. The batch file contains commands to execute each FE model sequentially, allowing for efficient and automated processing of the simulation tasks.

Finally, in Figure 3.4, the results obtained from Abaqus are post-processed and analysed to extract valuable insights into the structural response. This may involve visualizing stress distributions, displacement patterns, or other relevant data to evaluate the performance of the design.

By combining the capabilities of Ansys and Abaqus, engineers can benefit from a comprehensive and robust FE analysis workflow that enables accurate prediction of structural behaviour and performance. This integrated approach facilitates efficient design optimization and ensures the reliability and safety of engineering structures.

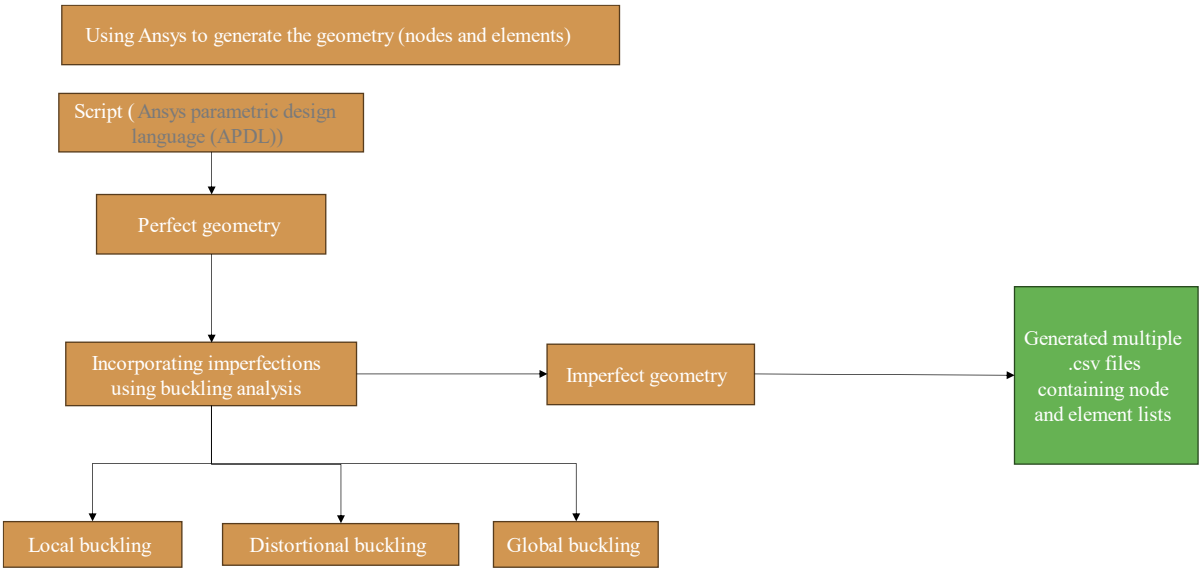

Figure 3.1 Generation of geometry.

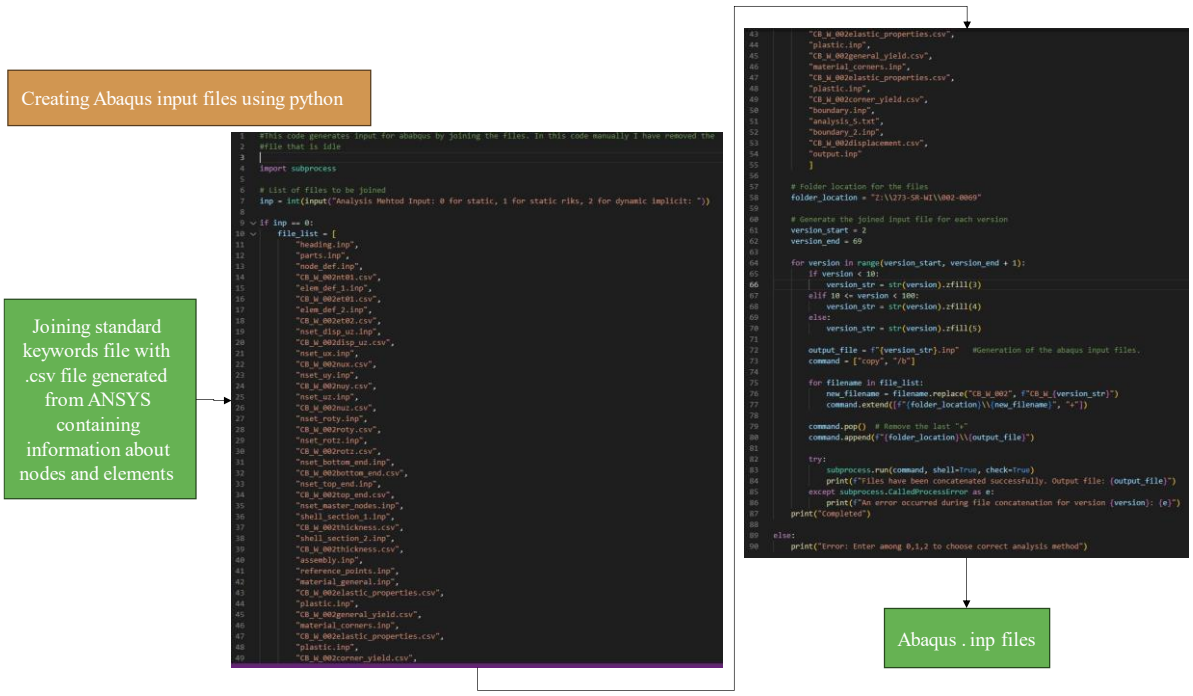

Figure 3.2 Creation of Abaqus input files.

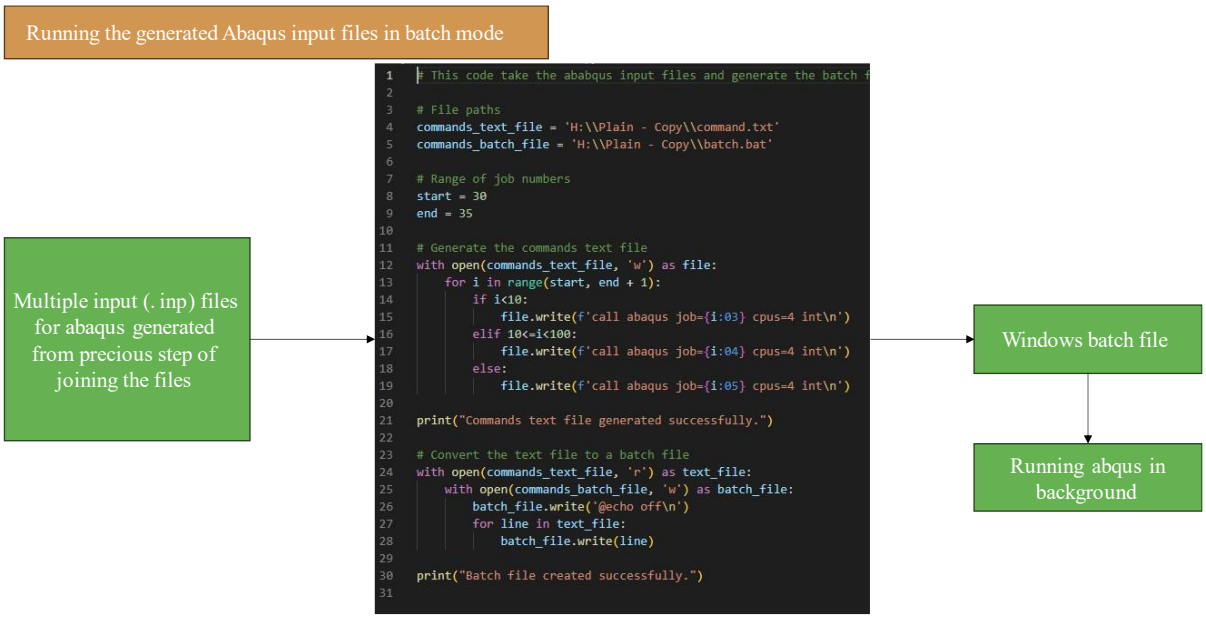

Figure 3.3 Analysis using batch mode.

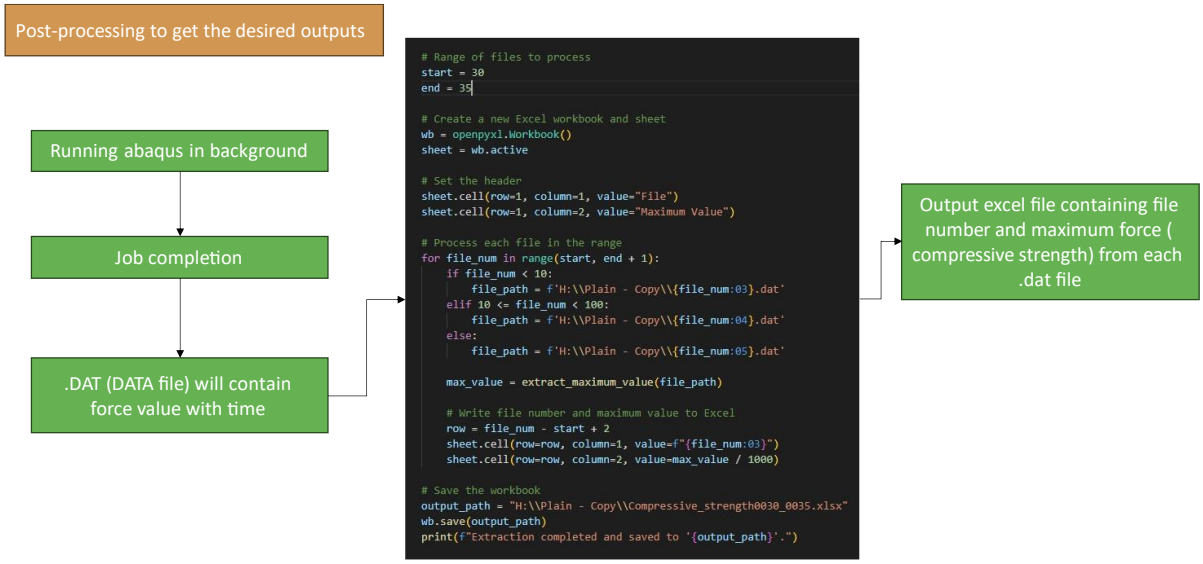

Figure 3.4 Post-processing

3.3 Modelling of CFS channel sections under eccentric compression

3.3.1 FE meshing and material properties

In the present study, a four-node shell element using quadratic shape functions, *S4R*, was assigned to the elements in ABAQUS software. Each node of this element type has five degrees of freedom, with three displacements and two in-surface rotational components. While *S4R* is a robust element type allowing as little as one element per buckling half-wave without degrading the solution, it can provide accurate predictions for thin-walled structures according to Schafer et al. [36]. Based on the previous study of the mesh sensitivity analysis [26, 27], appropriate mesh sizes were chosen for channel sections. Across the length and width, a mesh size of 5 mm × 5 mm was used for the FE models.

A true stress-strain model was used to simulate the behaviour of CFS elements. The engineering stress-strain curves obtained from coupon tests [32] were converted to true stress and true strain data using the following equation:

$$\begin{cases} \varepsilon_{true} = \ln(1 + \varepsilon_e) \\ \sigma_{true} = \sigma_e(1 + \varepsilon_e) \end{cases} \quad (1)$$

where σ_e and ε_e are the measured engineering stress and strain values based on the original cross-sectional area of the coupons, respectively. The engineering and true stress-strain curves of the tested beam-column elements are shown in Figure 3.5. The measured Poisson ratio, Young's modulus of elasticity, the yield stress, and the ultimate stress of the CFS material are equal to υ = 0.3, E = 203.4 GPa, F_y = 365 MPa, and F_u = 560 MPa, respectively.

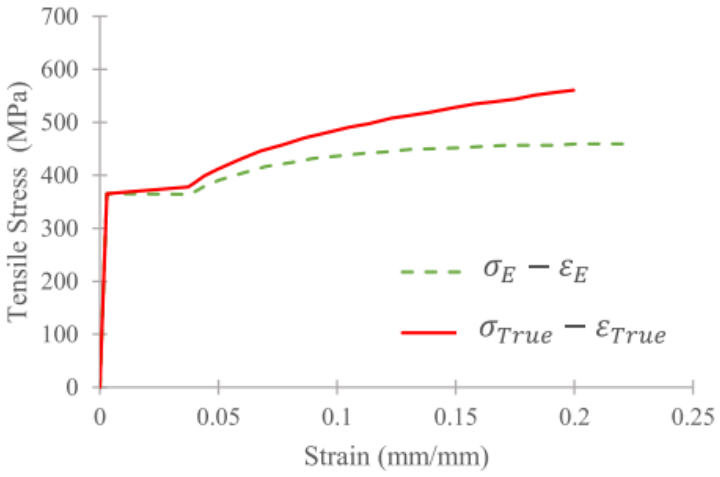

Figure 3.5 Material stress-strain relationship used in FE models (adopted from Torabian et al. [32])

3.3.2 Boundary conditions and loading conditions

The boundary conditions of the experimental test set-up were simulated in the FE models, as shown in Figure 3.6. Two reference points were placed using the "Rigid" constraint at the end sections of the lipped channel elements to simulate the support and apply eccentric compression. As shown in Figure 3.6, the nodal degrees of freedom at each end of the element were then coupled to their respective reference point, which was pinned about the minor- and major-axes. The coordinates of the reference points were varied to apply eccentricities to the element. While a concentrated load was applied to one of the reference points in a force-control manner (Rf-2 in Figure 3.6), the other reference point was restrained in the longitudinal direction (UZ) to simulate the support. Finally, a rigid link with a length of 152.4 mm in the

longitudinal direction was created between the reference points and the ends of the specimen to account for the depth of the clevis employed in the test set-up (see Figure 3.7).

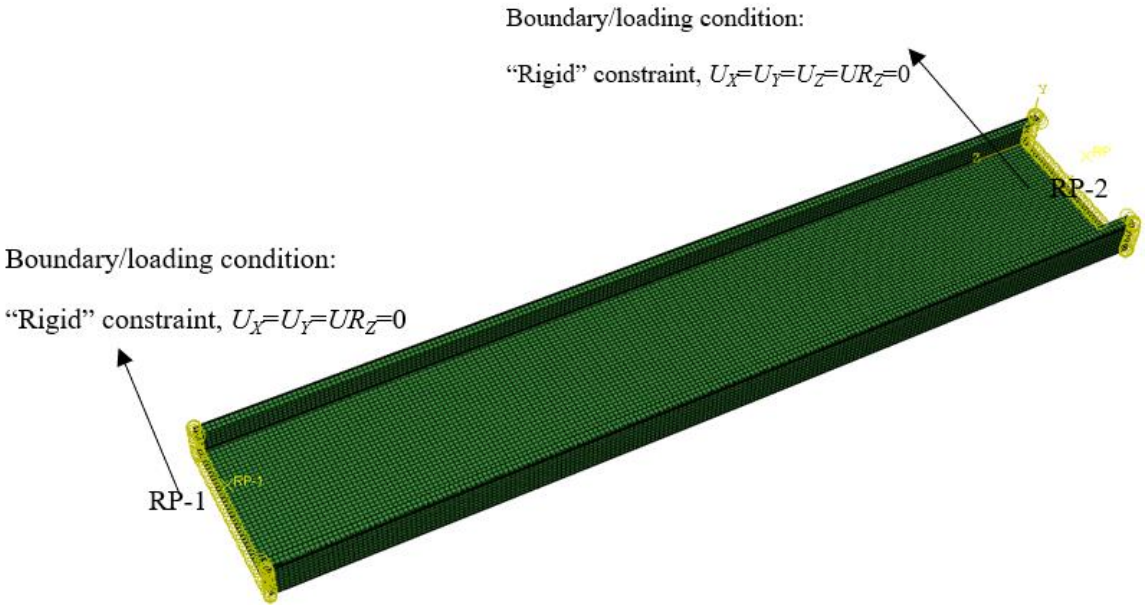

Figure 3.6 CFS element boundary conditions under eccentric compressive loads

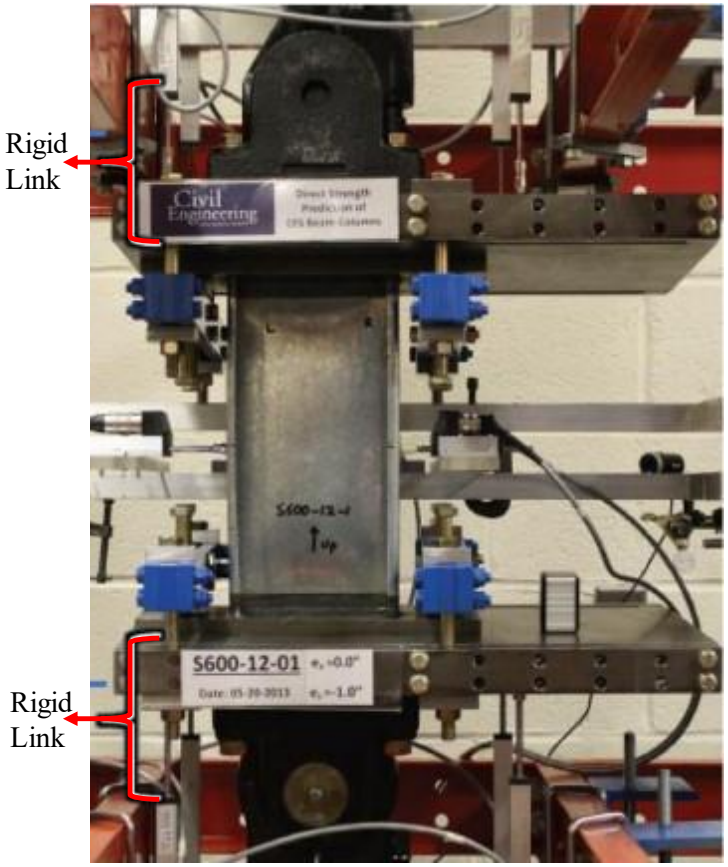

Figure 3.7 Lipped channel cross-section tested by Torabian et al. [32]

3.3.3 Geometric imperfection

The stability of CFS structural elements may be significantly influenced by the initial geometric imperfections because of their impact on the strength and post-buckling behaviour of the elements [33, 34]. Based on the work carried out by Schafer and Peköz [35], the dominant buckling mode shape derived from elastic buckling analysis can be employed to determine the general shape of imperfections. In this study, the Finite Strip Method was first used to predict the dominant buckling mode shape and its corresponding half-wavelength for each element [36]. For the CFS element with a thickness (t) smaller than 3 mm, the magnitude of the buckled shape was scaled to $0.34t$ and $0.94t$ for local buckling and distortional buckling, respectively, which corresponds to a Cumulative Distribution Function (CDF) value of 50% according to Schafer and Peköz [37].

A value of $Le/1500$ (where Le is the length of the member), as reported in previous studies [38, 39], was also taken for the global buckling imperfection magnitude. It should be noted that either a local or a distortional imperfection was incorporated into the FE models of short channels, depending on which mode had the lower critical buckling stress [38], while a combination of three buckling modes (local, distortional, and global) was introduced for the medium and long-length members [32].

3.3.4 FE validation

The accuracy of the developed FE models of the channels was validated against the experimental results of the study by Torabian et al. [32]. To predict the capacity of the CFS channels, the geometrical FE models with initial imperfection were generated in ANSYS [40], and the nonlinear inelastic post-buckling analysis was performed in ABAQUS [41] using the static RIKS arc-length method. Figure 3.8 and Table 1 demonstrate the cross-sectional dimensions and lengths of the beam-column specimens subjected to compressive loads with

nine different eccentricity values on the major (x) and minor (y) axes. The selected eccentricities imposed different combined actions on the CFS channels, including: (i) compression and a negative minor-axis bending moment; (ii) compression and a positive minor-axis bending moment; (iii) compression and a major-axis bending moment; and (iv) compression and bi-axial bending moments.

The capacity of CFS column channels under eccentric loading was predicted by the EF models and experiments, respectively, and the results, which are also compared in Table 2, illustrate a maximum estimation error of 5.7%. Figure 3.9 compares the axial force-displacement curves of test specimens, namely S600-305-13, S600-610-15 and S600-1219-17, with those obtained from FE simulations. It shows that the developed FE models could accurately predict the behaviour of CFS beam-columns over the entire loading range, including peak load, initial stiffness, ultimate capacity, and post-buckling behaviour. It should be noted that the slight difference between the initial stiffness of the tested specimens and the FE models can be attributed to the minor detachment of the end plate and loading plates as well as a small movement in the test rig's swivel joints [35]. The failure modes (local buckling, distortional buckling and global buckling) predicted by the FE were also in good agreement with those observed during experimental tests, as shown in Figure 3.10 for the S600-610-8 specimen under combined compression and bending about the major axis.

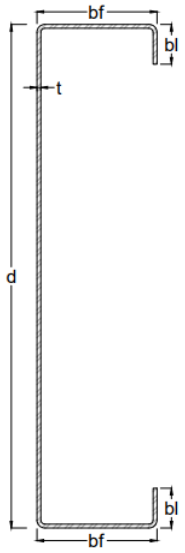

Figure 3.8 Nominal cross-sections of CFS channel sections

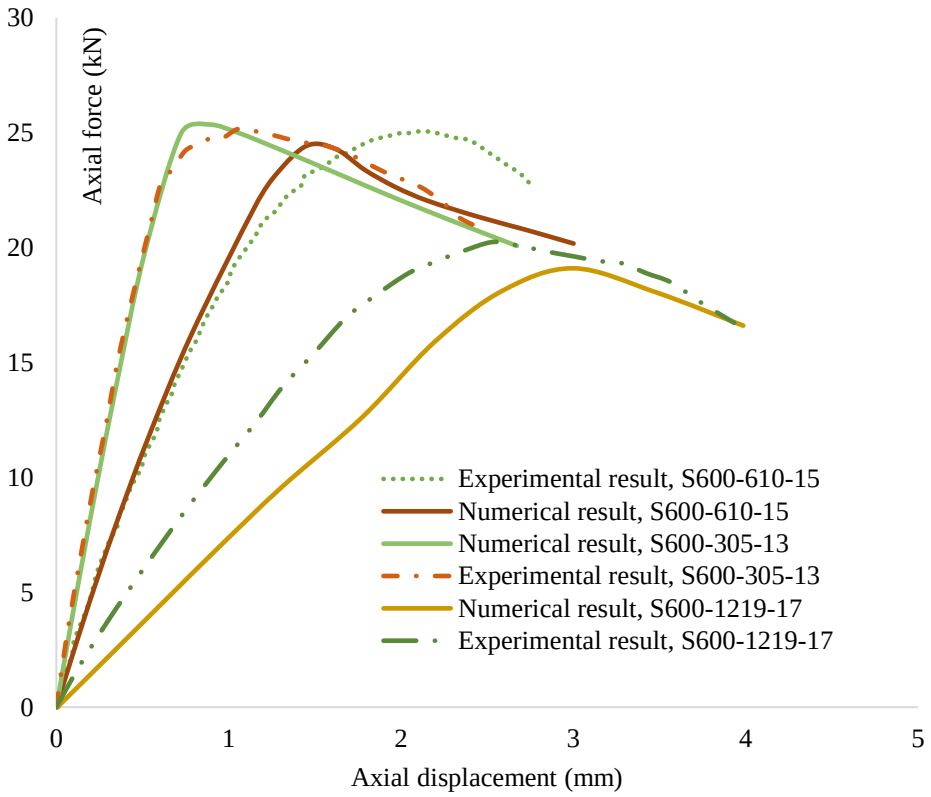

Figure 3.9 Axial force-displacement relationship resulting from experimental test against FE models for S600-305-13, S600-610-15 and S600-1219-17

Table 1. Validated models' variables and results

Section name	Web	Flange	Lip	Thickness	R	Length	Eccentricities		P_{test}	P_{FEA}	Percentage difference (%)
	d	b_f	b_l	t	r	L	e_x	e_y			
S600-305-1	152.05	34.95	9.5	1.45	2.87	305	-25.4	0.0	25.4	25.7	-1.3
S600-305-9						305	0.0	-190.5	20.6	20.0	2.7
S600-305-10						305	2.6	-38.1	48.9	48.2	1.4
S600-305-13						305	-15.5	-76.2	25.0	25.3	-1.2
S600-305-15						305	-15.5	-76.2	26.5	25.3	4.6
S600-610-6						610	31.8	0.0	16.1	16.5	-2.3
S600-610-8						610	0.0	-76.2	34.8	34.4	1.2
S600-610-9						610	0.0	-165.1	21.5	21.6	-0.5
S600-610-14						610	-3.8	-19.1	42.8	43.4	-1.2
S600-610-15						610	-14.2	-69.9	25.0	25.0	0.1
S600-1219-14						1219	-3.6	-17.8	27.2	28.8	-5.7
S600-1219-17						1219	-6.9	-101.6	20.0	19.1	4.6

Negative eccentricity in the x direction means that web of the specimens is in compression.

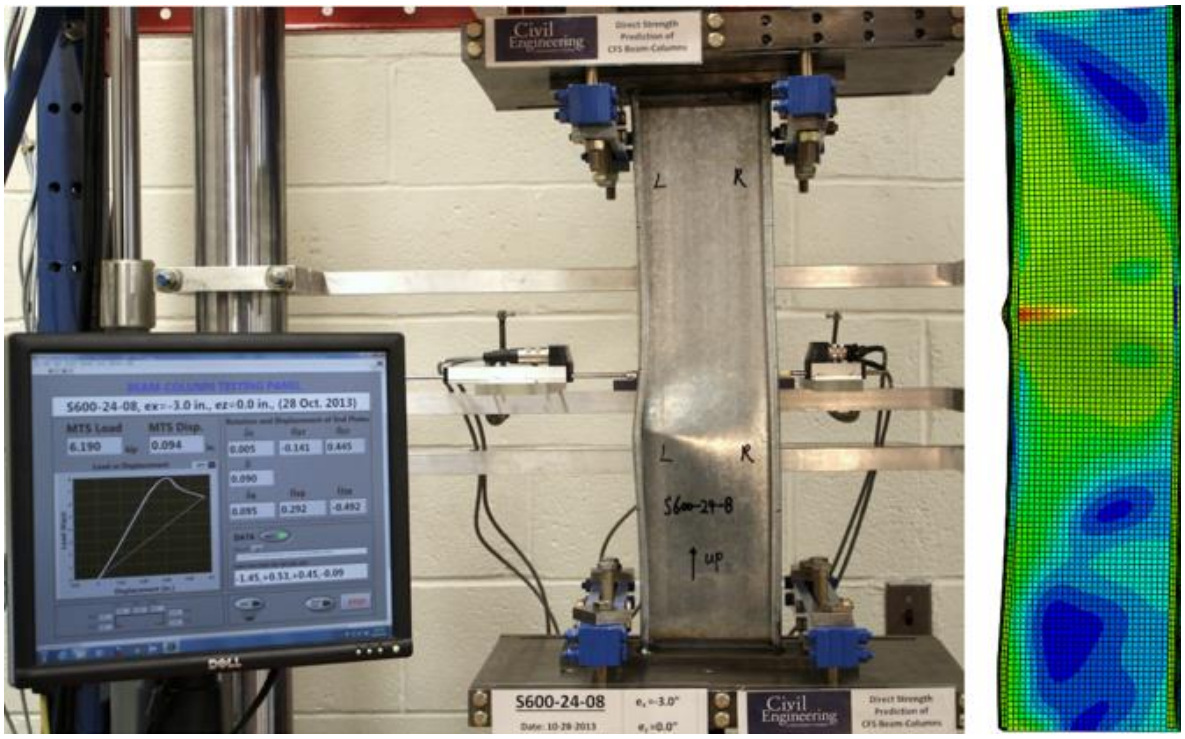

Figure 3.10 Failure mode determined by FE model versus experimental (S600-610-8) (test set-up adopted from [32]).

3.4 Modelling of edge-stiffened web holes in Cold-formed steel channel sections under axial compression

3.4.1 FE meshing and material properties

S4R shell elements were used to model the CFS channel sections. S4R elements allow each node to have three degrees of freedom both along the transitional and rotational directions. S4R elements are suitable for the analysis of nonlinear problems as they account for finite membrane strains and arbitrarily large rotations. Based on the previous study of the mesh sensitivity analysis [26, 27], appropriate mesh sizes were chosen for channel sections. Across the length and width, a mesh size of 5 mm × 5 mm was used for the FE models. Mesh refinement was made around the web opening and around corners for accurate FE analysis. The full stress-stain curves of coupons taken from the C190 × 45 × 15 and C240 × 45 × 15 channel sections are shown in Figure 3.11. The yield stress and the ultimate stress of the CFS

material are equal to F_y = 309.31 MPa and 285.17 MPa; F_u = 377.78 MPa and 379.35 MPa, respectively. Figures 3.12 and Table 3 display the dimension of the nominal cross section and Figure 3.13 shows the different opening spaces.

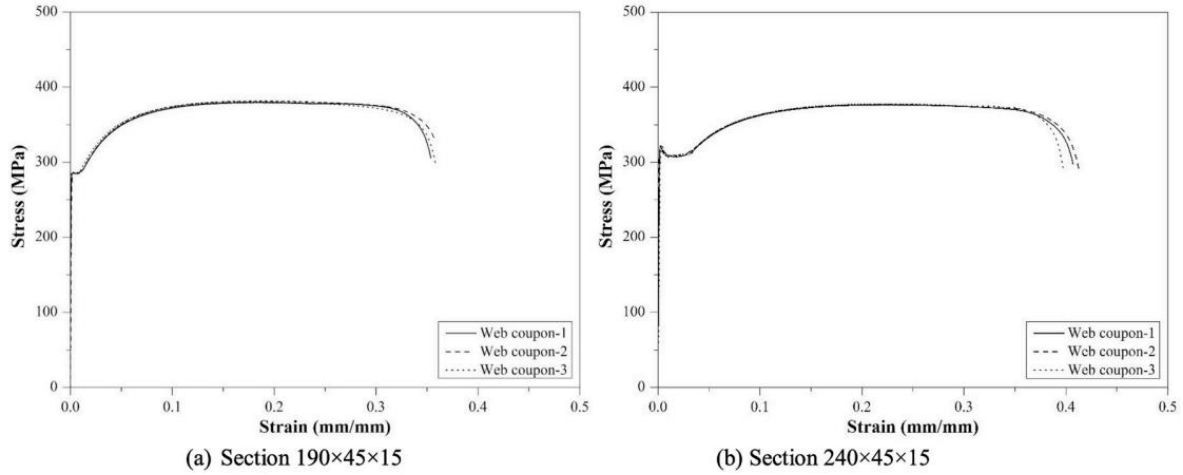

Figure 3.11 Material stress-strain relationship used in FE models (adopted from Chen et al. [4]).

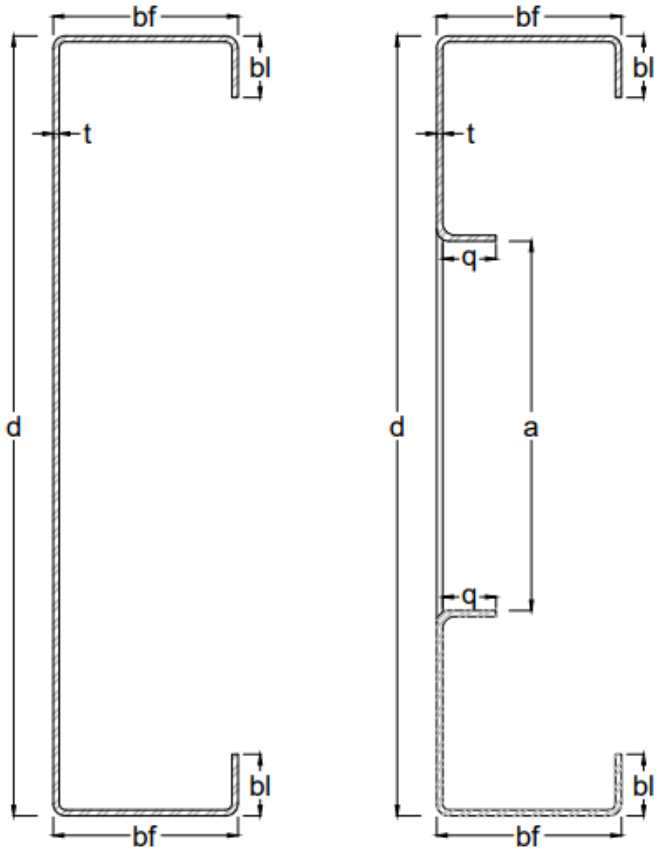

Figure 3.12 Nominal cross-sections of CFS channel sections.

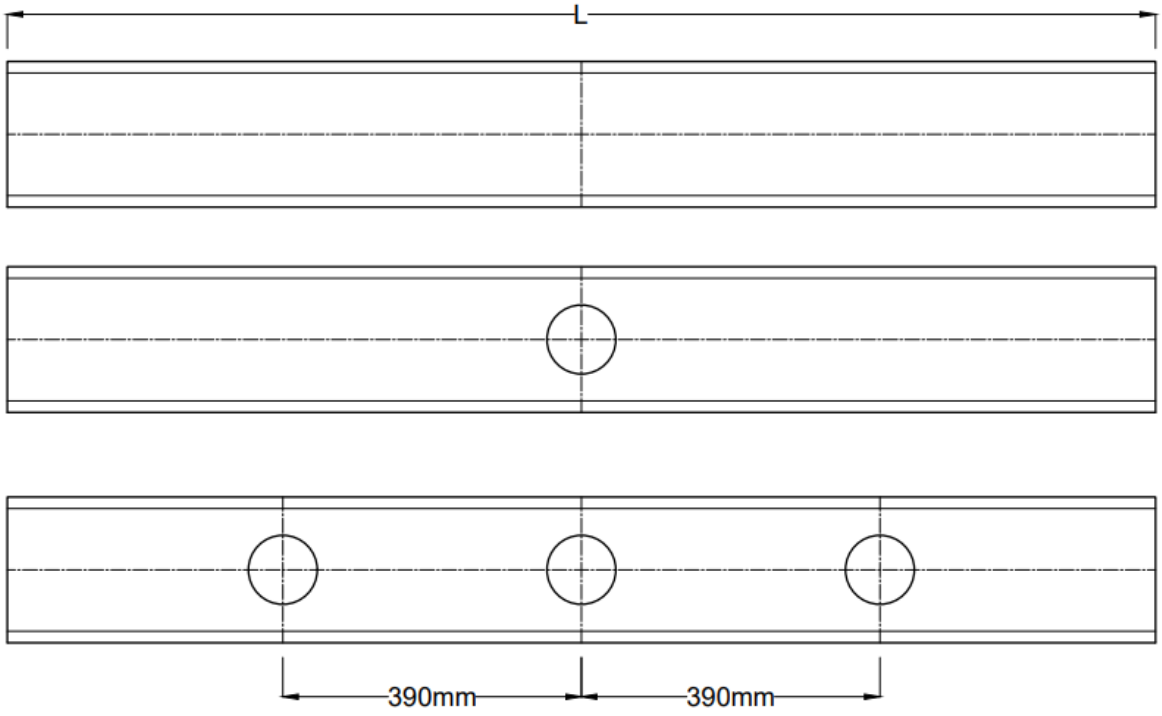

Figure 3.13 Different opening space.

3.4.2 Boundary conditions and loading conditions

The boundary conditions of the experimental test set-up were replicated in the FE models, as demonstrated in Figure 3.6. Two reference points were placed at the end sections of the lipped channels to simulate the support and apply axial compression. The nodal degrees of freedom at each end of the element were then rigidified to their respective reference point, which was pinned about the minor- and major-axes. The coordinates of the reference points shown in Figure 3.14 were fixed to apply the axial load to the channels. An axial load was applied to one of the reference points to simulate the loading, while the other reference point was restrained in the longitudinal direction (U_z) to simulate the supporting.

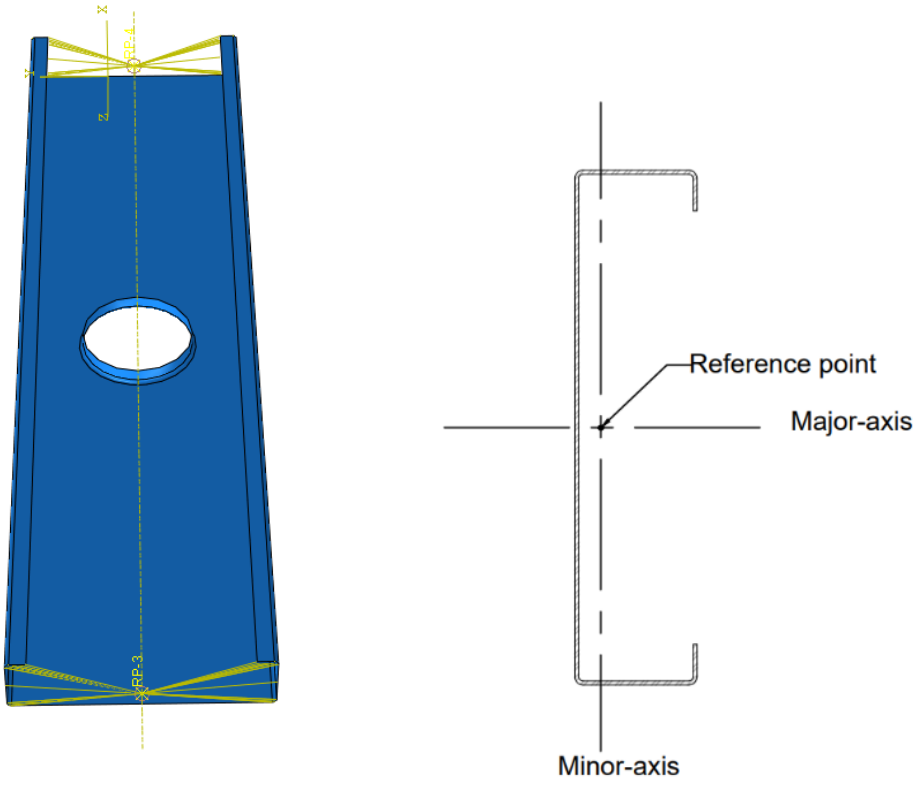

Figure 3.14 Reference point in the Coordinate System.

3.4.3 FE validations

The accuracy of the developed FE models of the channels was validated against the experimental results of the study by Chen et al. [4]. To predict the capacity of the CFS channels, the geometrical FE models with initial imperfection were generated in ANSYS, and the nonlinear inelastic post-buckling analysis was performed in ABAQUS using the static RIKS arc-length method. The validated models, including two different channel section sizes, are shown in Table 3. Figure 3.13 shows two different opening spacings were considered. Table 3 demonstrates the failure loads for six validated models, the experimental results, and the cross-sectional dimensions and lengths of the column specimens subjected to axial compressive loads (adopted from Chen et al. [4]).

The capacity of CFS column channels under axial loading was predicted by the FE models and experiments, respectively, and the results, which are compared in Table 2, illustrate a maximum

estimation error of 3.7%. Figures 3.15 and 3.16 show that the developed FE models could accurately predict the failure modes of CFS channels under axial loading. Figure 3.17 compares the axial force-displacement curves of test specimens, namely C190-1500EH1 and C240-1500EH3, and those obtained from FE validated models, showing the peak load, ultimate capacity, and post-buckling behaviour were also in good agreement. However, the slightly different initial stiffness between the tested specimens and the FE models should be noted. It can result from the minor detachment of the end plate and loading plates as well as a small movement in the test rig's swivel joints [35].

Table 2. Validated models' variables and results

Section name	Web	Flange	Lip	Thickness	Stiffener	Length	Dia	Opening space	Opening number	P_{test}	P_{FEA}	Percentage difference
	d	b_f	b_l	*t*	*q*	*L*	*a*	*s*	*n*			*%*
C190 x 45 x 15-L1500-EH1	189.5	45.6	15.9	1.53	13	1502.2	97.6	-	1	60.2	61.6	-2.3
C190 x 45 x 15-L1500-EH3	191.2	45.41	15.5	1.52	13	1501.8	96.8	390	3	62.3	63.8	-2.4
C190 x 45 x 15-L1300-EH1	189.6	44.8	15.2	1.48	13	1301.5	97	-	1	75.6	74.3	1.7
C190 x 45 x 15-L750-EH1	190.2	44.3	15.1	1.5	13	725.5	97.5	-	1	78.8	76.4	3.1
C240 x 45 x 15-L1500-EH1	238	45.7	15	1.75	13	1502	143.7	-	1	63.9	64.3	-0.6
C240 x 45 x 15-L1500-EH3	239.5	44.9	14.7	1.72	13	1502	142.7	390	3	66	68.5	-3.7
											Average	-0.7

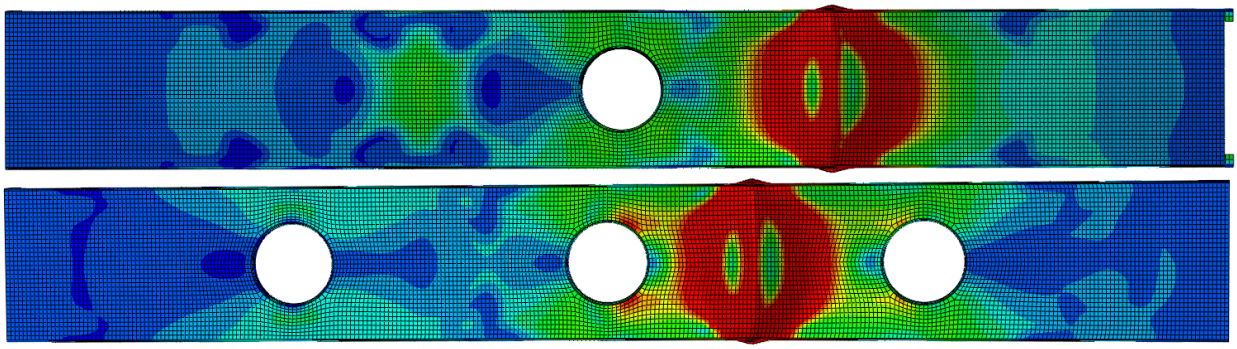

Figure 3.15 Failure models of C190-1500mm long specimens with edge-stiffened web opening.

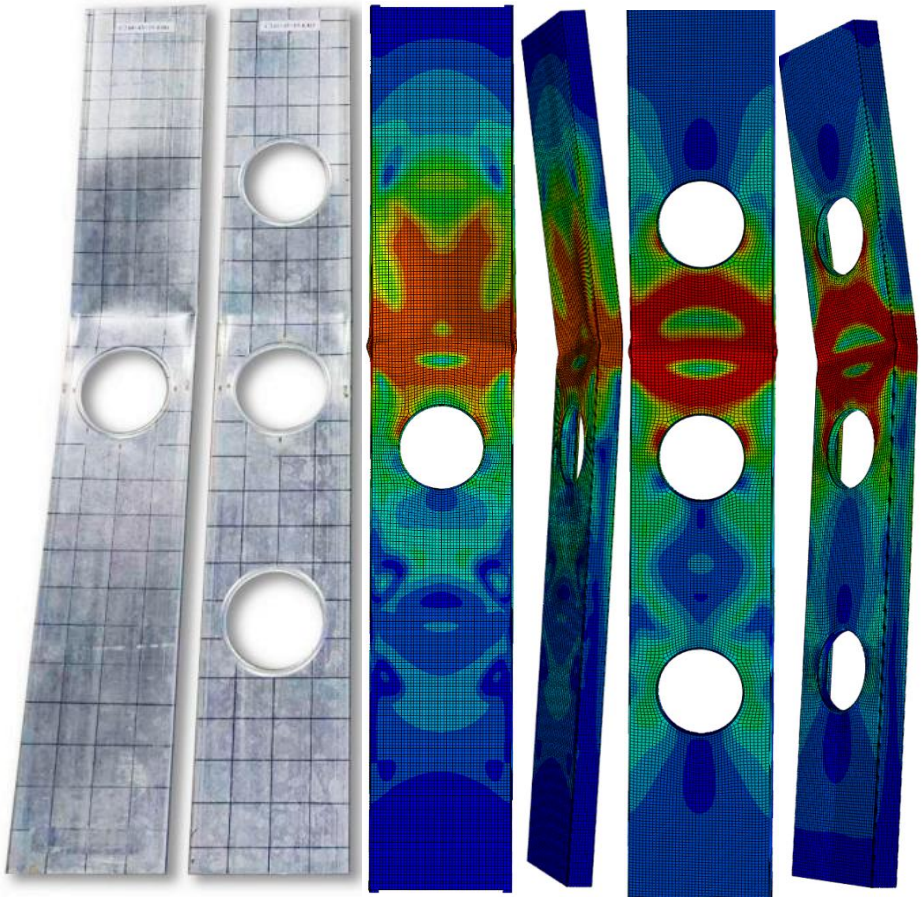

a) Failure mode adopted from Chen et al. [4] b) Failure mode from validated models

Figure 3.16 Failure models of C240-1500mm long specimens with edge-stiffened web opening.

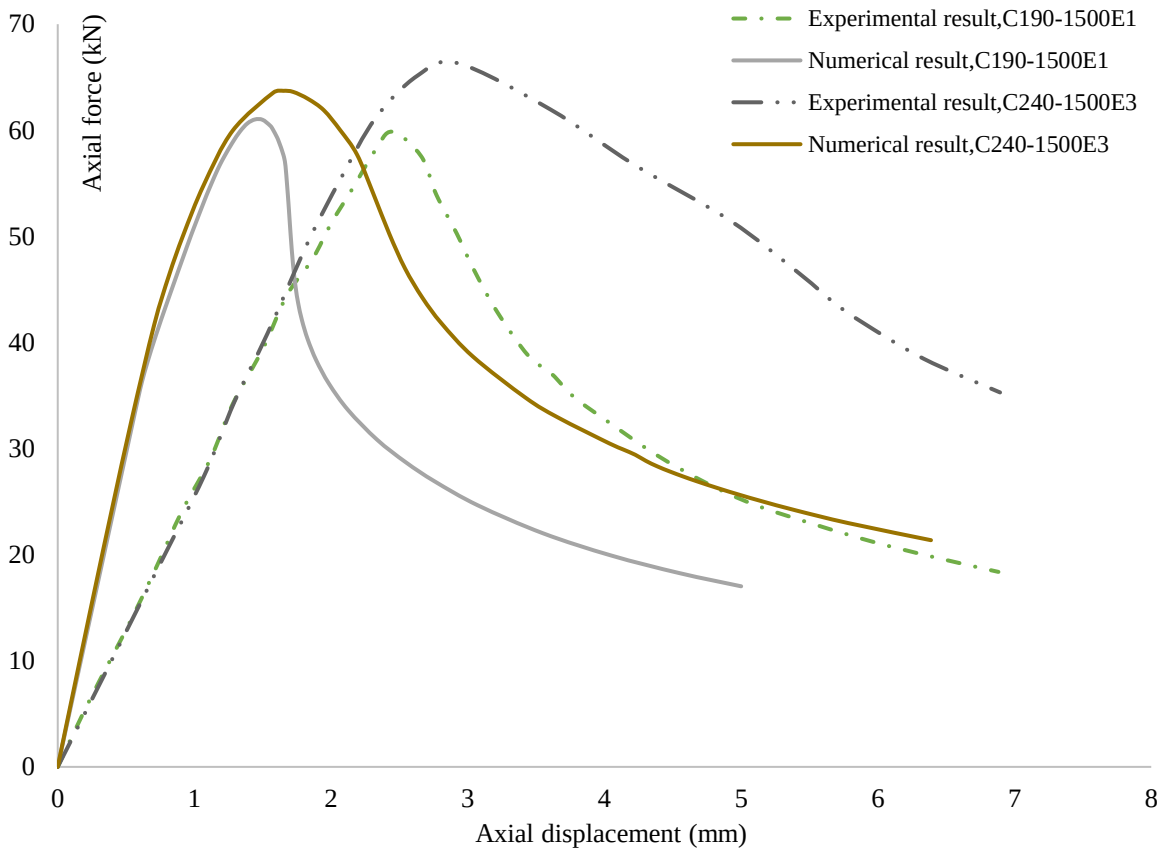

Figure 3.17 Axial force-displacement relationship resulting from an experimental test against FE models for C190-1500E1 and C240-1500E3.

Chapter 4: Current design rules

To predict the load-carrying capacity of CFS beam-column elements, the initial step involves determining their strength under pure axial compression and pure bending actions. This can be achieved by employing the traditional effective width method (EWM) as prescribed by the European design guidelines [29]. Alternatively, the Direct Strength Method (DSM) [35], available in AISI S100 [22] and AS/NZS 4600 [23], offers an alternative approach to estimate nominal pure compressive and bending strength values.

In the EWM, yield strength and reduced cross-section properties are utilized, while the DSM relies on gross cross-section properties, with a reduced strength value calculated based on the stability of the gross cross-section. The current design regulations for CFS beam-column members are briefly summarized in the following sections.

In steel design, determining the strength of a member subjected to multiple actions typically involves employing an interaction equation. For cold-formed steel (CFS) members under combined compression and bending actions, a simplified linear interactive equation recommended by AISI S100 [22] (Eq. (2)) and AS/NZS 4600 [23] (Eq. (3)) is commonly used:

$$\frac{P}{P_n} + \frac{M_x}{M_{nx}} + \frac{M_y}{M_{ny}} \leq 1.0 \quad (2)$$

$$\frac{N^*}{N_c} + \frac{M_x^*}{M_{bx}} + \frac{M_y^*}{M_{by}} \leq 1.0 \quad (3)$$

In the above equations, P, M_x and M_y ($N*$, M_x^* and M_y^* in AS/NZS 4600 [23]) are defined as the applied axial compression load and bending moments about the x- and y-axes, respectively. P_n (N_c in AS/NZS 4600 [23]) denotes the nominal axial compressive capacity, while M_{nx} and M_{ny} (M_{bx} and M_{by} in AS/NZS 4600 [23]) are nominal flexural strength about the x- and y-axes, respectively. Nominal pure strength (P_n, M_{nx} and M_{ny}) is typically determined by the

DSM equations supplied in Chapters E and F of the AISI S100 [22] as well as Chapter 7 of AS/NZS 4600 [23].

Chapter 5: Parametric study

5.1 General

A comprehensive parametric study was conducted using the experimentally validated FE models described in the previous section. This study aimed to investigate the efficiency of the code-prescribed compressive load-bending moment interaction equations and to develop more accurate interaction formulations for the CFS beam-columns.

The specimens used for the parametric study were labelled such that the nominal dimensions of the cross sections, the nominal length of specimens, the type of web opening, the diameter of web holes and the opening number were expressed as a label as shown in Figure 5.1. For example, the label "C240-L2000-T1-EH3-0.4*d*" can be interpreted as follows:

- "C240" means channel section with d = 240 mm, bf = 45 mm and bl = 15 mm.
- "L2000" is the nominal length of the specimen in millimetres, i.e., 1500 mm.
- "EH" identifies a web having an edge-stiffened web opening, "UH" identifies a web having an unstiffened web opening, and "NH" identifies a plain channel section having no web opening.
- "T1" means the thickness of the channel section, i.e., 1 mm.
- "3" represents the opening number.
- "0.4d" means the diameter of the web hole, i.e., 0.4d = 0.4 x 240 = 96 mm.

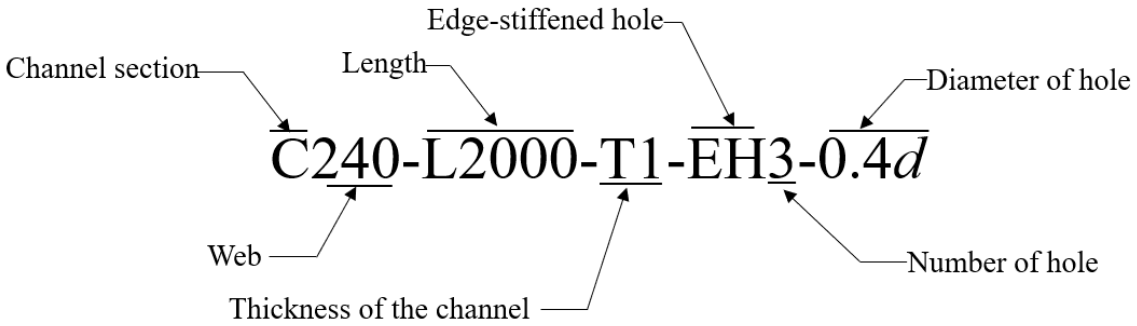

Figure 5.1 Specimen labelling

As shown in Table 3 and Figure 3.12, two sets of cross-sectional dimensions were selected to determine the effects of key design parameters. These dimensions include thicknesses of 1 mm, 2 mm, and 3 mm, and lengths of 1000 mm, 2000 mm and 2500 mm. The selected cross-sections cover a wide range of both overall ($\lambda=KL/r$) and web (h/t) slenderness ratios, where K, L, and r are defined as the effective length factor, the unbraced length of member and the thickness of the web, respectively.

Table 3. Parametric study variables

Section name	Thickness t (mm)	Length L (mm)	Hole diameter a (mm)	Hole number n
C190 x 45 x 15	1,2, and 3	1000, 2000 and 2500	a=0.4d, 0.5d and 0.6d	n=1,3 and 5 For L=2000, 2500
C240 x 45 x 15				n=1,2 and 3 for L=1000

The effects of all possible combinations of axial compression load and bending moments, including compression and major-axis bending, combined compression and minor-axis bending, were evaluated by selecting nine different combinations of loading conditions. Furthermore, the capacities of the cross-sections in the anchor points of the interaction curves were predicted using four alternative loading conditions: pure compression, pure bending about the major-axial, and pure minor-axial bending in two directions (i.e., bending moments putting

the web in compression or tension). These possible loading combinations were applied using various eccentricity values, as listed in Table 4. To account for the effects of the aforementioned design variables on the capacity of the beam-column, a total of 3078 FE models were developed. The yield stress (F_y), the ultimate stress (F_u), the elastic modulus (E), and the Poisson's ratio of the material (v) were taken as 350 MPa, 420 MPa, 210 GPa, and 0.3, respectively.

Table 4. Magnitude of the eccentricities.

Loading condition	Eccentricities	
	e_x (mm)	e_y (mm)
Pure compression	0	0
Pure bending about major axis	0	∞
Pure bending about minor axis (web in compression)	-∞	0
Pure bending about minor axis (web in tension)	∞	0
Minor-axis bending + compression load	10	0
	-10	0
	25	0
	-25	0
	50	0
	-50	0
Major-axis bending + compression load	0	50
	0	100
	0	200

5.2 Results and discussion

Table 4 presents the direction and magnitude of the selected eccentricities utilised in this study. Three negative and three positive eccentricities (e_x), which put the web in compression and tension, respectively, were employed to assess the combinations of a compressive load and minor-axis bending. Additionally, three different eccentricities along the y-axis (e_y) were also selected to generate combinations of a compressive load and major-axis bending.

The behaviour of the CFS channel sections was assessed using normalised two-dimensional (2D) strength interaction surfaces (P-M) under combinations of compression load and bending moments about either a major or minor axis. This assessment aimed to determine the accuracy of the interaction equation (Eq. (2)) prescribed in AISI S100 [22] and AS/NZS 4600 [23] under all selected eccentricities.

Subsequently, an optimization process was employed to minimize the errors between the results of the detailed FE models and the strength values estimated from the proposed equation (P_{Prop}), aiming to develop a more accurate interaction equation for the design of CFS beam-columns.

5.2.1 Assessment of beam-column under major-axial bending

Figures 5.2-5.9 illustrate the normalised peak compressive loads (P/P_n) and major-axis bending moments (M_x/M_{nx}) obtained from the validated FE models in the 2D interaction space. It should be noted that the anchor points of Figures 5.2-5.9 are P_n and M_{nx} obtained from the AISI S100 [22] and AS/NZS 4600 [23] under pure compression and pure major-axis bending, respectively. The main difference between these figures is in terms of the element slenderness ratio about the minor-axis ($\lambda_y = KL/r_y$), where r_y is the radius of gyration about the minor-axis. For better comparison, the data points are divided into two categories: (i) low slenderness ratios

$\lambda_y \leq 100$ (see Figures 5.2, 5.4, 5.6 and 5.8) and (ii) high slenderness ratios $\lambda_y > 100$ (see Figures 5.3, 5.5, 5.7 and 5.9). As expected, in all cases, the presence of a major-axis bending moment led to a reduction in the maximum compressive capacity of the CFS element. However, the reduction rate seems to be affected by the slenderness ratio of the elements.

Figures 5.2, 5.4, 5.6 and 5.8 indicate that the interaction equation (Eq. (2)) provided conservative estimations of the strength of CFS beam-columns with low slenderness ratios ($\lambda y \leq 100$) as the data points generally fell above Eq. (2). The typical failure modes of these elements were shown in Figure 6.10, where web local buckling was observed in the CFS channel sections with low slenderness ratios subjected to low eccentricities (i.e., e_y = 50 mm). For the majority of other specimens, either distortional or combined local-distortional buckling was observed, depending on the cross-sectional thickness and the eccentricity level. Specimens with the low thickness (i.e., t = 1 mm) experienced severe local buckling in their webs (see Figure 5.10 a)). For the elements with thicker plates (i.e., t = 3 mm), the contribution of the web local buckling was diminished, and consequently, the dominant failure mode changed to flange distortional buckling, as shown in Figure 5.10 b).

It can be observed from Figures 5.3, 5.5, 5.7 and 5.9 that the strength of CFS beam-columns with high slenderness ratios (i.e., λ_y >100) was consistently underestimated when using the code-prescribed interaction equation. The results also demonstrate that, regardless of the applied eccentricities, all high slender beam-columns experienced web local buckling and/or flange distortional buckling followed by global instability. Figure 5.11 demonstrates the failure modes of the CFS specimens with slenderness ratios of 162 under high eccentricities (i.e., e_y = 200 mm) obtained from the FE models. In general, by comparing Figures 5.2 to 5.9, it can be concluded that the presence of global buckling and increasing the eccentricity levels increased the errors obtained from the strength predictions of the code-prescribed interaction equation

(Eq. (2)). This emphasizes the necessity to develop more accurate design equations for such cases.

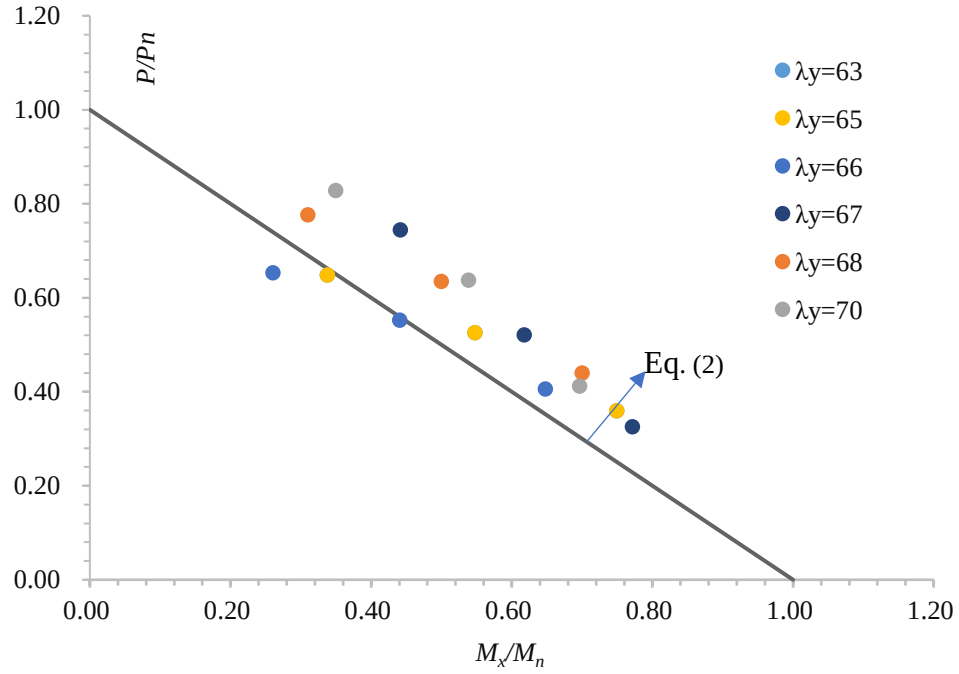

Figure 5.2 Interaction of P/P_n and M_x/M_{nx} for CFS beam-columns with plain section and $\lambda_y \leq 100$.

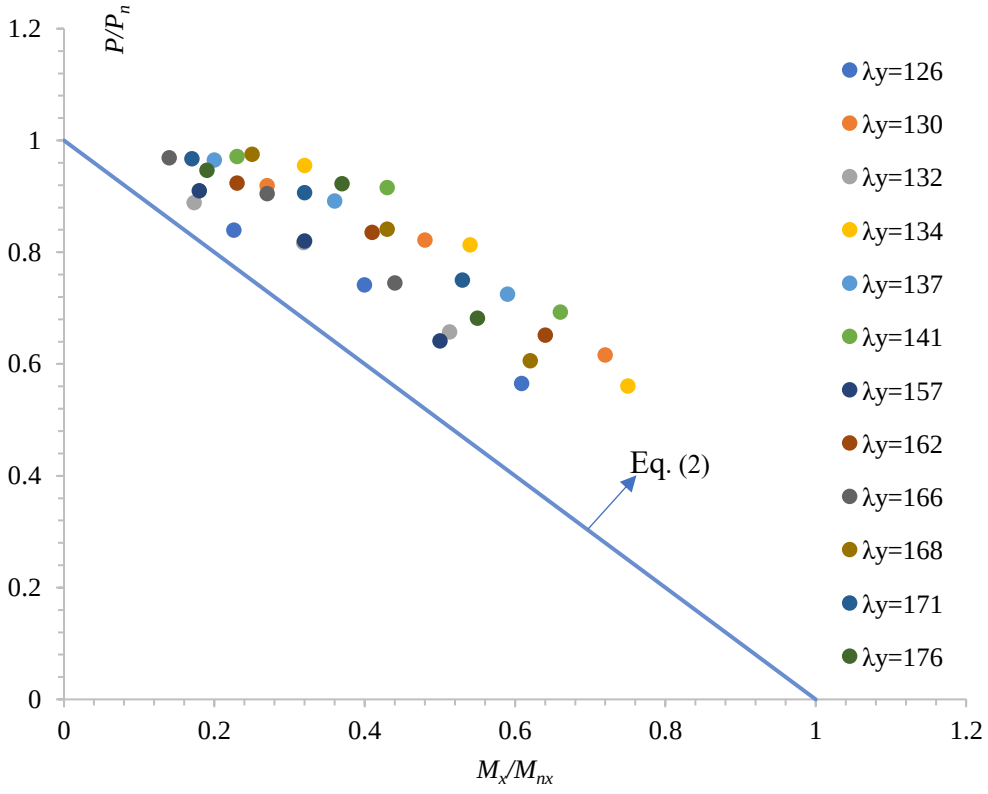

Figure 5.3 Interaction of P/P_n and M_x/M_{nx} for CFS beam-columns with plain section and $\lambda_y > 100$.

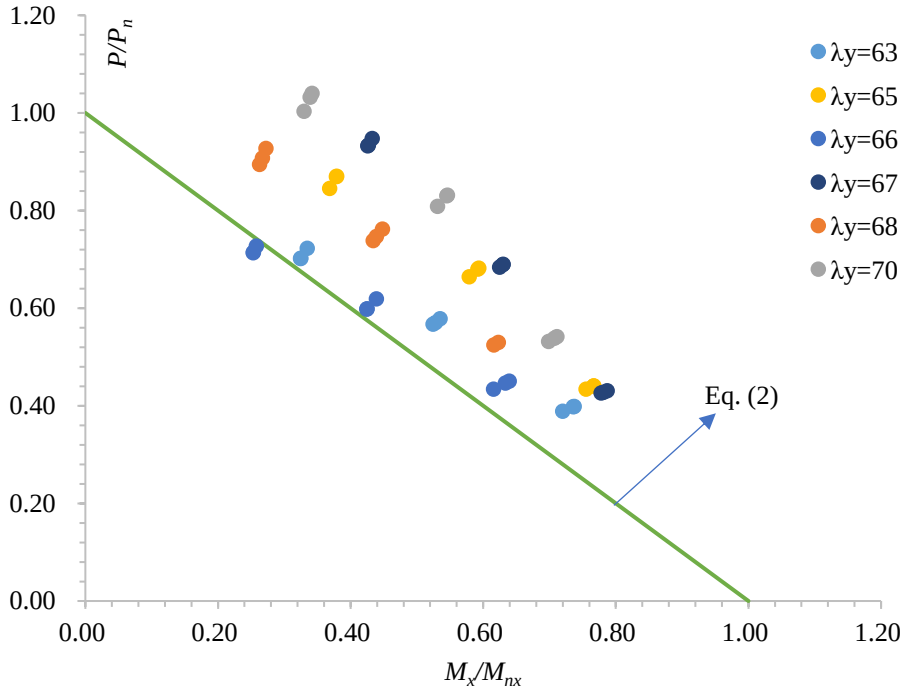

Figure 5.4 Interaction of P/P_n and Mx/M_{nx} for CFS beam-columns with unstiffened hole section (a/d=0.4) and $\lambda_y \leq 100$.

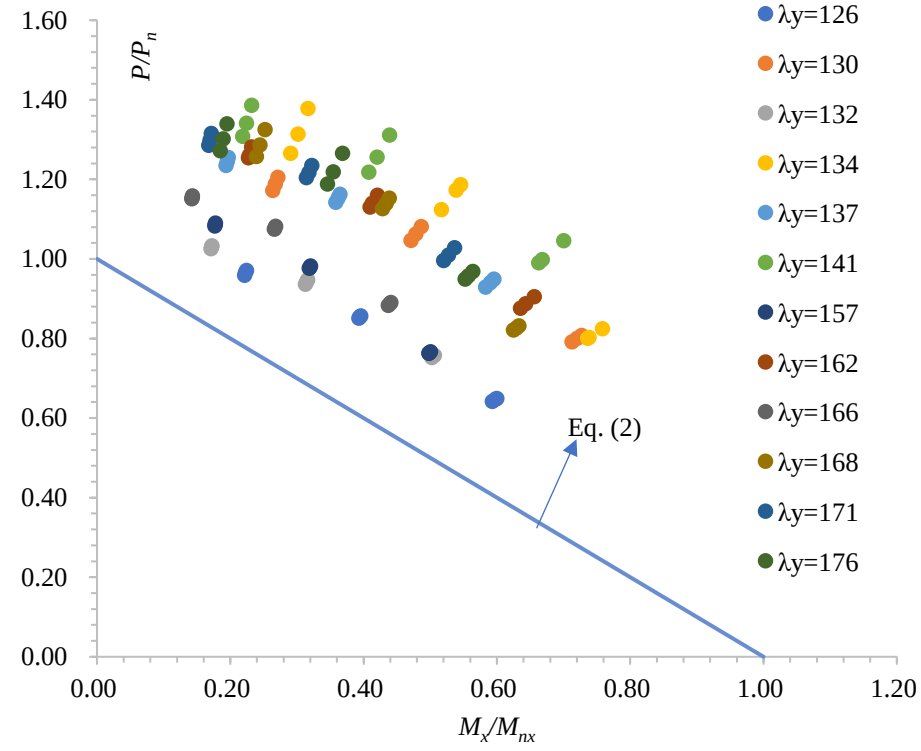

Figure 5.5 Interaction of P/P_n and M_x/M_{nx} for CFS beam-columns with unstiffened hole section (a/d=0.4) and λ_y >100.

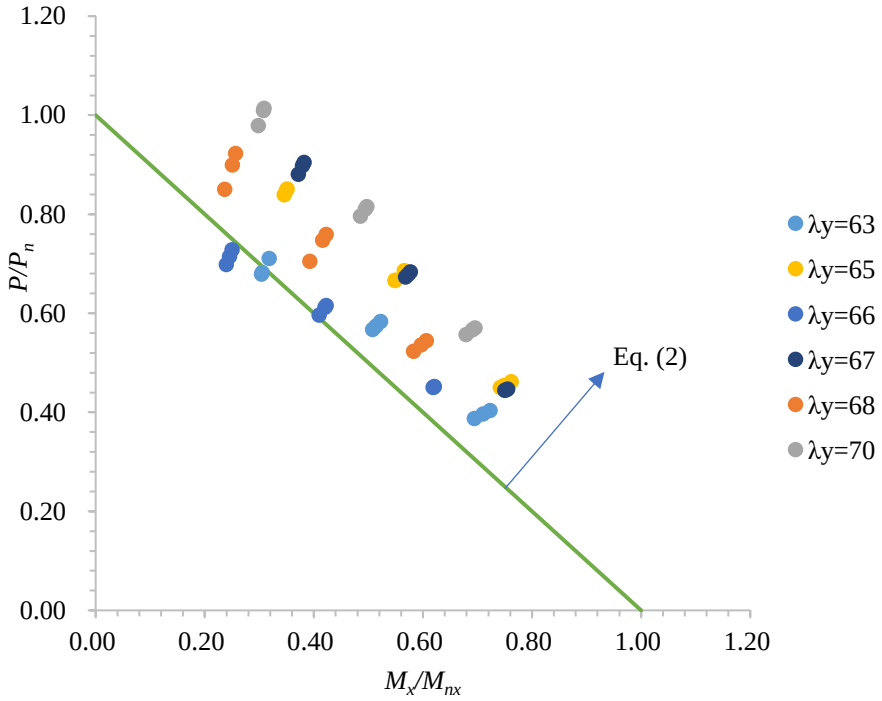

Figure 5.6 Interaction of P/P_n and M_x/M_{nx} for CFS beam-columns with unstiffened hole section (a/d=0.5) and $\lambda_y \leq 100$.

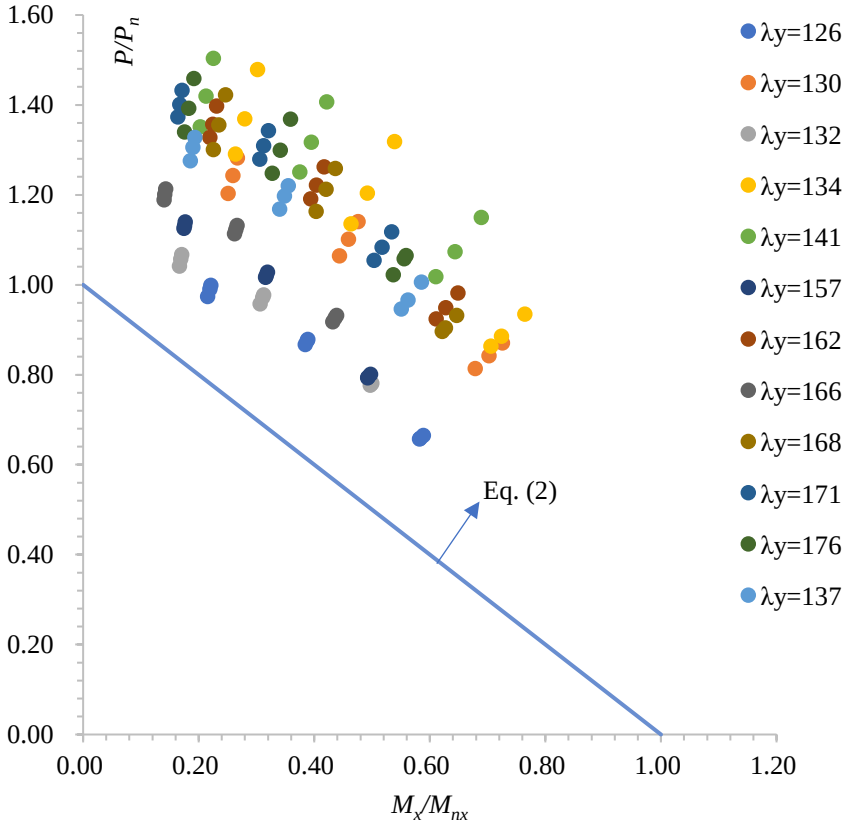

Figure 5.7 Interaction of P/P_n and M_x/M_{nx} for CFS beam-columns with unstiffened hole section (a/d=0.5) and λ_y >100.

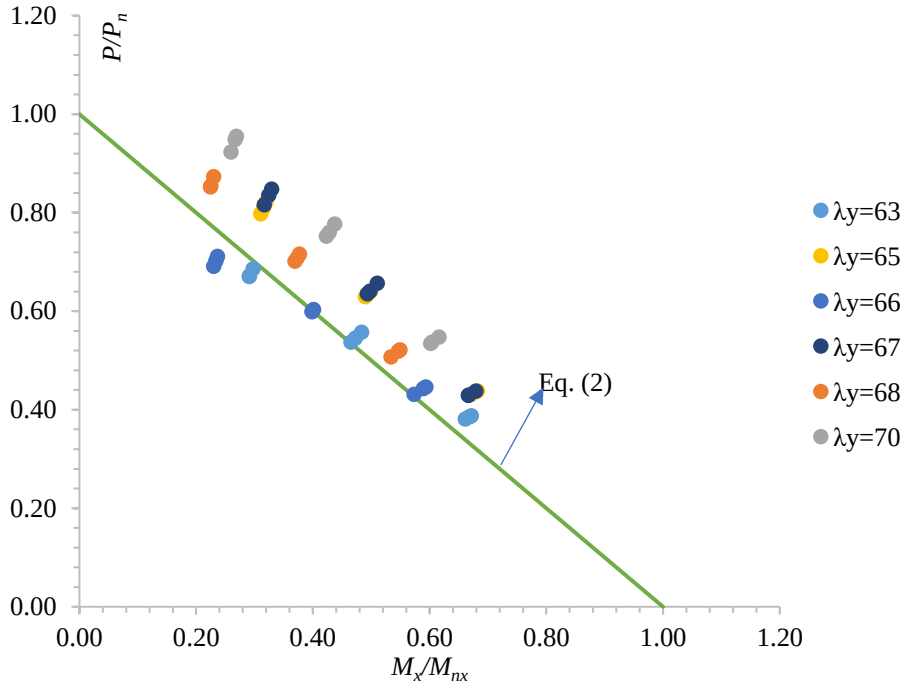

Figure 5.8 Interaction of P/P_n and M_x/M_{nx} for CFS beam-columns with unstiffened hole section (a/d=0.6) and $\lambda_y \leq 100$

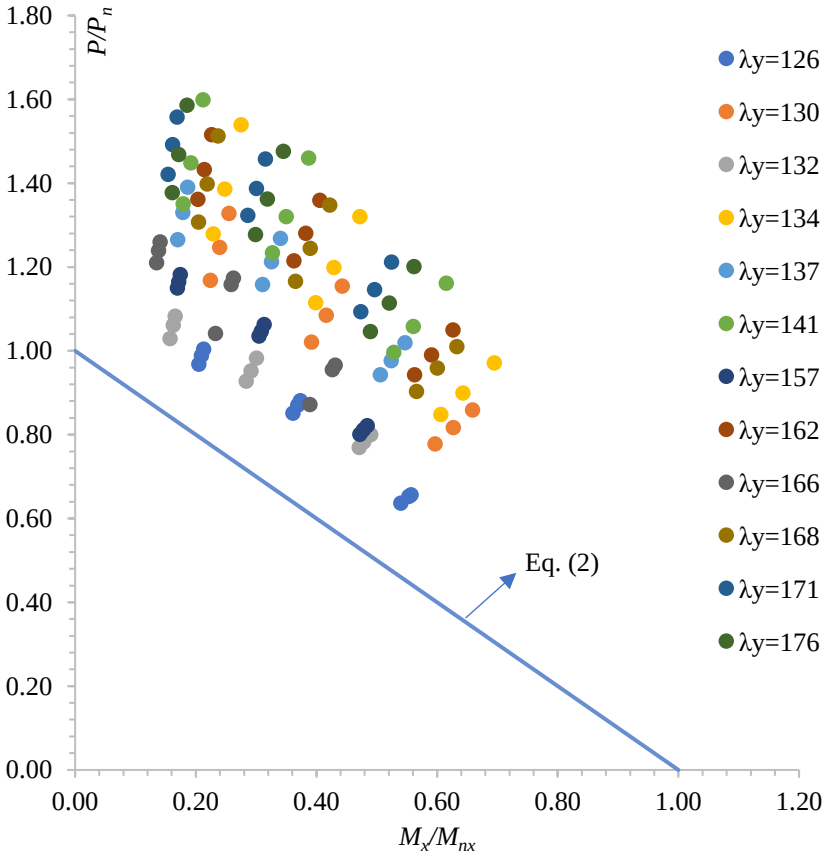

Figure 5.9 Interaction of P/P_n and M_x/M_{nx} for CFS beam-columns with unstiffened hole section (a/d=0.6) and λ_y >100.

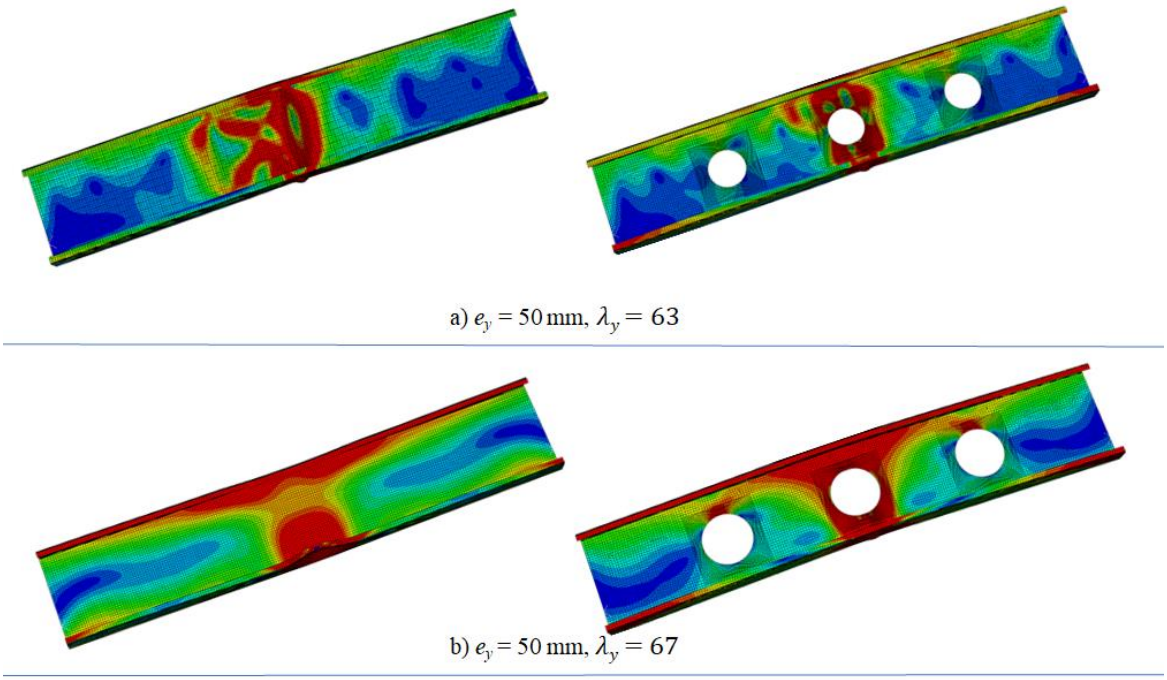

Figure 5.10 Failure modes of CFS beam-columns with λ_y <100 subjected to combined compression and major-axis bending actions.

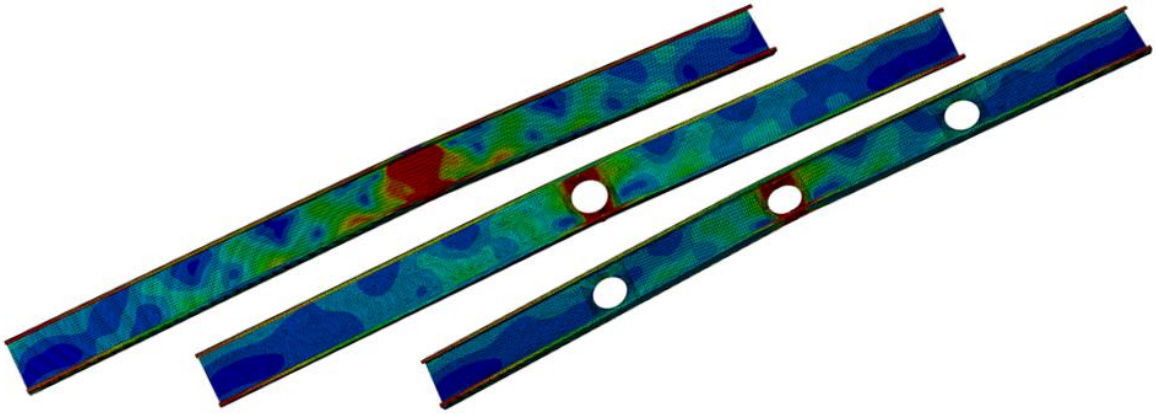

Figure 5.11 Failure modes of CFS beam-columns with λ_y = 162 and e_y = 200mm subjected to combined compression and major-axis bending actions.

5.2.2 Assessment of beam-column under minor-axial bending

In this section, the behaviour of the CFS beam-columns subjected to the combined compressive load and minor-axis bending moment is investigated. Figures 5.12-5.19 depict the normalised peak compressive loads (P/P_n) and minor-axis bending (M_y/M_{ny}) predicted by the validated FE models in 2D interaction space. Similar to Section 5.2.1, the anchor points of Figures 5.12-

5.19 (i.e., P_n and M_{ny}) were obtained from the AISI S100 [22] and AS/NZS 4600 [23] under pure compression and pure minor-axis bending. In this case, categorising the data points based on the cross-sectional web slenderness ratio (h/t) helps in a better understanding of the beam-column behaviour. Thus, the specimens were divided into two categories: (i) low web slenderness ratio $h/t < 100$, and (ii) high web slenderness ratio $h/t \geq 100$.

The results of this study indicate that the parameters significantly affecting the accuracy of the prescribed interaction equation (Eq. (2)) in AISI S100 [22] and AS/NZS 4600 [23] for elements under compression and minor-axis bending are: (i) the web slenderness ratio and (ii) the direction of the eccentricity. It can be seen in Figure 5.12 that most of the data points belonging to the elements (plain section) with low web slenderness (i.e., $h/t < 100$) were positioned above the interaction curve (Eq. (2)), although some points were located slightly below the curve. This implies that using the proposed interaction equation in AISI S100 [22] leads to generally accurate strength predictions of the low web slenderness elements subjected to compression and minor-axis bending. On the other hand, Figures 5.14, 5.16 and 5.18 present all the data points belonging to the elements which subjected to low web slenderness (i.e., $h/t < 100$) and different web openings were above the interaction curve (Eq. (2)); especially when combined compression and positive minor-axis bending, the prediction of strength is too conservative by 32% to 39% on average.

For the specimens with high (i.e., $h/t \geq 100$) web slenderness, as shown in Figures 5.13, 5.15, 5.17 and 5.19, Eq. (2) led to either underestimated or overestimated results, mainly when combined compression and positive minor-axis bending or combined compression and negative minor-axis bending were imposed, respectively.

Figure 5.20 illustrates the failure modes of the beam-columns with different web-slenderness ratios under various combinations of compression and minor-axis bending. It is shown that the

dominant failure mode of the beam-columns under combined actions of compression and positive minor-axis bending (i.e., web in tension/compression) induced distortional buckling in the flanges of the specimens (see Figure 5.20 (a)). On the contrary, imposing the combined compression and negative minor-axis bending on the elements (i.e., web in compression) resulted in interactive local- distortional, as shown in Figure 5.20 (b), Figure 5.20 (c) and Figure 5.20 (d) show the specimens with the same combined actions present different dominant failure modes due to different web slenderness ratios. With the increase in web slenderness ratios, the dominant failure mode varied from distortional buckling in the flanges to global buckling.

It is noted that the maximum value of P/P_n (i.e., e_x=10 mm) increased with the increase in the value of a/d from 0.4 to 0.6. This implies that the prediction of strength from interaction Eq. (2) becomes more overconservative subjected to the increase in diameters of web openings.

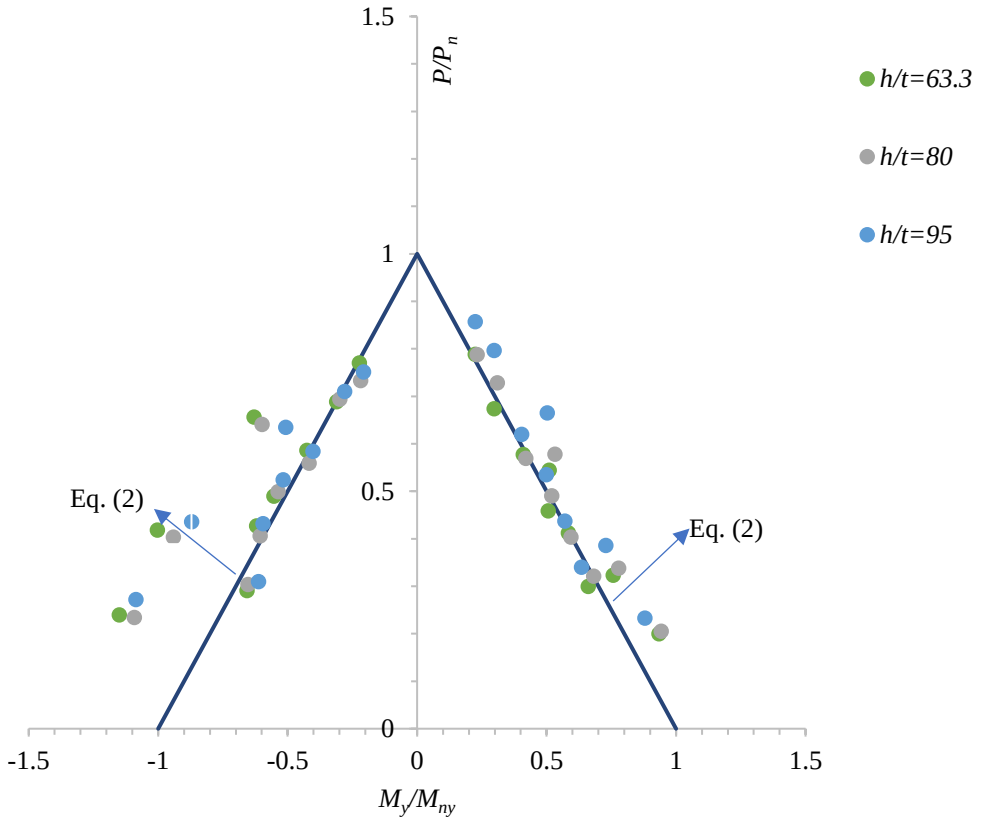

Figure 5.12 Interaction of P/P_n and M_y/M_{ny} for CFS beam-columns with plain section and $h/t \leq 100$.

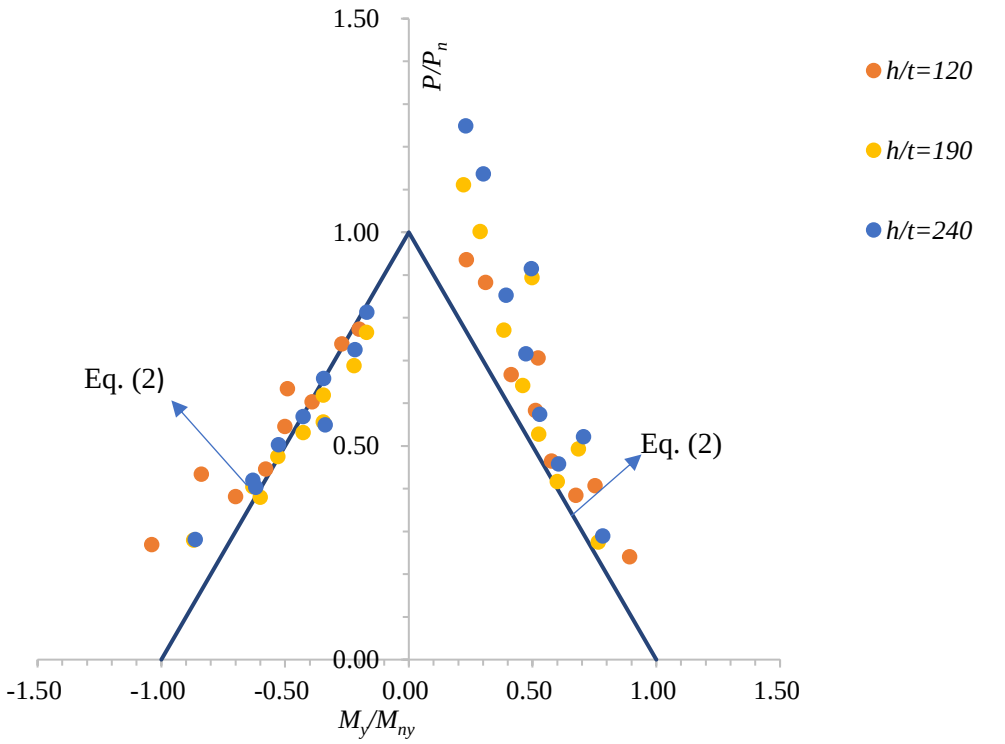

Figure 5.13 Interaction of P/P_n and M_y/M_{ny} for CFS beam-columns with plain section and h/t >100.

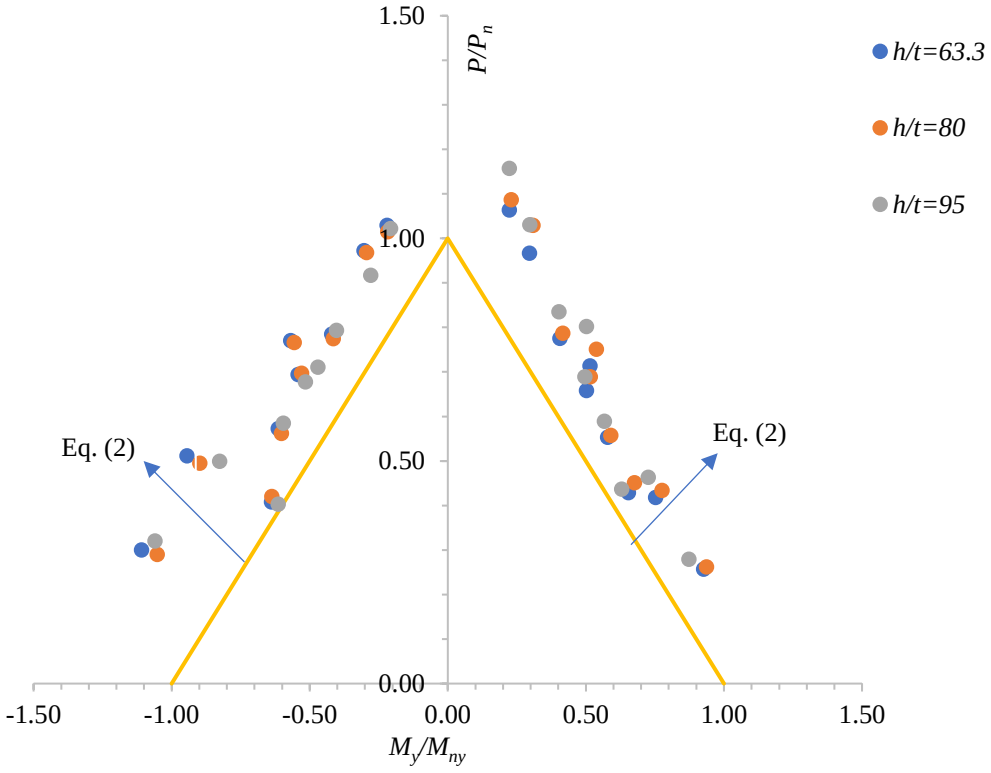

Figure 5.14 Interaction of P/P_n and M_y/M_{ny} for CFS beam-columns with unstiffened hole section (a/d=0.4) and h/t ≤ 100.

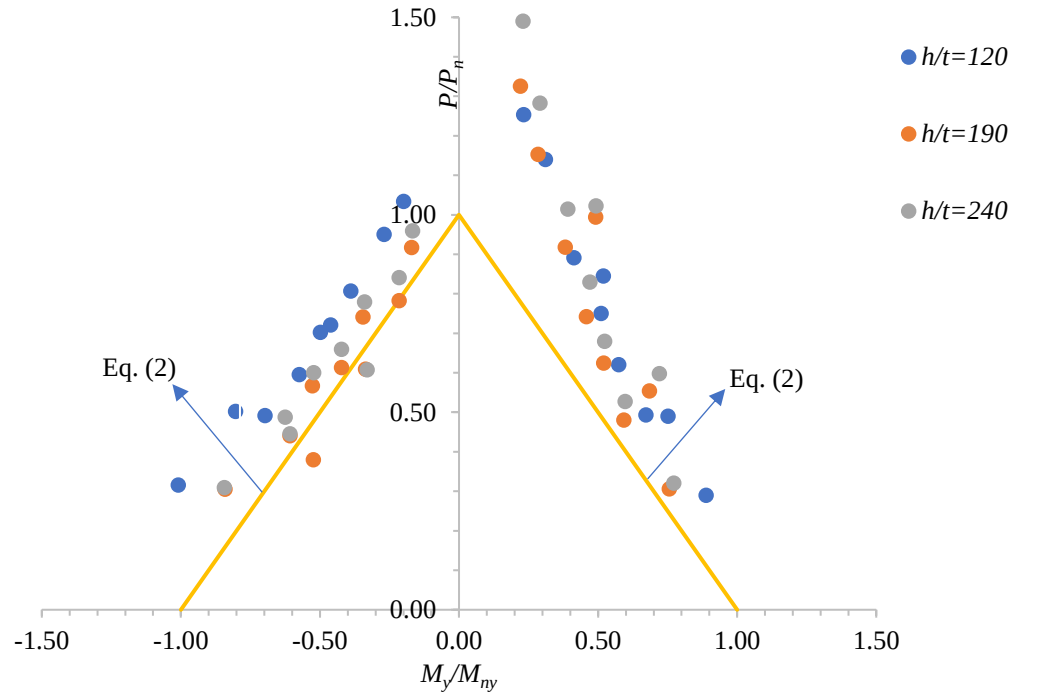

Figure 5.15 Interaction of P/P_n and M_y/M_{ny} for CFS beam-columns with unstiffened hole section (a/d=0.4) and h/t >100.

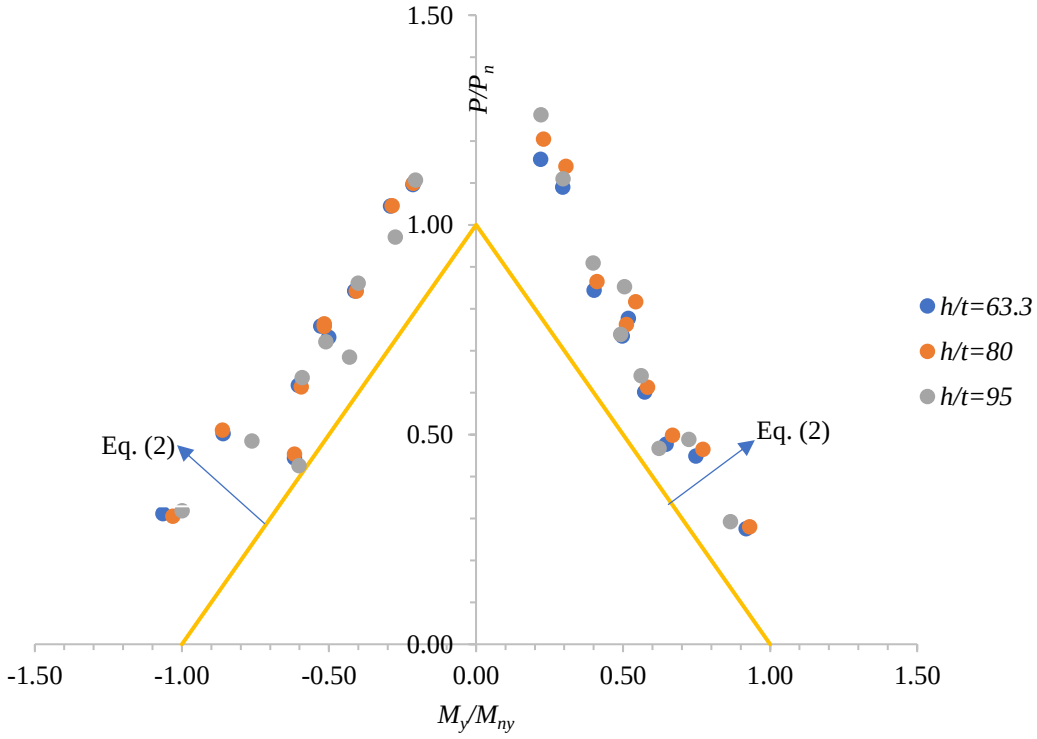

Figure 5.16 Interaction of P/P_n and M_y/M_{ny} for CFS beam-columns with unstiffened hole section (a/d=0.5) and $h/t \leq 100$.

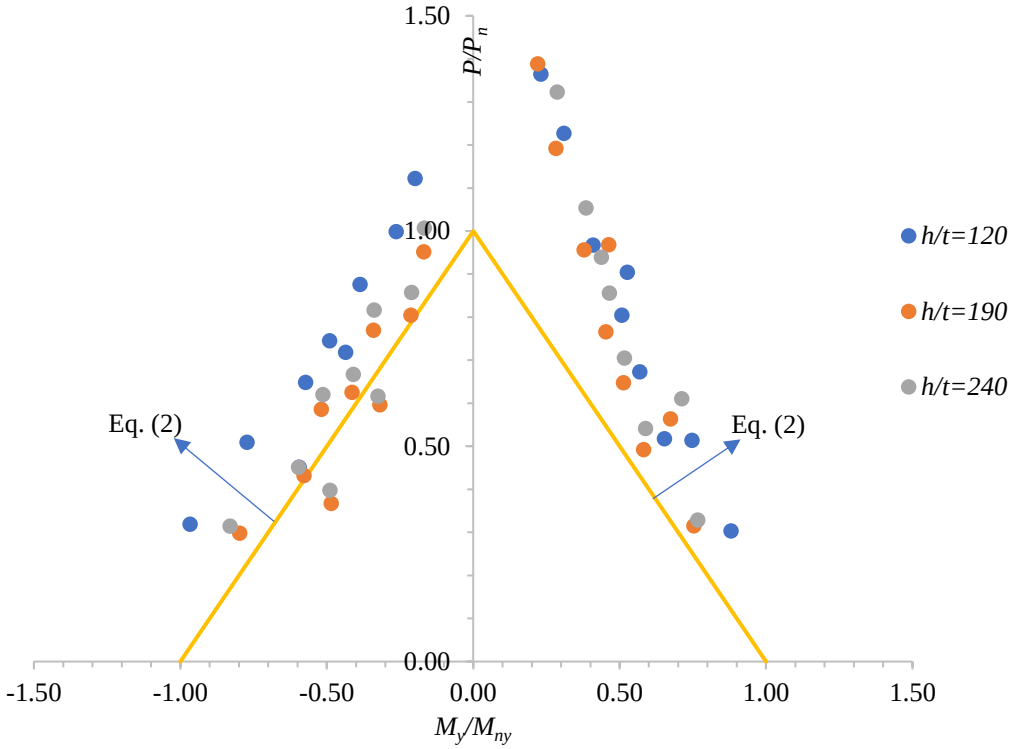

Figure 5.17 Interaction of P/P_n and M_y/M_{ny} for CFS beam-columns with unstiffened hole section (a/d=0.5) and h/t >100.

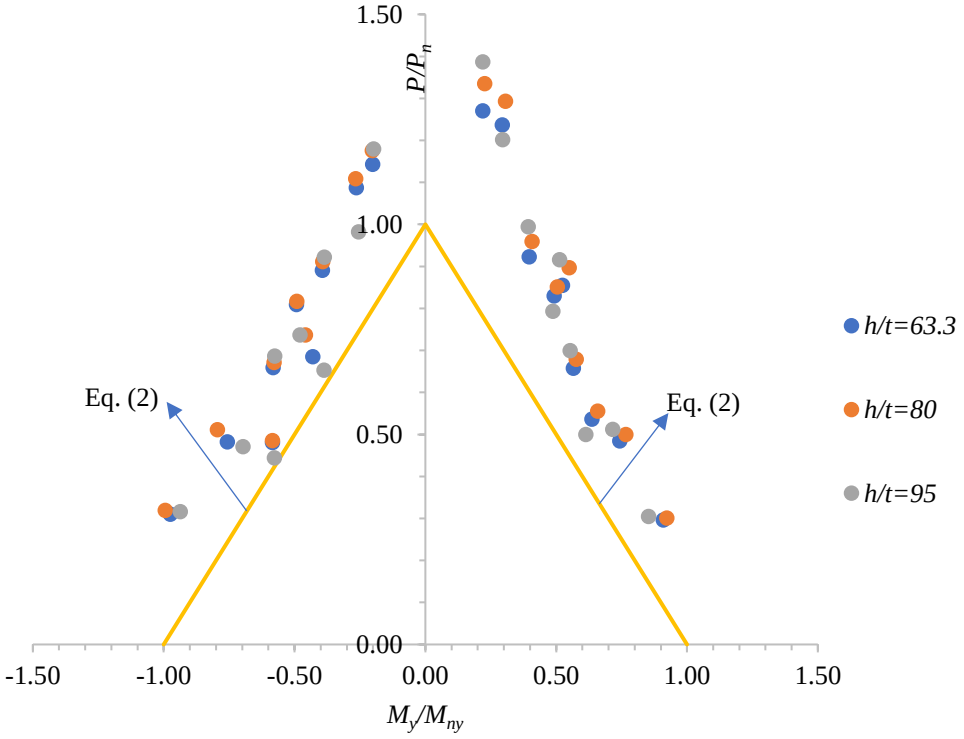

Figure 5.18 Interaction of P/P_n and M_y/M_{ny} for CFS beam-columns with unstiffened hole section (a/d=0.6) and $h/t \leq 100$.

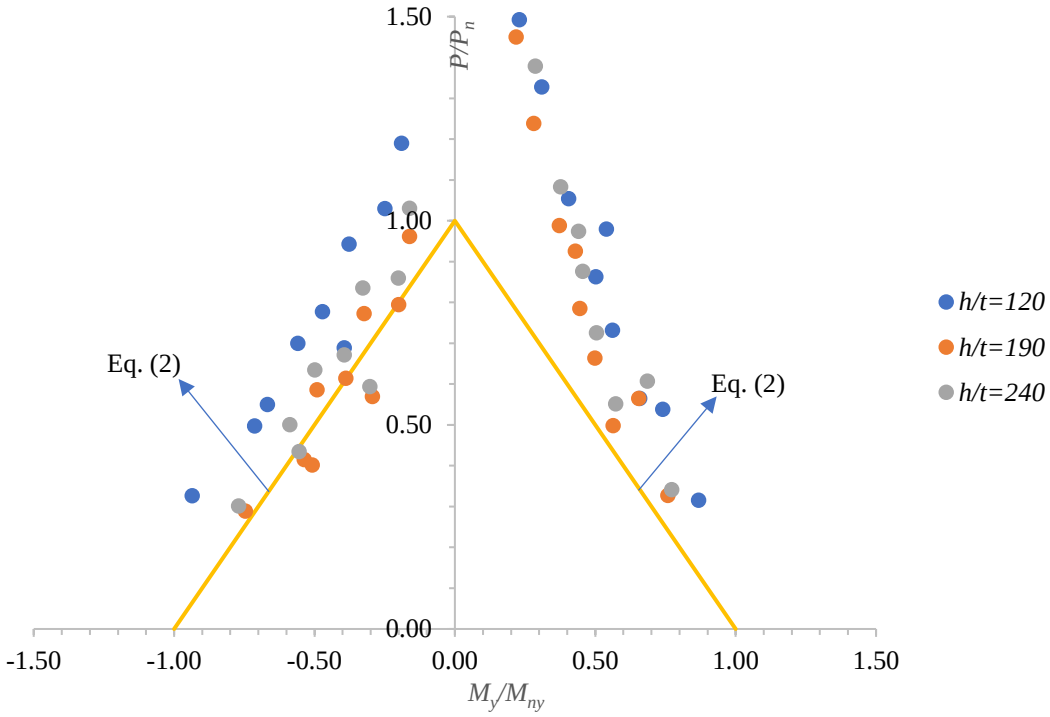

Figure 5.19 Interaction of P/P_n and M_y/M_{ny} for CFS beam-columns with unstiffened hole section (a/d=0.6) and $h/t >100$.

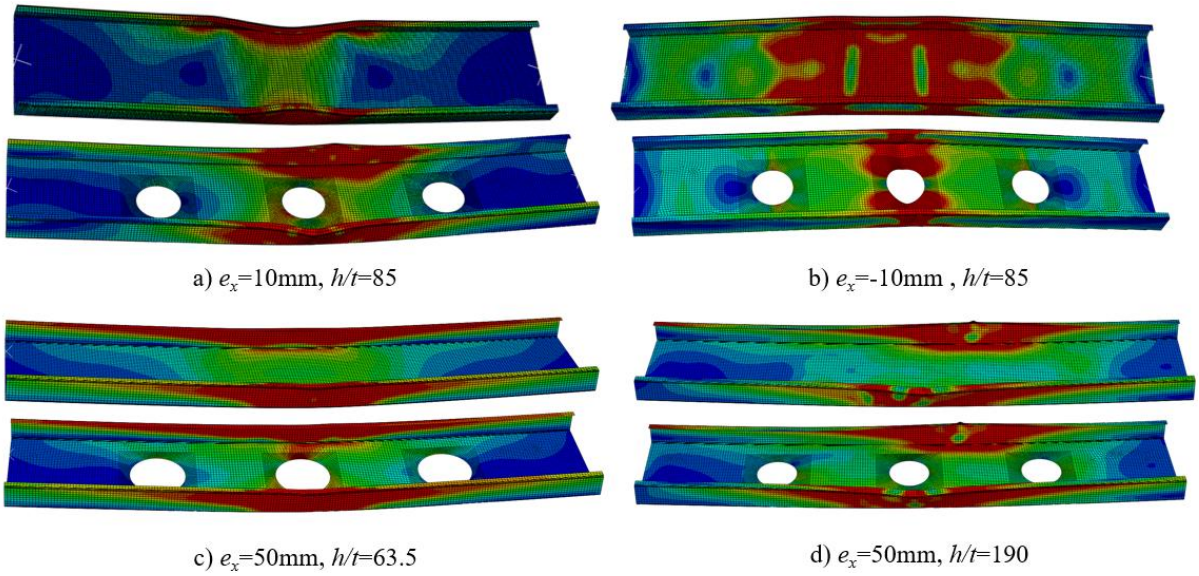

Figure 5.20 Failure modes of CFS beam-columns subject to combined compression and minor-axis bending.

Chapter 6: Proposed design equations

Based on the results of the validated FEA, modified interaction equations were proposed by adding new reduction factors that considered the effects of the element slenderness ratio (λ_y) and web slenderness ratio (h/t) as the key parameters identified in the previous section.

6.1 Plain section conditions

1) Eccentricity under major axial conditions

$$\frac{P}{P_n} + \frac{M_x}{M_{nx}} * 0.89 \leq 1.1 \quad (4)$$

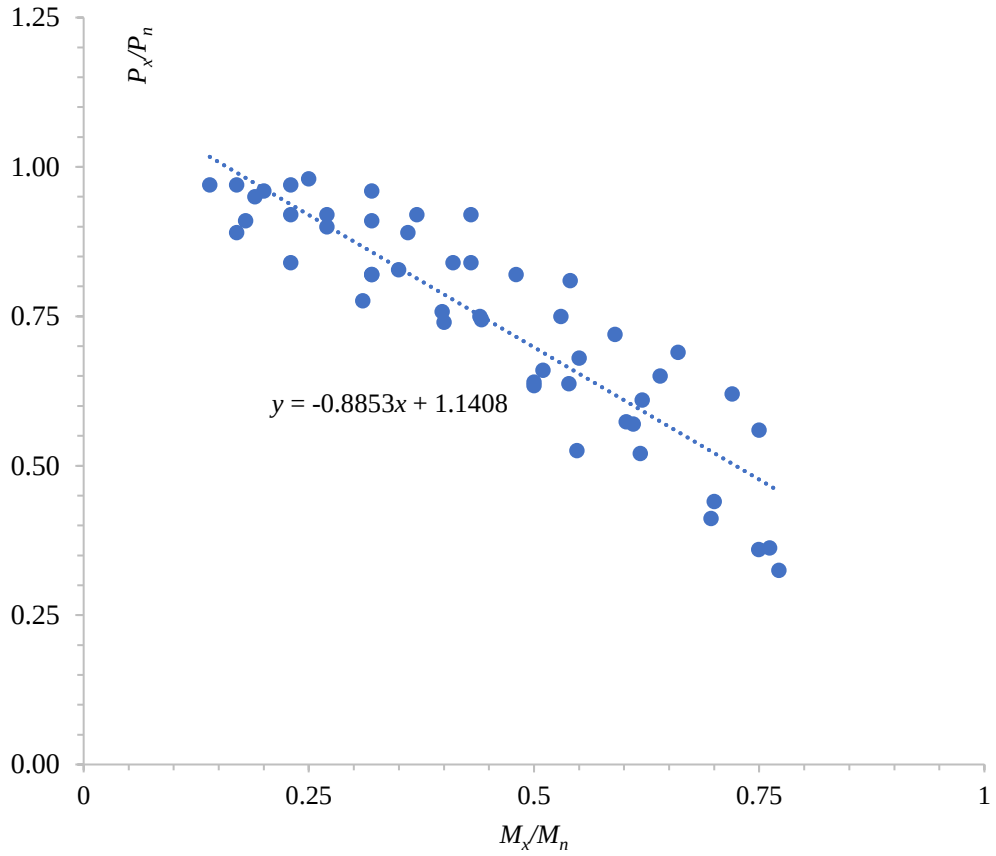

Figure 6.1 the relationship between P/P_n and M_x/M_{nx}

2) Eccentricity under minor axial conditions

$$\frac{P}{P_n} + \frac{M_y}{M_{ny}} * \alpha \leq 1 \quad (5)$$

Where α = 1 - *h/t* * 0.0009 if e_x > 0; or α = *h/t* * 0.0012+0.68

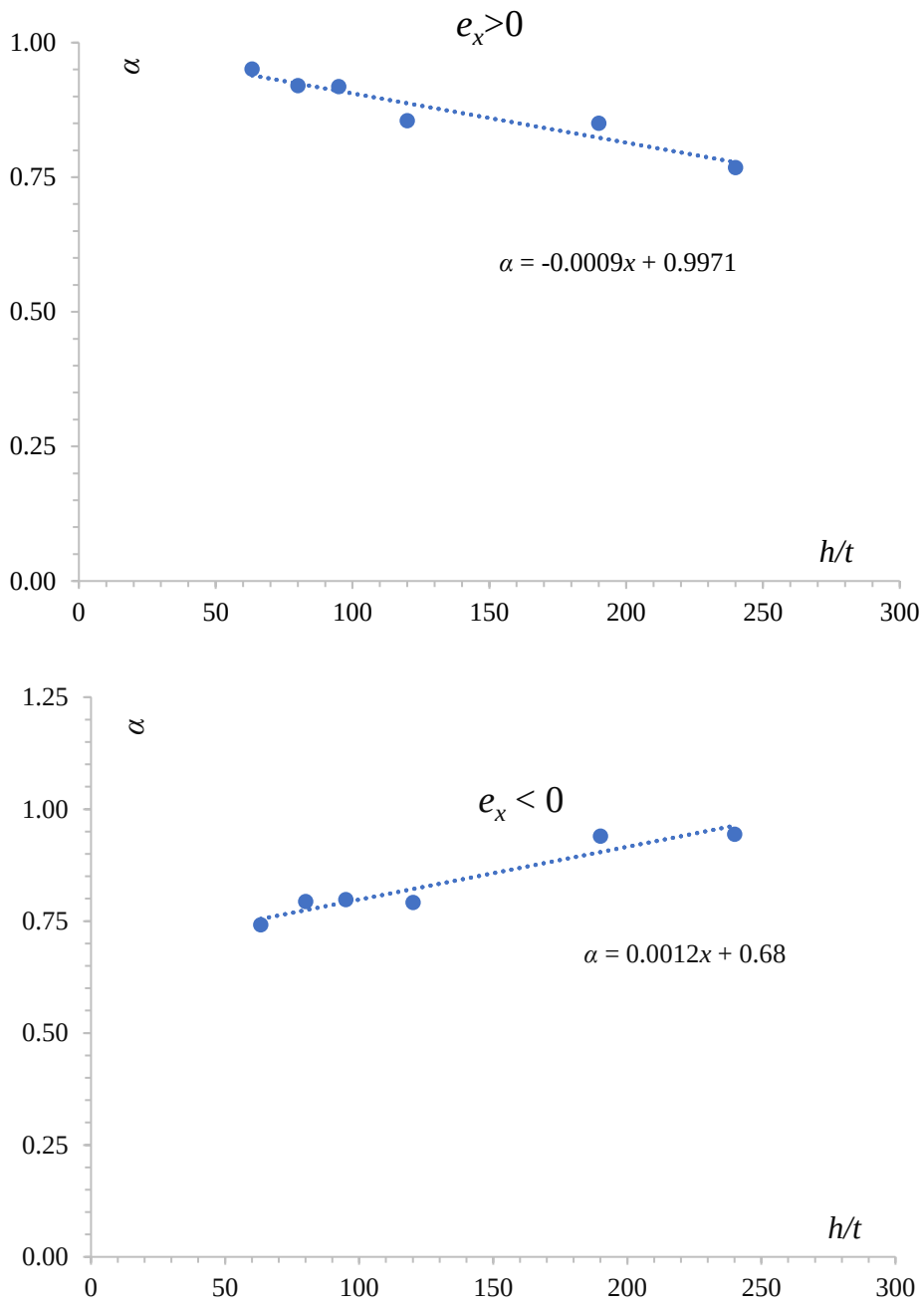

Figure 6.2 *α* factor versus web slenderness ratios of the CFS channel sections with e_x>0 and e_x<0

6.2 Unstiffened hole section conditions

1) Eccentricity under major axial conditions and minor axial (e_x < 0) conditions

$$\frac{P}{P_n}\alpha + \frac{M_x}{M_{nx}} \leq 1.0 \qquad (6)$$

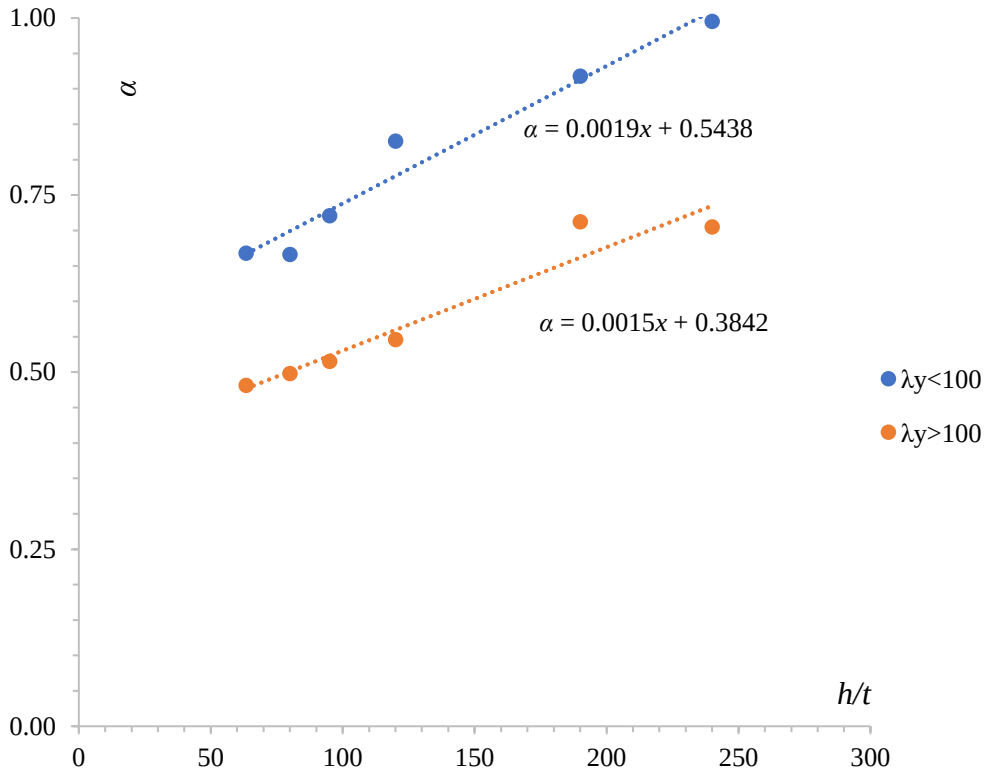

Figure 6.3 α factor versus web slenderness ratios of the CFS channel sections with $\lambda_y<100$ and $\lambda_y>100$

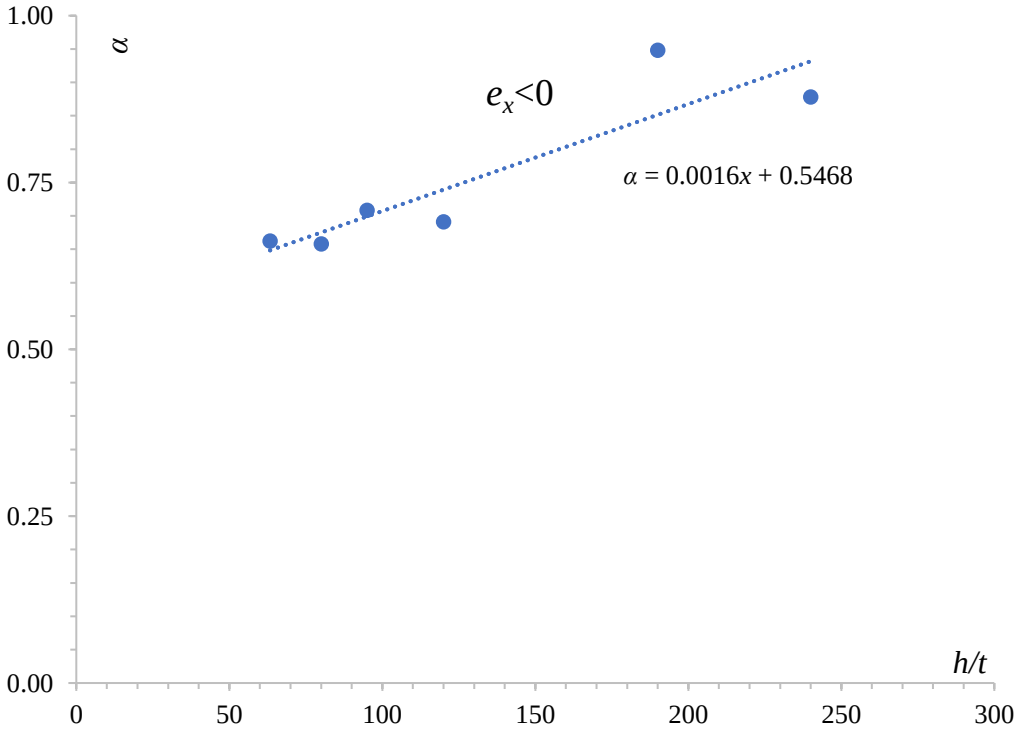

Figure 6.4 α factor versus web slenderness ratios of the CFS channel sections with $e_x<0$

Where α = h/t * 0.0019 + 0.54 if λ_y < 100; or α = h/t * 0.0015 + 0.38 if $\lambda_y \geq$ 100; or α = h/t * 0.0016 + 0.55 if e_x<0.

2) Eccentricity under minor axial conditions and e_x >0

$$\frac{P}{P_n} + \frac{M_x}{M_{nx}} * 1.6 \leq 1.6 \qquad (7)$$

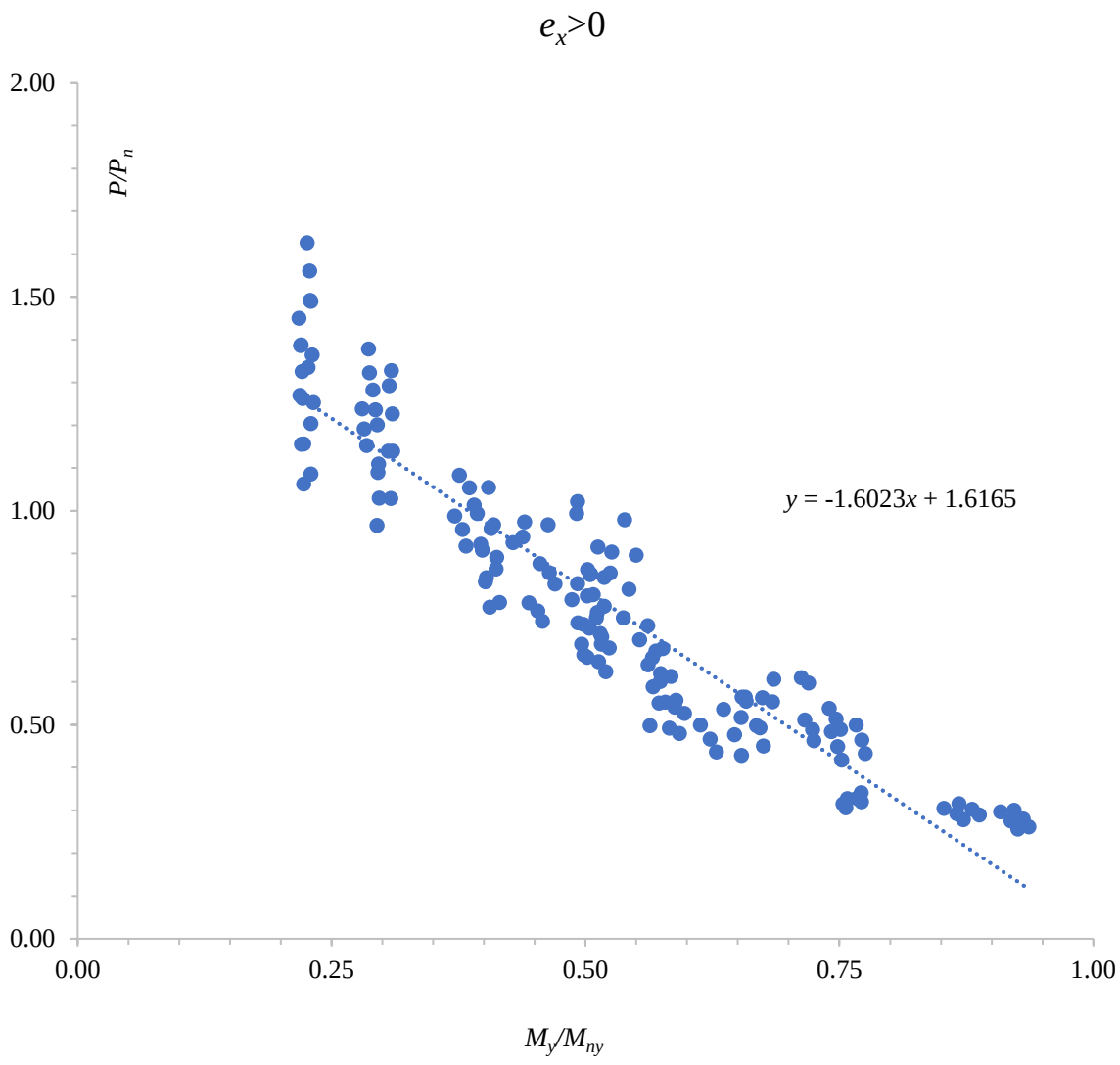

Figure 6.5 The relationship between P/P_n and M_y/M_{ny}

6.3 Reliability analysis

A reliability analysis was also carried out to assess the reliability of the proposed reduction factor equations for CFSS channel sections with unstiffened and edge-stiffened web holes. The

ASCE [46] provides an equation [Eq. 8] and suggests that the minimum target reliability index value for CFS structural members should be 2.5. The reliability of the design equations is considered reliable when the value of the reliability index (β) is 2.5 or above. The proposed equations were found to be trustworthy while calculating the strength capacity of CFS channel sections with plain section and unstiffened web holes (see Tables 5).

$$\varphi = 1.52 M_m F_m P_m e^{-\beta \sqrt{\{V_m{}^2 + V_f{}^2 + C_p V_p{}^2 + V_q{}^2\}}} \quad (8)$$

where β is the reliability index, φ for resistance factor (0.85), M_m and V_m for mean (1.1) and COV (0.1) of the material factor, F_m and V_f for mean (1.0) and COV (0.05) of the fabrication factor, P_m and V_P for mean and COV of the proposed equation, V_q for COV (0.21) of the load effect, C_p for correction factor $\left\lfloor 1 + \frac{1}{n} \right\rfloor \left\lfloor \frac{m}{m-2} \right\rfloor$, n for number of tests, and m for degree of freedom (m = n-1). Table 6 shows the comparison between the strength of CFS channel sections obtained using FE analysis (P_{FE}), code-prescribed interaction equations (P_{code}) and proposed interaction equation (P_{prop}).

Table 5 Reliability analysis results of proposed equations for CFS channel sections.

	Plain section		Unstiffened web holes	
	Eq. 4	Eq. 5	Eq. 6	Eq. 7
Total number of data	54	108	972	486
Mean, P_m	1.03	0.99	1.03	1.03
Coefficient of variation, V_p	0.08	0.07	0.09	0.07
Reliability index, β	2.78	2.71	2.77	2.87
Resistance factor, φ	0.85	0.85	0.85	0.85

6.4 Comparison the strength changes with different web openings of CFS channel sections subject to different eccentricities

Currently, accurately calculating the capacity of channel elements with edge stiffened holes by AISI S100 [22] and AS/NZS 4600 [23] is not possible. Comparing the capacity of these elements with two different web openings subjected to eccentricities becomes significantly necessary. Taking C190 specimens with 3 unstiffened or edge-stiffened web holes (a/d=0.5) as an example, Table 7 and Figures 6.6-6.8 show the strength changes of C190 specimens due to different web opening under different minor-axis eccentricities.

Table 6. Comparison between the strength of CFS channel sections obtained using FE analysis (P_{FE}), code-prescribed interaction equations (P_{code}) and proposed interaction equation (P_{prop}).

Specimen	λ_y	h/t	P_{EF}/P_{code} e_x=10 mm	P_{EF}/P_{prop} e_x=10 mm	P_{EF}/P_{code} e_x=-10 mm	P_{EF}/P_{prop} e_x=-10 mm	P_{EF}/P_{code} e_x=25 mm	P_{EF}/P_{prop} e_x=25 mm	P_{EF}/P_{code} e_x=-25 mm	P_{EF}/P_{prop} e_x=-25 mm	P_{EF}/P_{code} e_x=50 mm	P_{EF}/P_{prop} e_x=50 mm	P_{EF}/P_{code} e_x=-50 mm	P_{EF}/P_{prop} e_x=-50 mm	P_{EF}/P_{code} e_y=50 mm	P_{EF}/P_{prop} e_y=50 mm	P_{EF}/P_{code} e_y=100 mm	P_{EF}/P_{prop} e_y=100 mm	P_{EF}/P_{code} e_y=200 mm	P_{EF}/P_{prop} e_y=200 mm
C240-L1000-T1-NH	66	240	1.41	0.92	0.89	0.99	1.23	1.08	1.02	1.00	1.07	0.90	1.14	1.12	0.91	0.80	0.99	0.86	1.1	0.9
C240-L1000-T1-UH1-0.4d	66	240	1.51	1.13	0.94	0.90	1.30	1.07	1.06	1.03	1.10	0.97	1.16	1.14	0.97	0.96	1.02	1.02	1.09	1.09
C240-L1000-T1-UH1-0.5d	66	240	1.41	1.05	0.92	0.88	1.30	1.08	1.03	1.00	1.10	0.98	1.13	1.11	0.94	0.94	1.04	1.04	1.07	1.07
C240-L1000-T1-UH1-0.6d	66	240	1.40	1.04	0.88	0.84	1.30	1.07	0.95	0.92	1.11	0.98	1.06	1.04	0.92	0.92	1.00	0.99	1.03	1.03
C240-L1000-T1-UH2-0.4d	66	240	1.48	1.10	0.93	0.89	1.31	1.09	1.05	1.02	1.11	0.99	1.16	1.14	0.98	0.98	1.06	1.06	1.08	1.08
C240-L1000-T1-UH2-0.5d	66	240	1.37	1.02	0.93	0.89	1.32	1.09	0.69	0.67	1.12	0.99	0.80	0.79	0.98	0.98	1.03	1.03	1.07	1.07
C240-L1000-T1-UH2-0.6d	66	240	1.41	1.05	0.88	0.85	1.30	1.07	0.97	0.94	1.14	1.01	1.03	1.01	0.94	0.93	1.00	1.00	1.00	1.00
C240-L1000-T1-UH3-0.4d	66	240	1.51	1.13	0.94	0.90	1.32	1.09	1.05	1.02	1.09	0.97	1.15	1.13	0.97	0.97	1.02	1.02	1.05	1.05
C240-L1000-T1-UH3-0.5d	66	240	1.38	1.03	0.94	0.90	1.32	1.09	1.05	1.02	1.10	0.97	1.14	1.12	0.96	0.96	1.01	1.00	1.07	1.07
C240-L1000-T1-UH3-0.6d	66	240	1.41	1.05	0.90	0.86	1.29	1.06	0.99	0.96	1.11	0.98	1.07	1.05	0.95	0.95	1.00	1.00	1.04	1.04
C240-L2000-T1-NH	132	240	1.44	0.95	0.94	0.99	1.19	1.09	1.00	0.98	1.06	0.93	1.05	1.03	1.06	0.95	1.14	1.00	1.2	1.0
C240-L2000-T1-UH1-0.4d	132	240	1.61	1.12	1.06	1.00	1.31	0.99	1.09	1.04	1.12	0.92	1.12	1.08	1.21	0.94	1.26	1.02	1.26	1.07
C240-L2000-T1-UH1-0.5d	132	240	1.66	1.15	1.07	1.02	1.33	1.01	1.09	1.04	1.12	0.92	0.89	0.86	1.24	0.96	1.29	1.04	1.28	1.08
C240-L2000-T1-UH1-0.6d	132	240	1.69	1.16	1.08	1.02	1.36	1.03	1.07	1.03	1.11	0.91	1.10	1.07	1.25	0.97	1.28	1.03	1.06	0.89
C240-L2000-T1-UH3-0.4d	132	240	1.57	1.09	1.06	1.00	1.30	0.99	1.08	1.04	1.12	0.93	1.11	1.08	1.20	0.93	1.26	1.01	1.26	1.07
C240-L2000-T1-UH3-0.5d	132	240	1.61	1.11	1.07	1.01	1.32	1.00	1.08	1.03	1.13	0.93	0.89	0.86	1.23	0.95	1.28	1.03	1.28	1.08
C240-L2000-T1-UH3-0.6d	132	240	1.67	1.15	1.06	1.01	1.33	1.00	1.07	1.02	1.12	0.92	1.09	1.06	1.22	0.95	1.21	0.97	1.26	1.06
C240-L2000-T1-UH5-0.4d	132	240	1.57	1.09	1.05	1.00	1.30	0.99	1.08	1.03	1.12	0.93	1.11	1.08	1.20	0.93	1.25	1.01	1.25	1.06
C240-L2000-T1-UH5-0.5d	132	240	1.60	1.11	1.05	0.99	1.32	1.00	1.05	1.01	1.13	0.93	0.91	0.88	1.21	0.94	1.26	1.01	1.27	1.07
C240-L2000-T1-UH5-0.6d	132	240	1.67	1.15	1.04	0.99	1.33	1.00	1.05	1.01	1.13	0.92	1.08	1.05	1.19	0.92	1.24	1.00	1.24	1.04
C240-L2500-T1-NH	166	240	1.48	0.97	0.98	0.99	1.25	1.16	1.00	0.99	1.10	0.99	1.03	1.01	1.11	1.00	1.17	1.04	1.2	1.0
C240-L2500-T1-UH1-0.4d	166	240	1.73	1.16	1.14	1.07	1.41	1.03	1.13	1.08	1.20	0.94	1.13	1.09	1.30	1.00	1.35	1.07	1.33	1.10
C240-L2500-T1-UH1-0.5d	166	240	1.80	1.21	1.18	1.11	1.45	1.05	1.16	1.11	1.21	0.95	1.14	1.10	1.36	1.04	1.40	1.10	1.37	1.13
C240-L2500-T1-UH1-0.6d	166	240	1.88	1.26	1.21	1.14	1.47	1.06	1.18	1.12	1.21	0.94	1.16	1.11	1.40	1.07	1.44	1.13	1.40	1.15
C240-L2500-T1-UH3-0.4d	166	240	1.72	1.16	1.13	1.06	1.40	1.02	1.12	1.07	1.20	0.95	1.12	1.08	1.30	1.00	1.34	1.06	1.33	1.10
C240-L2500-T1-UH3-0.5d	166	240	1.79	1.20	1.17	1.11	1.44	1.04	1.16	1.10	1.22	0.96	1.13	1.09	1.34	1.03	1.39	1.09	1.36	1.12
C240-L2500-T1-UH3-0.6d	166	240	1.85	1.24	1.19	1.12	1.46	1.05	1.16	1.11	1.23	0.96	1.13	1.09	1.38	1.06	1.42	1.12	1.38	1.13
C240-L2500-T1-UH5-0.4d	166	240	1.72	1.16	1.13	1.07	1.40	1.02	1.12	1.07	1.20	0.95	1.12	1.08	1.29	0.99	1.34	1.06	1.32	1.09
C240-L2500-T1-UH5-0.5d	166	240	1.78	1.20	1.15	1.09	1.44	1.05	1.14	1.09	1.22	0.96	1.12	1.08	1.33	1.02	1.38	1.09	1.35	1.11
C240-L2500-T1-UH5-0.6d	166	240	1.84	1.24	1.14	1.08	1.47	1.06	1.06	1.01	1.23	0.96	1.00	0.96	1.35	1.03	1.27	1.00	1.26	1.03
C240-L1000-T2-NH	68	120	1.23	0.95	1.12	0.92	1.16	1.08	1.27	1.12	1.13	1.04	1.31	1.12	1.08	0.95	1.14	0.98	1.13	0.96
C240-L1000-T2-UH1-0.4d	68	120	1.39	1.06	1.19	1.00	1.24	1.06	1.32	1.19	1.18	1.07	1.34	1.26	1.21	1.00	1.24	1.06	1.21	1.09
C240-L1000-T2-UH1-0.5d	68	120	1.43	1.09	1.13	0.95	1.27	1.07	1.25	1.12	1.19	1.08	1.31	1.23	1.18	0.97	1.21	1.04	1.20	1.08
C240-L1000-T2-UH1-0.6d	68	120	1.49	1.13	1.05	0.88	1.29	1.09	1.17	1.05	1.18	1.06	1.25	1.17	1.10	0.91	1.11	0.95	1.10	0.99
C240-L1000-T2-UH2-0.4d	68	120	1.36	1.05	1.20	1.01	1.24	1.06	1.33	1.20	1.18	1.07	1.34	1.26	1.23	1.02	1.26	1.09	1.23	1.10
C240-L1000-T2-UH2-0.5d	68	120	1.42	1.09	1.14	0.96	1.26	1.07	1.26	1.13	1.19	1.07	1.29	1.21	1.21	1.00	1.23	1.06	1.22	1.10
C240-L1000-T2-UH2-0.6d	68	120	1.50	1.14	1.06	0.89	1.29	1.08	1.18	1.05	1.20	1.08	1.26	1.17	1.13	0.93	1.14	0.97	1.14	1.01
C240-L1000-T2-UH3-0.4d	68	120	1.36	1.05	1.18	1.00	1.24	1.06	1.31	1.18	1.18	1.07	1.32	1.24	1.19	0.98	1.22	1.05	1.21	1.09
C240-L1000-T2-UH3-0.5d	68	120	1.43	1.09	1.15	0.97	1.26	1.07	1.28	1.15	1.18	1.07	1.29	1.20	1.11	0.92	1.14	0.98	1.17	1.05

Specimen	λ_y	h/t	P_{EF}/P_{code} e_x=10 mm	P_{EF}/P_{prop} e_x=10 mm	P_{EF}/P_{code} e_x=-10 mm	P_{EF}/P_{prop} e_x=-10 mm	P_{EF}/P_{code} e_x=25 mm	P_{EF}/P_{prop} e_x=25 mm	P_{EF}/P_{code} e_x=-25 mm	P_{EF}/P_{prop} e_x=-25 mm	P_{EF}/P_{code} e_x=50 mm	P_{EF}/P_{prop} e_x=50 mm	P_{EF}/P_{code} e_x=-50 mm	P_{EF}/P_{prop} e_x=-50 mm	P_{EF}/P_{code} e_y=50 mm	P_{EF}/P_{prop} e_y=50 mm	P_{EF}/P_{code} e_y=100 mm	P_{EF}/P_{prop} e_y=100 mm	P_{EF}/P_{code} e_y=200 mm	P_{EF}/P_{prop} e_y=200 mm
C240-L1000-T2-UH3-0.6d	68	120	1.52	1.15	1.08	0.91	1.28	1.08	1.21	1.08	1.18	1.06	1.26	1.18	1.11	0.91	1.13	0.96	1.13	1.01
C240-L2000-T2-NH	137	120	1.19	0.97	1.01	0.95	1.10	1.04	1.05	0.96	1.06	0.99	1.08	0.96	1.16	1.04	1.25	1.10	1.31	1.13
C240-L2000-T2-UH1-0.4d	137	120	1.45	1.02	1.23	0.98	1.26	0.98	1.20	1.02	1.17	0.98	1.19	1.07	1.45	0.90	1.53	1.02	1.55	1.13
C240-L2000-T2-UH1-0.5d	137	120	1.53	1.07	1.28	1.01	1.32	1.02	1.25	1.05	1.18	0.99	1.08	0.96	1.52	0.94	1.58	1.04	1.59	1.15
C240-L2000-T2-UH1-0.6d	137	120	1.63	1.14	1.31	1.04	1.38	1.05	1.28	1.07	1.24	1.02	1.24	1.09	1.58	0.97	1.61	1.05	1.57	1.12
C240-L2000-T2-UH3-0.4d	137	120	1.45	1.02	1.22	0.98	1.26	0.98	1.20	1.02	1.17	0.98	1.19	1.06	1.44	0.89	1.51	1.01	1.53	1.12
C240-L2000-T2-UH3-0.5d	137	120	1.54	1.08	1.26	1.00	1.31	1.01	1.24	1.04	1.17	0.98	1.04	0.93	1.50	0.92	1.55	1.02	1.53	1.10
C240-L2000-T2-UH3-0.6d	137	120	1.64	1.14	1.28	1.01	1.37	1.04	1.25	1.05	1.22	1.01	1.22	1.08	1.51	0.92	1.54	1.00	1.50	1.07
C240-L2000-T2-UH5-0.4d	137	120	1.45	1.02	1.21	0.97	1.26	0.98	1.19	1.01	1.16	0.98	1.18	1.06	1.43	0.89	1.50	1.00	1.51	1.10
C240-L2000-T2-UH5-0.5d	137	120	1.54	1.08	1.23	0.98	1.30	1.00	1.20	1.01	1.15	0.96	1.01	0.90	1.46	0.90	1.51	0.99	1.50	1.08
C240-L2000-T2-UH5-0.6d	137	120	1.64	1.14	1.23	0.98	1.35	1.03	1.20	1.01	1.21	1.00	1.18	1.04	1.44	0.88	1.47	0.96	1.45	1.03
C240-L2500-T2-NH	171	120	1.17	0.98	0.97	0.96	1.08	1.04	0.99	0.92	1.04	0.98	1.02	0.92	1.14	1.02	1.22	1.08	1.27	1.11
C240-L2500-T2-UH1-0.4d	171	120	1.49	1.02	1.24	0.97	1.31	0.97	1.20	0.99	1.20	0.97	1.18	1.02	1.49	0.91	1.56	1.01	1.56	1.11
C240-L2500-T2-UH1-0.5d	171	120	1.60	1.09	1.34	1.05	1.39	1.02	1.27	1.05	1.25	1.00	1.23	1.06	1.60	0.97	1.66	1.07	1.65	1.16
C240-L2500-T2-UH1-0.6d	171	120	1.73	1.17	1.44	1.12	1.48	1.08	1.35	1.10	1.31	1.03	1.28	1.10	1.73	1.04	1.77	1.13	1.74	1.20
C240-L2500-T2-UH3-0.4d	171	120	1.49	1.02	1.23	0.97	1.30	0.97	1.20	0.99	1.19	0.96	1.17	1.02	1.47	0.90	1.54	1.00	1.54	1.09
C240-L2500-T2-UH3-0.5d	171	120	1.60	1.08	1.32	1.03	1.38	1.01	1.26	1.04	1.24	0.99	1.22	1.05	1.57	0.95	1.62	1.05	1.60	1.12
C240-L2500-T2-UH3-0.6d	171	120	1.72	1.16	1.38	1.07	1.46	1.06	1.32	1.08	1.29	1.02	1.26	1.08	1.65	1.00	1.69	1.08	1.64	1.14
C240-L2500-T2-UH5-0.4d	171	120	1.48	1.01	1.23	0.96	1.30	0.97	1.19	0.98	1.19	0.96	1.17	1.01	1.45	0.89	1.52	0.99	1.52	1.08
C240-L2500-T2-UH5-0.5d	171	120	1.59	1.08	1.31	1.02	1.37	1.01	1.25	1.03	1.23	0.98	1.21	1.04	1.54	0.93	1.59	1.02	1.56	1.09
C240-L2500-T2-UH5-0.6d	171	120	1.71	1.15	1.33	1.04	1.44	1.05	1.28	1.04	1.28	1.01	1.22	1.05	1.58	0.95	1.61	1.03	1.57	1.09
C240-L1000-T3-NH	70	80	1.11	0.97	1.24	0.89	1.12	1.06	1.34	1.13	1.15	1.08	1.01	0.83	1.18	1.04	1.18	1.02	1.11	0.94
C240-L1000-T3-UH1-0.4d	70	80	1.28	1.00	1.34	1.09	1.21	1.05	1.41	1.25	1.20	1.10	1.36	1.27	1.37	1.05	1.37	1.12	1.25	1.09
C240-L1000-T3-UH1-0.5d	70	80	1.34	1.04	1.29	1.04	1.24	1.07	1.41	1.25	1.22	1.11	1.37	1.27	1.32	1.01	1.30	1.05	1.26	1.08
C240-L1000-T3-UH1-0.6d	70	80	1.42	1.09	1.22	0.98	1.27	1.09	1.34	1.17	1.24	1.12	1.35	1.25	1.22	0.92	1.19	0.95	1.14	0.97
C240-L1000-T3-UH2-0.4d	70	80	1.28	1.00	1.36	1.11	1.21	1.05	1.42	1.26	1.20	1.10	1.35	1.26	1.38	1.06	1.38	1.12	1.25	1.08
C240-L1000-T3-UH2-0.5d	70	80	1.35	1.05	1.30	1.05	1.24	1.06	1.41	1.24	1.21	1.11	1.36	1.26	1.32	1.01	1.31	1.06	1.27	1.09
C240-L1000-T3-UH2-0.6d	70	80	1.44	1.10	1.22	0.98	1.27	1.08	1.34	1.17	1.23	1.11	1.34	1.23	1.22	0.93	1.21	0.97	1.16	0.99
C240-L1000-T3-UH3-0.4d	70	80	1.29	1.01	1.32	1.08	1.21	1.05	1.39	1.23	1.20	1.10	1.34	1.25	1.33	1.02	1.34	1.09	1.23	1.07
C240-L1000-T3-UH3-0.5d	70	80	1.36	1.05	1.28	1.03	1.24	1.06	1.37	1.21	1.21	1.11	1.34	1.24	1.28	0.98	1.28	1.04	1.24	1.06
C240-L1000-T3-UH3-0.6d	70	80	1.45	1.11	1.20	0.96	1.27	1.08	1.31	1.14	1.22	1.11	1.31	1.21	1.18	0.90	1.18	0.94	1.14	0.98
C240-L2000-T3-NH	141	80	1.04	0.98	0.99	0.93	1.01	0.97	1.04	0.92	1.00	0.95	1.01	0.86	1.20	1.07	1.35	1.18	1.35	1.16
C240-L2000-T3-UH1-0.4d	141	80	1.34	0.95	1.29	0.97	1.21	0.95	1.24	1.01	1.13	0.96	1.09	0.95	1.62	0.93	1.75	1.09	1.65	1.16
C240-L2000-T3-UH1-0.5d	141	80	1.46	1.02	1.38	1.03	1.28	1.00	1.30	1.05	1.18	0.99	1.13	0.97	1.73	0.98	1.83	1.12	1.84	1.26
C240-L2000-T3-UH1-0.6d	141	80	1.60	1.11	1.46	1.08	1.38	1.05	1.37	1.09	1.24	1.02	1.17	1.00	1.81	1.01	1.85	1.12	1.78	1.20
C240-L2000-T3-UH3-0.4d	141	80	1.34	0.95	1.26	0.95	1.20	0.95	1.23	1.00	1.13	0.96	1.06	0.92	1.57	0.89	1.68	1.05	1.75	1.22
C240-L2000-T3-UH3-0.5d	141	80	1.45	1.02	1.33	0.99	1.27	0.99	1.27	1.03	1.17	0.98	1.07	0.92	1.63	0.92	1.71	1.05	1.72	1.18
C240-L2000-T3-UH3-0.6d	141	80	1.60	1.11	1.38	1.02	1.36	1.04	1.31	1.05	1.21	1.00	1.07	0.91	1.64	0.92	1.67	1.01	1.62	1.09
C240-L2000-T3-UH5-0.4d	141	80	1.33	0.94	1.25	0.94	1.20	0.94	1.21	0.99	1.12	0.95	1.03	0.90	1.53	0.87	1.63	1.02	1.67	1.17
C240-L2000-T3-UH5-0.5d	141	80	1.45	1.02	1.29	0.97	1.26	0.98	1.24	1.00	1.15	0.97	1.02	0.88	1.55	0.88	1.63	1.00	1.63	1.12
C240-L2000-T3-UH5-0.6d	141	80	1.60	1.11	1.31	0.97	1.34	1.02	1.26	1.01	1.19	0.99	0.99	0.84	1.53	0.85	1.56	0.94	1.52	1.03

Specimen	λ_y	h/t	P_{EF}/P_{code} e_x=10 mm	P_{EF}/P_{prop} e_x=10 mm	P_{EF}/P_{code} e_x=-10 mm	P_{EF}/P_{prop} e_x=-10 mm	P_{EF}/P_{code} e_x=25 mm	P_{EF}/P_{prop} e_x=25 mm	P_{EF}/P_{code} e_x=-25 mm	P_{EF}/P_{prop} e_x=-25 mm	P_{EF}/P_{code} e_x=50 mm	P_{EF}/P_{prop} e_x=50 mm	P_{EF}/P_{code} e_x=-50 mm	P_{EF}/P_{prop} e_x=-50 mm	P_{EF}/P_{code} e_y=50 mm	P_{EF}/P_{prop} e_y=50 mm	P_{EF}/P_{code} e_y=100 mm	P_{EF}/P_{prop} e_y=100 mm	P_{EF}/P_{code} e_y=200 mm	P_{EF}/P_{prop} e_y=200 mm
C240-L2500-T3-NH	176	80	1.02	0.98	0.95	0.95	0.99	0.96	0.98	0.88	1.00	0.95	1.01	0.87	1.14	1.02	1.30	1.14	1.24	1.07
C240-L2500-T3-UH1-0.4d	176	80	1.33	0.92	1.25	0.92	1.21	0.91	1.20	0.95	1.15	0.94	1.17	0.99	1.53	0.86	1.63	1.00	1.50	1.03
C240-L2500-T3-UH1-0.5d	176	80	1.44	0.98	1.35	0.99	1.29	0.96	1.27	1.00	1.21	0.98	1.23	1.03	1.65	0.92	1.73	1.04	1.61	1.08
C240-L2500-T3-UH1-0.6d	176	80	1.57	1.07	1.45	1.05	1.38	1.02	1.35	1.05	1.27	1.02	1.28	1.06	1.77	0.98	1.82	1.08	1.76	1.16
C240-L2500-T3-UH3-0.4d	176	80	1.32	0.91	1.23	0.91	1.20	0.91	1.19	0.94	1.15	0.94	1.16	0.98	1.49	0.84	1.57	0.96	1.52	1.04
C240-L2500-T3-UH3-0.5d	176	80	1.43	0.98	1.31	0.96	1.28	0.95	1.25	0.98	1.20	0.97	1.21	1.01	1.58	0.88	1.64	0.99	1.62	1.09
C240-L2500-T3-UH3-0.6d	176	80	1.56	1.06	1.38	1.00	1.37	1.01	1.30	1.01	1.25	1.00	1.25	1.03	1.64	0.91	1.68	1.00	1.63	1.08
C240-L2500-T3-UH5-0.4d	176	80	1.32	0.91	1.21	0.89	1.20	0.90	1.17	0.93	1.14	0.93	1.15	0.97	1.46	0.82	1.53	0.94	1.53	1.05
C240-L2500-T3-UH5-0.5d	176	80	1.42	0.97	1.27	0.93	1.27	0.94	1.22	0.96	1.19	0.96	1.19	0.99	1.52	0.85	1.58	0.95	1.56	1.05
C240-L2500-T3-UH5-0.6d	176	80	1.55	1.05	1.32	0.96	1.35	0.99	1.26	0.97	1.23	0.98	1.21	1.00	1.54	0.85	1.58	0.94	1.54	1.01
C190-L1000-T1-NH	63	190	1.39	0.94	0.90	0.96	1.18	1.06	1.03	0.98	1.04	0.91	1.15	1.07	0.99	0.86	1.07	0.92	1.11	0.93
C190-L1000-T1-UH1-0.4d	63	190	1.48	1.11	0.95	0.86	1.23	1.03	1.05	0.99	1.07	0.95	1.15	1.10	1.03	0.96	1.11	1.06	1.13	1.09
C190-L1000-T1-UH1-0.5d	63	190	1.49	1.11	0.93	0.84	1.24	1.03	1.02	0.95	1.08	0.96	1.11	1.07	0.99	0.92	1.11	1.05	1.13	1.09
C190-L1000-T1-UH1-0.6d	63	190	1.47	1.09	0.87	0.79	1.23	1.02	0.96	0.89	1.09	0.97	1.04	0.99	0.96	0.89	1.02	0.96	1.04	1.00
C190-L1000-T1-UH2-0.4d	63	190	1.48	1.11	0.96	0.87	1.24	1.03	1.07	1.00	1.07	0.95	1.17	1.12	1.06	0.99	1.09	1.03	1.11	1.07
C190-L1000-T1-UH2-0.5d	63	190	1.48	1.10	0.95	0.86	1.25	1.03	1.04	0.98	1.08	0.96	1.13	1.09	1.03	0.96	1.08	1.02	1.08	1.04
C190-L1000-T1-UH2-0.6d	63	190	1.36	1.01	0.87	0.79	1.24	1.02	0.96	0.90	1.09	0.97	1.04	1.00	0.98	0.92	1.04	0.99	1.06	1.02
C190-L1000-T1-UH3-0.4d	63	190	1.49	1.11	0.95	0.86	1.24	1.03	1.05	0.98	1.06	0.95	1.15	1.10	1.03	0.96	1.10	1.04	1.14	1.10
C190-L1000-T1-UH3-0.5d	63	190	1.43	1.07	0.91	0.83	1.24	1.03	1.01	0.95	1.07	0.95	1.10	1.05	0.98	0.92	1.09	1.03	1.11	1.07
C190-L1000-T1-UH3-0.6d	63	190	1.35	1.01	0.86	0.78	1.22	1.01	0.95	0.89	1.09	0.96	1.03	0.99	0.96	0.90	1.00	0.95	1.05	1.02
C190-L2000-T1-NH	126	190	1.29	0.96	0.91	0.98	1.10	1.02	0.97	0.93	1.02	0.91	0.93	0.88	1.07	0.95	1.14	1.00	1.17	1.01
C190-L2000-T1-UH1-0.4d	126	190	1.44	1.01	1.01	0.89	1.21	0.93	1.04	0.95	1.07	0.89	0.91	0.86	1.20	0.87	1.25	0.97	1.25	1.03
C190-L2000-T1-UH1-0.5d	126	190	1.49	1.04	1.02	0.91	1.24	0.95	1.04	0.95	1.08	0.89	0.87	0.81	1.22	0.89	1.27	0.97	1.25	1.03
C190-L2000-T1-UH1-0.6d	126	190	1.53	1.06	1.01	0.89	1.27	0.97	1.01	0.92	1.07	0.88	0.94	0.88	1.22	0.88	1.25	0.96	1.21	0.99
C190-L2000-T1-UH3-0.4d	126	190	1.44	1.00	1.00	0.88	1.20	0.92	1.04	0.95	1.07	0.89	0.90	0.85	1.19	0.87	1.25	0.96	1.25	1.03
C190-L2000-T1-UH3-0.5d	126	190	1.47	1.03	1.02	0.90	1.22	0.93	1.04	0.95	1.07	0.89	0.85	0.80	1.21	0.88	1.26	0.97	1.24	1.02
C190-L2000-T1-UH3-0.6d	126	190	1.52	1.05	1.00	0.88	1.23	0.94	1.00	0.91	1.06	0.87	0.91	0.85	1.20	0.87	1.24	0.95	1.21	0.99
C190-L2000-T1-UH5-0.4d	126	190	1.43	1.00	1.00	0.89	1.20	0.92	1.03	0.94	1.07	0.89	0.90	0.84	1.18	0.86	1.24	0.96	1.24	1.02
C190-L2000-T1-UH5-0.5d	126	190	1.46	1.02	1.00	0.88	1.22	0.93	1.02	0.93	1.08	0.89	0.89	0.84	1.19	0.86	1.25	0.96	1.24	1.02
C190-L2000-T1-UH5-0.6d	126	190	1.51	1.05	0.97	0.86	1.24	0.94	0.98	0.89	1.07	0.88	0.88	0.82	1.17	0.85	1.21	0.93	1.18	0.96
C190-L2500-T1-NH	157	190	1.33	0.97	0.94	0.98	1.16	1.09	0.96	0.93	1.05	0.96	1.00	0.96	1.09	0.97	1.14	1.01	1.14	0.99
C190-L2500-T1-UH1-0.4d	157	190	1.55	1.05	1.09	0.96	1.30	0.96	1.09	0.98	1.14	0.91	1.10	1.01	1.27	0.90	1.30	0.97	1.27	1.01
C190-L2500-T1-UH1-0.5d	157	190	1.62	1.09	1.19	1.05	1.34	0.98	1.11	1.00	1.16	0.92	1.11	1.02	1.32	0.93	1.35	1.00	1.30	1.03
C190-L2500-T1-UH1-0.6d	157	190	1.69	1.14	1.13	0.99	1.38	1.00	1.10	0.99	1.16	0.91	1.09	1.01	1.36	0.96	1.38	1.02	1.31	1.03
C190-L2500-T1-UH3-0.4d	157	190	1.55	1.05	1.09	0.95	1.30	0.96	1.09	0.98	1.14	0.91	1.09	1.01	1.26	0.90	1.30	0.97	1.26	1.01
C190-L2500-T1-UH3-0.5d	157	190	1.61	1.09	1.12	0.98	1.34	0.98	1.11	1.00	1.16	0.92	1.10	1.02	1.31	0.93	1.34	1.00	1.29	1.02
C190-L2500-T1-UH3-0.6d	157	190	1.67	1.12	1.12	0.98	1.36	0.99	1.10	0.98	1.16	0.91	1.08	0.99	1.34	0.95	1.36	1.00	1.29	1.02
C190-L2500-T1-UH5-0.4d	157	190	1.54	1.05	1.09	0.95	1.30	0.95	1.08	0.98	1.14	0.91	1.09	1.01	1.26	0.90	1.30	0.97	1.26	1.01
C190-L2500-T1-UH5-0.5d	157	190	1.60	1.08	1.11	0.98	1.33	0.97	1.10	0.99	1.16	0.91	1.10	1.01	1.30	0.92	1.33	0.99	1.29	1.02
C190-L2500-T1-UH5-0.6d	157	190	1.66	1.12	1.11	0.97	1.34	0.98	1.09	0.98	1.16	0.91	1.08	0.99	1.32	0.93	1.34	0.99	1.27	1.00
C190-L1000-T2-NH	65	95	1.17	0.96	1.14	0.91	1.11	1.05	1.31	1.13	1.11	1.04	1.36	1.13	1.16	1.01	1.18	1.01	1.12	0.95

Specimen	λ_y	h/t	P_{EF}/P_{code} e_x=10 mm	P_{EF}/P_{prop} e_x=10 mm	P_{EF}/P_{code} e_x=-10 mm	P_{EF}/P_{prop} e_x=-10 mm	P_{EF}/P_{code} e_x=25 mm	P_{EF}/P_{prop} e_x=25 mm	P_{EF}/P_{code} e_x=-25 mm	P_{EF}/P_{prop} e_x=-25 mm	P_{EF}/P_{code} e_x=50 mm	P_{EF}/P_{prop} e_x=50 mm	P_{EF}/P_{code} e_x=-50 mm	P_{EF}/P_{prop} e_x=-50 mm	P_{EF}/P_{code} e_y=50 mm	P_{EF}/P_{prop} e_y=50 mm	P_{EF}/P_{code} e_y=100 mm	P_{EF}/P_{prop} e_y=100 mm	P_{EF}/P_{code} e_y=200 mm	P_{EF}/P_{prop} e_y=200 mm
C190-L1000-T2-UH1-0.4d	65	95	1.31	1.01	1.19	0.97	1.19	1.02	1.33	1.18	1.16	1.05	1.39	1.30	1.25	1.01	1.27	1.08	1.21	1.08
C190-L1000-T2-UH1-0.5d	65	95	1.34	1.03	1.12	0.91	1.21	1.03	1.25	1.10	1.16	1.05	1.33	1.24	1.20	0.96	1.21	1.03	1.20	1.08
C190-L1000-T2-UH1-0.6d	65	95	1.39	1.06	1.05	0.86	1.24	1.05	1.17	1.03	1.17	1.06	1.25	1.16	1.13	0.90	1.12	0.94	1.10	0.98
C190-L1000-T2-UH2-0.4d	65	95	1.30	1.00	1.20	0.98	1.19	1.02	1.34	1.19	1.16	1.05	1.39	1.29	1.21	0.98	1.24	1.06	1.21	1.08
C190-L1000-T2-UH2-0.5d	65	95	1.35	1.03	1.14	0.93	1.21	1.03	1.27	1.12	1.16	1.05	1.35	1.25	1.19	0.95	1.25	1.06	1.22	1.09
C190-L1000-T2-UH2-0.6d	65	95	1.42	1.08	1.08	0.88	1.22	1.03	1.19	1.05	1.17	1.06	1.28	1.18	1.14	0.91	1.14	0.96	1.12	1.00
C190-L1000-T2-UH3-0.4d	65	95	1.30	1.00	1.18	0.97	1.19	1.01	1.33	1.18	1.15	1.05	1.38	1.29	1.25	1.01	1.27	1.08	1.19	1.07
C190-L1000-T2-UH3-0.5d	65	95	1.36	1.04	1.11	0.91	1.21	1.03	1.25	1.10	1.16	1.05	1.32	1.22	1.20	0.96	1.22	1.03	1.19	1.07
C190-L1000-T2-UH3-0.6d	65	95	1.43	1.08	1.04	0.85	1.23	1.04	1.17	1.03	1.16	1.04	1.25	1.16	1.11	0.89	1.13	0.95	1.12	1.00
C190-L2000-T2-NH	130	95	1.09	0.98	0.99	0.94	1.03	0.99	1.04	0.94	0.98	0.92	0.92	0.80	1.19	1.05	1.30	1.14	1.34	1.14
C190-L2000-T2-UH1-0.4d	130	95	1.33	0.94	1.21	0.93	1.19	0.93	1.20	1.00	1.11	0.94	1.03	0.91	1.48	0.90	1.57	1.05	1.53	1.15
C190-L2000-T2-UH1-0.5d	130	95	1.41	0.99	1.26	0.97	1.24	0.96	1.24	1.02	1.14	0.96	1.06	0.93	1.55	0.94	1.62	1.07	1.60	1.18
C190-L2000-T2-UH1-0.6d	130	95	1.50	1.05	1.28	0.98	1.29	0.99	1.26	1.03	1.17	0.98	1.09	0.95	1.58	0.95	1.60	1.05	1.52	1.11
C190-L2000-T2-UH3-0.4d	130	95	1.33	0.94	1.20	0.92	1.18	0.93	1.19	0.99	1.07	0.90	1.02	0.90	1.46	0.89	1.54	1.03	1.52	1.14
C190-L2000-T2-UH3-0.5d	130	95	1.41	0.99	1.25	0.96	1.23	0.95	1.23	1.02	1.09	0.91	1.03	0.90	1.50	0.91	1.56	1.04	1.54	1.14
C190-L2000-T2-UH3-0.6d	130	95	1.50	1.05	1.24	0.95	1.28	0.98	1.22	1.00	1.11	0.93	1.02	0.89	1.49	0.89	1.50	0.98	1.44	1.05
C190-L2000-T2-UH5-0.4d	130	95	1.33	0.94	1.18	0.91	1.18	0.92	1.19	0.99	1.06	0.90	1.00	0.88	1.44	0.88	1.52	1.02	1.50	1.13
C190-L2000-T2-UH5-0.5d	130	95	1.40	0.99	1.21	0.93	1.22	0.95	1.21	1.00	1.08	0.90	0.99	0.87	1.45	0.88	1.51	1.00	1.49	1.10
C190-L2000-T2-UH5-0.6d	130	95	1.49	1.04	1.19	0.90	1.26	0.97	1.18	0.97	1.09	0.91	0.96	0.83	1.39	0.83	1.41	0.93	1.37	1.00
C190-L2500-T2-NH	162	95	1.08	0.98	0.96	0.96	1.02	0.99	0.99	0.90	1.01	0.96	1.03	0.90	1.15	1.02	1.25	1.09	1.29	1.11
C190-L2500-T2-UH1-0.4d	162	95	1.38	0.95	1.24	0.93	1.24	0.93	1.20	0.97	1.16	0.94	1.19	1.01	1.51	0.90	1.58	1.03	1.56	1.13
C190-L2500-T2-UH1-0.5d	162	95	1.49	1.02	1.33	1.00	1.32	0.97	1.27	1.02	1.21	0.97	1.24	1.05	1.63	0.96	1.68	1.08	1.63	1.16
C190-L2500-T2-UH1-0.6d	162	95	1.62	1.09	1.42	1.06	1.40	1.03	1.35	1.06	1.27	1.00	1.29	1.08	1.74	1.02	1.77	1.12	1.68	1.17
C190-L2500-T2-UH3-0.4d	162	95	1.38	0.95	1.23	0.93	1.24	0.92	1.20	0.96	1.16	0.93	1.18	1.01	1.49	0.89	1.55	1.01	1.53	1.11
C190-L2500-T2-UH3-0.5d	162	95	1.48	1.01	1.31	0.98	1.31	0.97	1.26	1.00	1.20	0.96	1.23	1.04	1.58	0.93	1.63	1.04	1.58	1.12
C190-L2500-T2-UH3-0.6d	162	95	1.61	1.09	1.38	1.03	1.39	1.01	1.31	1.03	1.25	0.99	1.26	1.06	1.65	0.96	1.66	1.05	1.58	1.11
C190-L2500-T2-UH5-0.4d	162	95	1.38	0.94	1.23	0.92	1.23	0.92	1.20	0.96	1.15	0.93	1.18	1.01	1.48	0.88	1.54	1.00	1.51	1.09
C190-L2500-T2-UH5-0.5d	162	95	1.48	1.00	1.29	0.97	1.30	0.96	1.25	0.99	1.19	0.95	1.22	1.03	1.55	0.91	1.58	1.02	1.53	1.09
C190-L2500-T2-UH5-0.6d	162	95	1.59	1.08	1.33	0.99	1.37	1.00	1.28	1.01	1.24	0.98	1.24	1.04	1.56	0.91	1.58	1.00	1.51	1.06
C190-L1000-T3-NH	67	63.3	1.05	0.97	1.29	0.88	1.08	1.04	1.42	1.18	1.13	1.08	1.39	1.11	1.19	1.03	1.14	0.97	1.09	0.92
C190-L1000-T3-UH1-0.4d	67	63.3	1.22	0.95	1.38	1.10	1.17	1.02	1.49	1.31	1.19	1.09	1.43	1.32	1.38	1.06	1.32	1.08	1.21	1.06
C190-L1000-T3-UH1-0.5d	67	63.3	1.28	0.99	1.28	1.01	1.20	1.03	1.40	1.22	1.20	1.10	1.41	1.30	1.28	0.97	1.25	1.02	1.20	1.05
C190-L1000-T3-UH1-0.6d	67	63.3	1.36	1.04	1.17	0.92	1.24	1.05	1.29	1.11	1.22	1.11	1.32	1.21	1.16	0.88	1.14	0.92	1.10	0.95
C190-L1000-T3-UH2-0.4d	67	63.3	1.22	0.96	1.32	1.05	1.17	1.01	1.45	1.27	1.19	1.09	1.43	1.32	1.36	1.04	1.32	1.08	1.22	1.07
C190-L1000-T3-UH2-0.5d	67	63.3	1.29	1.00	1.27	1.01	1.20	1.03	1.40	1.22	1.20	1.10	1.41	1.30	1.29	0.98	1.26	1.03	1.20	1.05
C190-L1000-T3-UH2-0.6d	67	63.3	1.37	1.05	1.16	0.91	1.23	1.05	1.28	1.11	1.21	1.10	1.32	1.21	1.18	0.89	1.17	0.94	1.12	0.97
C190-L1000-T3-UH3-0.4d	67	63.3	1.23	0.96	1.34	1.07	1.17	1.01	1.46	1.28	1.18	1.09	1.41	1.30	1.36	1.04	1.31	1.08	1.20	1.06
C190-L1000-T3-UH3-0.5d	67	63.3	1.30	1.00	1.23	0.98	1.20	1.03	1.36	1.19	1.19	1.09	1.37	1.27	1.25	0.95	1.24	1.01	1.19	1.04
C190-L1000-T3-UH3-0.6d	67	63.3	1.38	1.06	1.12	0.88	1.23	1.04	1.24	1.07	1.21	1.09	1.28	1.18	1.13	0.86	1.13	0.91	1.10	0.95
C190-L2000-T3-NH	134	63.3	0.97	0.98	1.00	0.92	0.96	0.94	1.04	0.91	1.00	0.96	0.95	0.79	1.27	1.13	1.35	1.18	1.30	1.11
C190-L2000-T3-UH1-0.4d	134	63.3	1.26	0.90	1.30	0.96	1.16	0.92	1.26	1.01	1.09	0.93	1.08	0.93	1.70	0.97	1.73	1.11	1.54	1.12

Specimen	λ_y	h/t	P_{EF}/P_{code} e_x=10 mm	P_{EF}/P_{prop} e_x=10 mm	P_{EF}/P_{code} e_x=-10 mm	P_{EF}/P_{prop} e_x=-10 mm	P_{EF}/P_{code} e_x=25 mm	P_{EF}/P_{prop} e_x=25 mm	P_{EF}/P_{code} e_x=-25 mm	P_{EF}/P_{prop} e_x=-25 mm	P_{EF}/P_{code} e_x=50 mm	P_{EF}/P_{prop} e_x=50 mm	P_{EF}/P_{code} e_x=-50 mm	P_{EF}/P_{prop} e_x=-50 mm	P_{EF}/P_{code} e_y=50 mm	P_{EF}/P_{prop} e_y=50 mm	P_{EF}/P_{code} e_y=100 mm	P_{EF}/P_{prop} e_y=100 mm	P_{EF}/P_{code} e_y=200 mm	P_{EF}/P_{prop} e_y=200 mm
C190-L2000-T3-UH1-0.5d	134	63.3	1.38	0.97	1.37	1.00	1.24	0.96	1.32	1.05	1.14	0.96	1.12	0.96	1.78	1.00	1.86	1.17	1.70	1.21
C190-L2000-T3-UH1-0.6d	134	63.3	1.53	1.07	1.44	1.03	1.34	1.02	1.36	1.06	1.20	0.99	1.16	0.98	1.82	1.01	1.79	1.10	1.67	1.16
C190-L2000-T3-UH3-0.4d	134	63.3	1.26	0.90	1.28	0.94	1.16	0.91	1.24	0.99	1.08	0.92	1.05	0.90	1.62	0.93	1.71	1.10	1.54	1.12
C190-L2000-T3-UH3-0.5d	134	63.3	1.39	0.98	1.34	0.97	1.23	0.96	1.29	1.02	1.12	0.94	1.06	0.91	1.65	0.93	1.70	1.06	1.61	1.15
C190-L2000-T3-UH3-0.6d	134	63.3	1.53	1.07	1.35	0.97	1.32	1.01	1.30	1.02	1.17	0.97	1.06	0.90	1.63	0.91	1.63	1.00	1.54	1.07
C190-L2000-T3-UH5-0.4d	134	63.3	1.27	0.90	1.25	0.92	1.15	0.91	1.22	0.98	1.07	0.91	1.02	0.88	1.56	0.89	1.64	1.05	1.58	1.15
C190-L2000-T3-UH5-0.5d	134	63.3	1.38	0.97	1.28	0.93	1.22	0.95	1.25	0.99	1.11	0.93	1.01	0.86	1.55	0.88	1.60	1.00	1.57	1.12
C190-L2000-T3-UH5-0.6d	134	63.3	1.53	1.06	1.28	0.92	1.30	1.00	1.25	0.98	1.15	0.95	0.99	0.83	1.51	0.84	1.51	0.93	1.45	1.01
C190-L2500-T3-NH	168	63.3	1.01	0.99	0.99	0.95	0.99	0.96	1.01	0.91	1.00	0.96	1.05	0.90	1.23	1.09	1.28	1.12	1.23	1.05
C190-L2500-T3-UH1-0.4d	168	63.3	1.29	0.89	1.27	0.90	1.19	0.89	1.22	0.95	1.14	0.93	1.20	1.00	1.58	0.88	1.57	0.97	1.45	1.02
C190-L2500-T3-UH1-0.5d	168	63.3	1.39	0.95	1.34	0.95	1.26	0.94	1.28	0.98	1.19	0.96	1.24	1.02	1.67	0.92	1.70	1.03	1.53	1.06
C190-L2500-T3-UH1-0.6d	168	63.3	1.50	1.02	1.41	1.00	1.34	0.99	1.33	1.01	1.24	0.99	1.28	1.04	1.75	0.96	1.77	1.06	1.64	1.11
C190-L2500-T3-UH3-0.4d	168	63.3	1.29	0.89	1.25	0.89	1.18	0.89	1.21	0.93	1.13	0.92	1.19	0.99	1.53	0.86	1.59	0.99	1.46	1.02
C190-L2500-T3-UH3-0.5d	168	63.3	1.38	0.94	1.31	0.93	1.25	0.93	1.26	0.96	1.18	0.95	1.22	1.01	1.59	0.88	1.63	1.00	1.58	1.09
C190-L2500-T3-UH3-0.6d	168	63.3	1.49	1.01	1.34	0.95	1.32	0.97	1.28	0.97	1.22	0.98	1.24	1.01	1.62	0.88	1.63	0.98	1.56	1.06
C190-L2500-T3-UH5-0.4d	168	63.3	1.28	0.88	1.23	0.88	1.17	0.89	1.19	0.92	1.13	0.92	1.18	0.98	1.50	0.84	1.56	0.96	1.47	1.03
C190-L2500-T3-UH5-0.5d	168	63.3	1.37	0.94	1.27	0.90	1.23	0.92	1.23	0.94	1.16	0.94	1.20	0.99	1.53	0.84	1.57	0.96	1.52	1.05
C190-L2500-T3-UH5-0.6d	168	63.3	1.47	1.00	1.28	0.90	1.30	0.96	1.23	0.93	1.20	0.96	1.20	0.97	1.51	0.83	1.53	0.92	1.47	0.99

Table 7. Percentage of strength change of C190 specimens due to different web opening.

Specimen	x = -50 mm		x = -25 mm		x = -10 mm		0	x = 10 mm		x = 25 mm		x = 50 mm	
	(kN)	(%)	(kN)	(%)	(kN)	(%)		(kN)	(%)	(kN)	(%)	(kN)	(%)
C190-L1000-T1-NH	11.82	-	17.11	-	23.50	-	32.56	37.81	-	20.85	-	11.64	-
C190-L1000-T1-UH3-0.5d	10.15	-14.08	14.61	-14.62	20.05	-14.70	27.56	32.58	-13.84	19.89	-4.62	11.52	-1.03
C190-L1000-T1-EH3-0.5d	12.01	1.63	17.48	2.16	24.08	2.45	33.66	38.15	0.90	20.54	-1.49	11.52	-1.06
C190-L2000-T1-NH	7.80	-	11.74	-	15.04	-	19.24	21.90	-	14.01	-	9.11	-
C190-L2000-T1-UH3-0.5d	6.91	-11.42	10.57	-10.00	13.67	-9.11	17.77	21.30	-2.73	13.51	-3.62	8.57	-6.01
C190-L2000-T1-EH3-0.5d	8.01	2.69	12.06	2.69	15.33	1.89	19.87	22.04	0.61	13.94	-0.50	9.04	-0.83
C190-L2500-T1-NH	7.20	-	9.38	-	11.60	-	14.23	16.83	-	11.68	-	7.99	-
C190-L2500-T1-UH3-0.5d	6.69	-7.03	8.82	-5.91	10.98	-5.39	13.65	16.56	-1.62	11.29	-3.36	7.58	-5.18
C190-L2500-T1-EH3-0.5d	7.34	1.99	9.69	3.30	11.89	2.42	14.56	16.82	-0.08	11.85	1.44	8.02	0.31
C190-L1000-T2-NH	29.35	-	47.07	-	68.54	-	100.42	71.77	-	41.67	-	25.14	-
C190-L1000-T2-UH3-0.5d	26.97	-8.09	41.10	-12.68	58.00	-15.38	88.50	72.25	0.66	41.40	-0.65	24.76	-1.54
C190-L1000-T2-EH3-0.5d	29.02	-1.11	47.14	0.14	67.88	-0.97	98.66	72.90	1.56	41.51	-0.38	24.96	-0.72
C190-L2000-T2-NH	16.54	-	27.98	-	37.89	-	50.93	42.51	-	28.54	-	18.16	-
C190-L2000-T2-UH3-0.5d	16.24	-1.77	27.52	-1.64	37.04	-2.25	49.39	42.35	-0.38	28.18	-1.27	17.81	-1.95

Specimen	x = -50 mm		x = -25 mm		x = -10 mm		0	x = 10 mm		x = 25 mm		x = 50 mm	
	(kN)	(%)	(kN)	(%)	(kN)	(%)		(kN)	(%)	(kN)	(%)	(kN)	(%)
C190-L2000-T2-EH3-0.5d	16.02	-3.14	27.67	-1.12	37.48	-1.08	50.00	42.44	-0.15	28.18	-1.28	17.81	-1.94
C190-L2500-T2-NH	16.08	-	21.76	-	28.00	-	35.39	31.95	-	23.10	-	16.30	-
C190-L2500-T2-UH3-0.5d	15.94	-0.85	21.59	-0.77	27.75	-0.89	35.01	31.67	-0.90	22.79	-1.33	16.07	-1.43
C190-L2500-T2-EH3-0.5d	15.93	-0.91	21.59	-0.76	27.73	-0.97	34.90	31.63	-1.01	22.76	-1.47	16.08	-1.34
C190-L1000-T3-NH	44.41	-	77.51	-	121.63	-	193.39	100.85	-	59.95	-	36.98	-
C190-L1000-T3-UH3-0.5d	41.06	-7.55	66.34	-14.41	96.63	-20.55	142.91	102.63	1.76	59.26	-1.14	36.39	-1.58
C190-L1000-T3-EH3-0.5d	42.36	-4.62	69.86	-9.87	102.71	-15.56	154.01	102.60	1.74	59.34	-1.00	36.53	-1.21
C190-L2000-T3-NH	25.38	-	42.73	-	60.09	-	84.75	58.81	-	40.04	-	27.20	-
C190-L2000-T3-UH3-0.5d	23.83	-6.10	40.71	-4.72	56.12	-6.61	76.49	58.52	-0.50	39.45	-1.49	25.61	-5.86
C190-L2000-T3-EH3-0.5d	23.85	-6.03	41.20	-3.58	56.98	-5.17	77.81	58.54	-0.47	39.46	-1.46	25.60	-5.89
C190-L2500-T3-NH	23.96	-	32.88	-	43.22	-	56.11	44.22	-	32.39	-	23.11	-
C190-L2500-T3-UH3-0.5d	23.31	-2.71	31.83	-3.22	41.40	-4.22	52.87	43.65	-1.29	31.86	-1.61	22.72	-1.68
C190-L2500-T3-EH3-0.5d	23.36	-2.48	31.93	-2.90	41.52	-3.93	52.99	43.63	-1.35	31.85	-1.67	22.72	-1.65

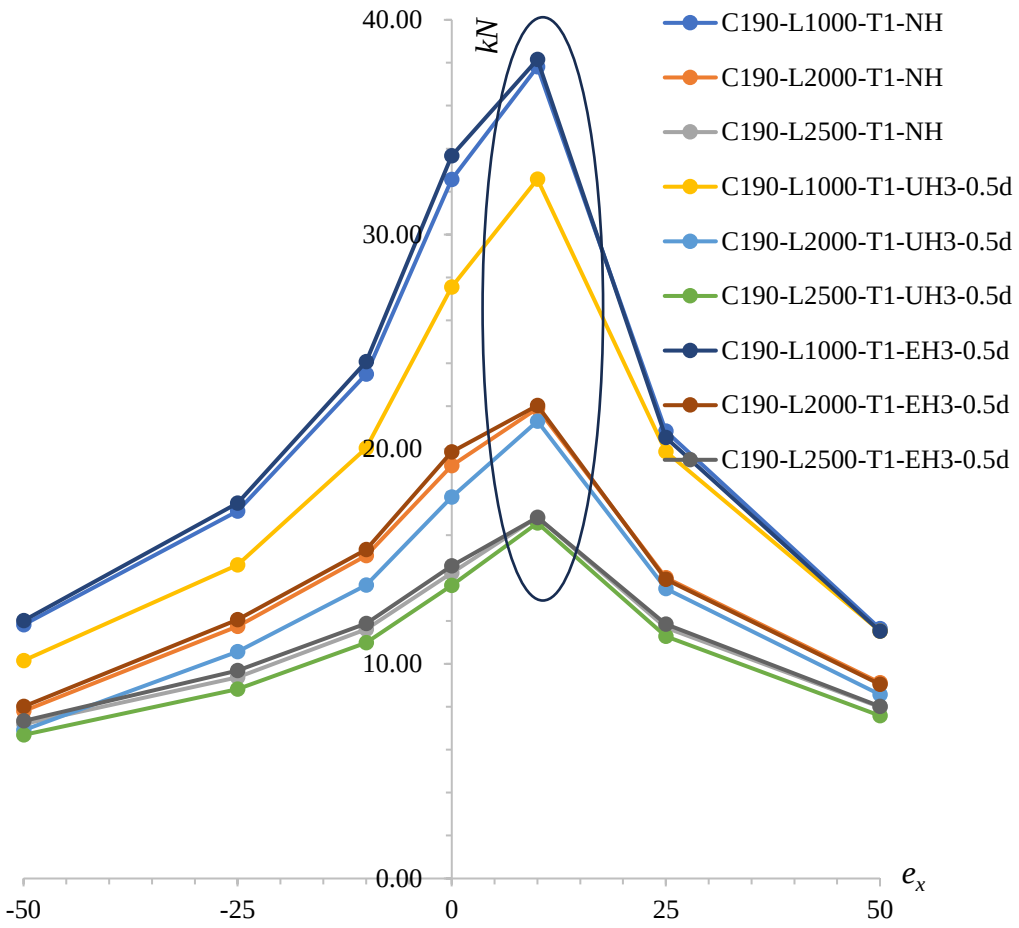

Figure 6.6 The strength of C190-1 mm thickness specimens with different web openings due to minor-axis eccentricities

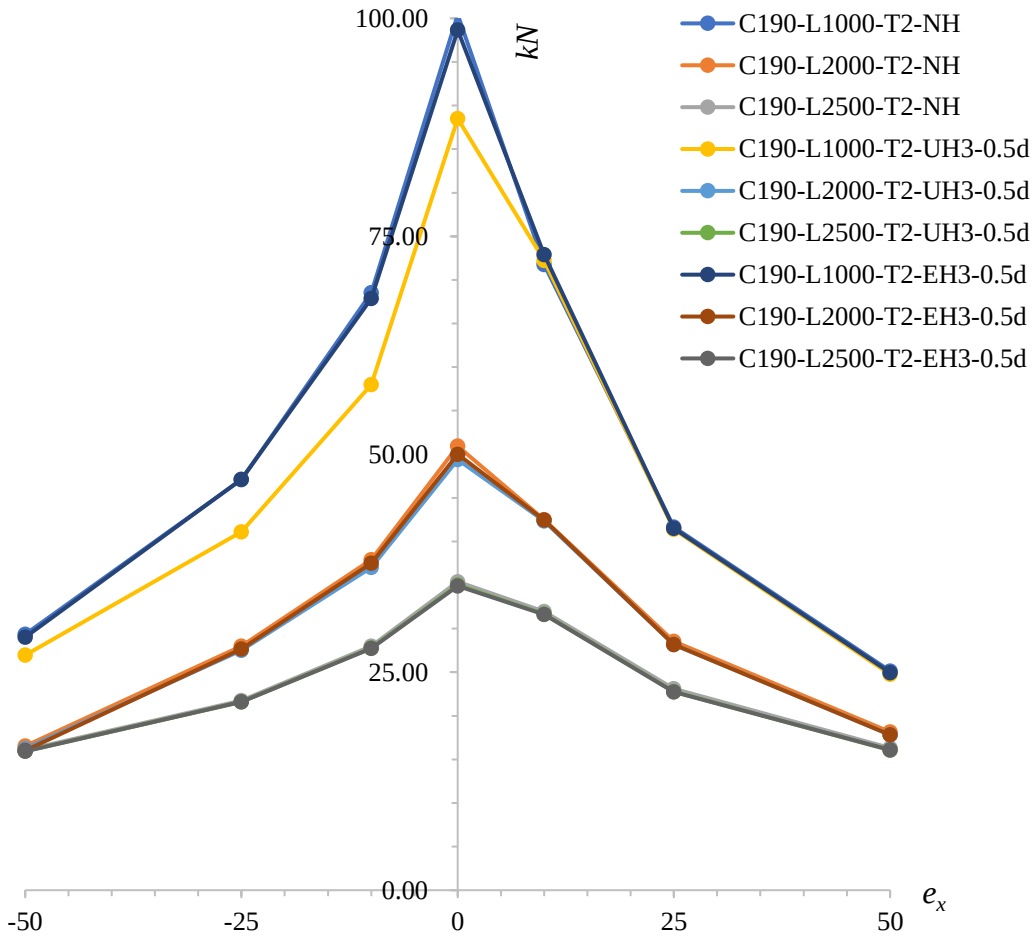

Figure 6.7 The strength of C190-2 mm thickness specimens with different web openings due to minor-axis eccentricities

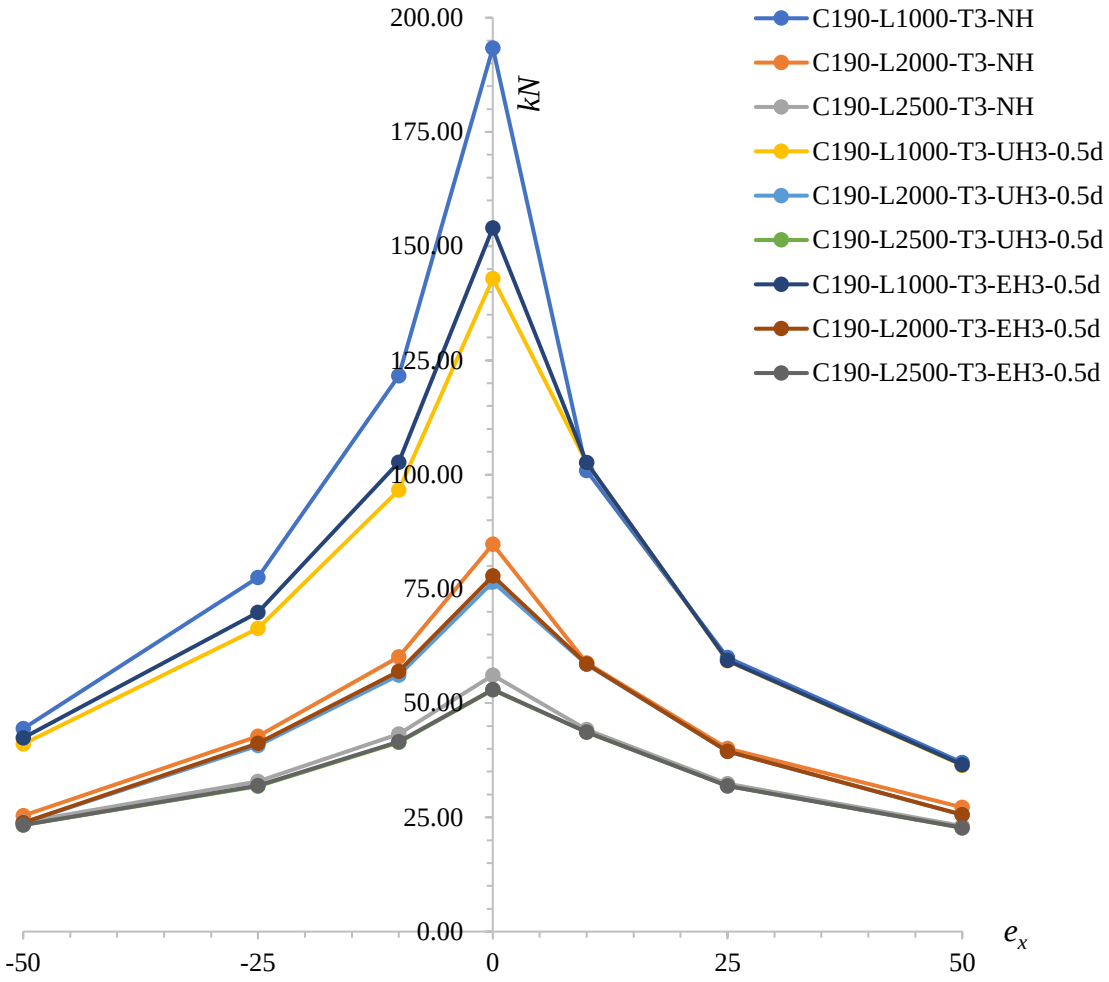

Figure 6.8 The strength of C190-3 mm thickness specimens with different web openings due to minor-axis eccentricities

Table 6 displays the percentage of strength change accurately subjected to different web openings due to eccentricities ranging from e_x = -50 mm to e_x = 50 mm. Figures 6.6 to 6.8 present the influence of web opening due to the eccentricities through curves. Web openings can cause a significant increase or decrease in strength under compression (e_x<0); however, the influence could be mitigated by increasing the thickness and length of the specimens. Figure 6.6 indicates that specimens with edge-stiffened web holes (thickness = 1 mm) exhibit greater strength compared to those with unstiffened web holes and even plain sections. Conversely, in Figure 6.8, specimens with edge-stiffened web holes (thickness = 3 mm) do not show a

significant strength increase compared to those with unstiffened web holes. Furthermore, as the length of specimens increases, the impact of edge-stiffened holes becomes negligible.

It can be noted that a number of beam-column elements with high web slenderness ratios under combined compression and positive minor-axis bending exhibited higher strength than those under pure compression. These data points, specified by an oval in Figure 6.6, correspond to the specimens with thin plate thickness (i.e., t = 1 mm and h/t = 190), subjected to pure compression and low eccentricity (i.e., e_x = 10 mm). In these cases, the higher capacity under combined actions can be justified by the effect of the tensile stresses that emerged from the bending in the web of the cross-section, which led to a delay in the web's local buckling. As shown in Figure 6.9, when e_x = 0 and e_x = 5 mm, it presents similar failure modes; however, at e_x = 10 mm, a completely different failure mode is evident. Applying higher eccentricities (i.e., e_x = 25 or 50 mm) induces significant compressive stresses in the flanges caused by the minor-axis bending, which consequently results in the distortional buckling of the flanges.

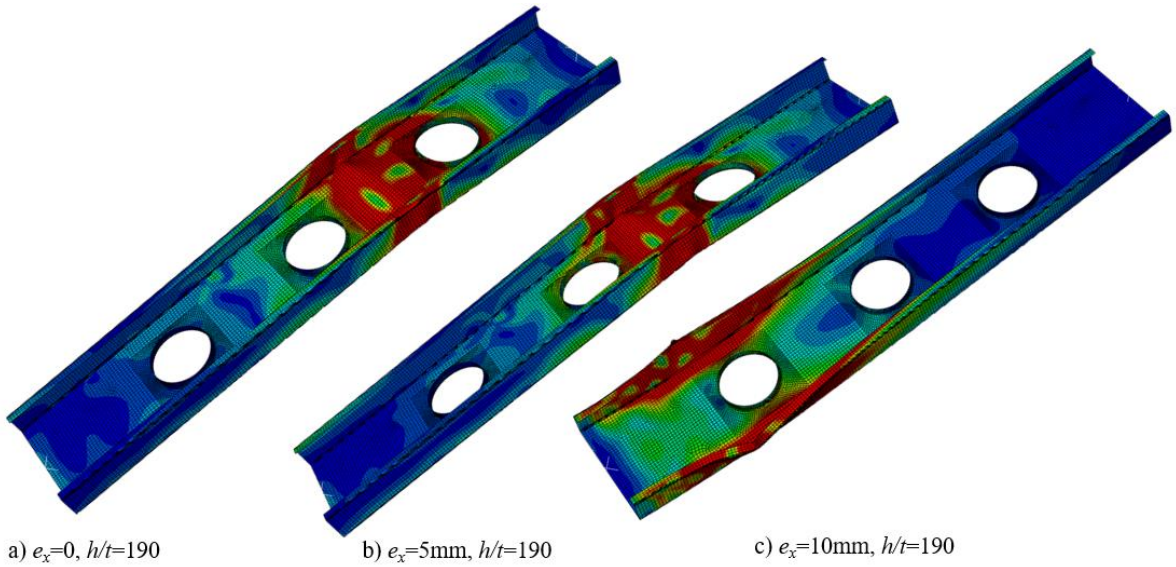

Figure 6.9 The failure modes of C190-1 mm thickness specimens due to axial compression and minor-axis eccentricities.

Chapter 7: Conclusions

This research aims to improve the accuracy of the linear interaction equations recommended by AISI S100 [22] and AS/NZS 4600 [23] for the design of CFS single-section beam-column elements with different web openings. To achieve this goal, experimentally validated FE models of CFS beam-columns, considering geometric imperfections and material nonlinearity, were employed to conduct a comprehensive parametric study. The developed dataset comprised a wide range of key design parameters, including different cross-sectional geometries, lengths, the number and diameter of web holes, as well as directions and values of load eccentricities, to study various combinations of axial compression and bending moments about minor and major axes. The FEA results were then used to assess the accuracy of current design specifications, including AISI S100 [22] and AS/NZS 4600 [23], to predict the load-carrying capacity of CFS beam-column elements. Subsequently, by minimising the errors between the strength results obtained from the validated FE models and the predicted values using the current design specifications, new interaction equations were proposed, considering the element and web slenderness ratios. Based on the presented results, the following conclusions were drawn:

- The key factors affecting the behaviour of CFS cross-sections subjected to the combined action of compression and major-axis bending were the element slenderness ratio (λ_y), the eccentricity magnitude and the thickness of the specimens.

- For the CFS channel sections subjected to combined compression and minor-axis bending, the web slenderness ratio (h/t) and the sign of the eccentricity were the most important parameters affecting their behaviour.

- The accuracy of the interaction equations specified in the design codes, in general, is influenced by the following three main factors: (i) element slenderness ratio (λ_y), (ii) web slenderness ratio (h/t) and (iii) the value and direction of the eccentricities (e_y and e_x).

- With the diameter of unstiffened holes increasing, the strength of the element decreases significantly, while the edge-stiffened holes on the web can enhance the capacity of the element. Especially for high web slenderness and low element slenderness ratios, edge-stiffened holes on the web under compression (i.e., e_x<0) can make a great contribution to increase the strength of the element.

- The contribution of different web openings subjected to tension (i.e., e_x>0) or high element slenderness ratio (i.e., λ_y>150) can be almost ignored.

- Four modified interaction equations were proposed by adding new reduction factors that considered the effects of the element slenderness ratio (λ_y), the web slenderness ratio (h/t) and the eccentricity magnitude as the key parameters.

Chapter 8: Limitations of current study and future study

These are the limitations of the current study:

- The research is confined to only one specific grade of CFS (G350).
- Only two cross-sectional dimensions (C190 x 45 x 15 and C240 x 45 x 15) were investigated numerically.
- Only one length of edge stiffener (q = 13 mm) was considered.
- Only combined compression and minor-axis bending, and combined compression and major-axis bending were considered.
- The diameter of web holes ranged only from 0.4d, 0.5d and 0.6d.

Therefore, the proposed reduction factor equations were limited to the considered parameters using FEA analysis. However, it is known from previous research studies that the length of edge stiffener of channel sections will also influence the structural behaviour of CFS channel sections. Therefore, the following are recommendations for further research:

- Conduct experimental research on the CFS channel sections with edge-stiffened web holes under eccentric loading.
- Investigate different loading condition like combined compression and bi-axial bending.
- Further exploration is needed to examine the parametric effects of the varied length of edge stiffener, cross-section dimensions and other grades of CFS.

References

[1] McCrum, D. P., Simon, J., Grimes, M., Broderick, B. M., Lim, J. B., & Wrzesien, A. M. (2019). Experimental cyclic performance of cold-formed steel bolted moment resisting frames. Engineering Structures, 181, 1-14.

[2] Mojtabaei, S. M., Kabir, M. Z., Hajirasouliha, I., & Kargar, M. (2018). Analytical and experimental study on the seismic performance of cold-formed steel frames. Journal of Constructional Steel Research, 143, 18-31.

[3] Phan, D. T., Mojtabaei, S. M., Hajirasouliha, I., Ye, J., & Lim, J. B. (2020). Coupled element and structural level optimisation framework for cold-formed steel frames. Journal of Constructional Steel Research, 168, 105867.

[4] Chen, B., Roy, K., Uzzaman, A., Raftery, G. M., Nash, D., Clifton, G. C., ... & Lim, J. B. (2019). Effects of edge-stiffened web openings on the behaviour of cold-formed steel channel sections under compression. Thin-Walled Structures, 144, 106307.

[5] Chen, B., Roy, K., Uzzaman, A., Raftery, G. M., & Lim, J. B. (2020). Parametric study and simplified design equations for cold-formed steel channels with edge-stiffened holes under axial compression. Journal of Constructional Steel Research, 172, 106161.

[6] Fang, Z., Roy, K., Chen, B., Sham, C. W., Hajirasouliha, I., & Lim, J. B. (2021). Deep learning-based procedure for structural design of cold-formed steel channel sections with edge-stiffened and un-stiffened holes under axial compression. Thin-Walled Structures, 166, 108076.

[7] Mojtabaei, S. M., Becque, J., & Hajirasouliha, I. (2021). Structural size optimization of single and built-up cold-formed steel beam-column members. Journal of Structural Engineering, 147(4), 04021030.

[8] Papargyriou, I., & Hajirasouliha, I. (2021). More efficient design of CFS strap-braced frames under vertical and seismic loading. Journal of Constructional Steel Research, 185, 106886.

[9] Yilmaz, F., Mojtabaei, S. M., Hajirasouliha, I., & Becque, J. (2023). Behaviour and performance of OSB-sheathed cold-formed steel stud wall panels under combined vertical and seismic loading. Thin-Walled Structures, 183, 110419.

[10] Mojtabaei, S. M., Becque, J., & Hajirasouliha, I. (2020). Local buckling in cold-formed steel moment-resisting bolted connections: Behaviour, capacity, and design. Journal of Structural Engineering, 146(9), 04020167.

[11] Mojtabaei, S. M., Becque, J., & Hajirasouliha, I. (2021). Behaviour and design of cold-formed steel bolted connections subjected to combined actions. Journal of Structural Engineering, 147(4), 04021013.

[12] Torabian, S., Zheng, B., & Schafer, B. W. (2015). Experimental response of cold-formed steel lipped channel beam-columns. Thin-walled structures, 89, 152-168.

[13] Torabian, S., Fratamico, D. C., & Schafer, B. W. (2016). Experimental response of cold-formed steel Zee-section beam-columns. Thin-walled structures, 98, 496-517.

[14] AISI (American Iron and Steel Institute), North American Specification for the Design of Cold-Formed Steel Structural Members, AISI S100-12, AISI, Washington, DC, 2012.

[15] Li, Y., Li, Y., & Song, Y. (2014). Experimental investigation on ultimate capacity of eccentrically-compressed cold-formed beam-columns with lipped channel sections.

[16] Cheng, S. S., Kim, B., & Li, L. Y. (2013). Lateral–torsional buckling of cold-formed channel sections subject to combined compression and bending. Journal of Constructional Steel Research, 80, 174-180.

[17] Ma, J. L., Chan, T. M., & Young, B. (2019). Cold-formed high-strength steel rectangular and square hollow sections under combined compression and bending. Journal of Structural Engineering, 145(12), 04019154.

[18] ANSI/AISC (American National Standards Institute of steel Construction), Specification for Structural Steel Buildings, ANSI/AISC 360-10, AISC, Chicago, 2010.

[19] CEN (European Committee for Standardization), Eurocode 3: Design of Steel Structures—Part 1–1: General Rules and Rules for Buildings, CEN, Brussels, Belgium, 2005.

[20] AS (Australia Standards), Standards Australia International, AS, New South Wales, Australia, 1990.

[21] Li, Q. Y., & Young, B. (2021). Tests of cold-formed steel built-up open section members under eccentric compressive load. Journal of Constructional Steel Research, 184, 106775.

[22] AISI (American Iron and Steel Institute), North American Specification for the Design of Cold-Formed Steel Structural Members (AISI S100-16), AISI, Washington, DC, 2016.

[23] AS/NZS 4600 (Australian Standard/New Zealand Standard), Cold-formed steel structures. Sydney/Wellington, 2018.

[24] ANSI/AISC (American National Standards Institute of steel Construction), Specification for Structural Steel Buildings, ANSI/AISC 360-16, AISC, Chicago, 2016.

[25] Li, Q. Y., & Young, B. (2022). Design of cold-formed steel built-up open section members under combined compression and bending. Thin-Walled Structures, 172, 108890.

[26] Hasanali, M., Mojtabaei, S. M., Clifton, G. C., Hajirasouliha, I., Torabian, S., & Lim, J. B. (2022). Capacity and design of cold-formed steel warping-restrained beam-column elements. Journal of Constructional Steel Research, 190, 107139.

[27] Hasanali, M., Mojtabaei, S. M., Hajirasouliha, I., Clifton, G. C., & Lim, J. B. (2023). More accurate design equations for cold-formed steel members subjected to combined axial compressive load and bending. Thin-Walled Structures, 185, 110588.

[28] Howick, Floor Joist System, (2013) Auckland, New Zealand.

[29] CEN (European Committee for Standardization), Eurocode 3: Design of steel structures-Part 1-3: General rules: Supplementary rules for cold-formed members and sheeting. Brussels, 2022.

[30] CEN (European Committee for Standardization), Eurocode 3: Design of steel structures-Part 1-1: General rules and rules for buildings. Brussels, 2020.

[31] CEN (European Committee for Standardization), Eurocode 3: Design of steel structures-Part 1-5: Plated structural elements. Brussels, 2020.

[32] Torabian, S., Zheng, B., & Schafer, B. W. (2016). Direct strength prediction of cold-formed steel beam-columns. Research Rep. RP16-3. Ithaca, NY: American Iron and Steel Institute.

[33] Yu, C., & Schafer, B. W. (2006). Distortional buckling tests on cold-formed steel beams. Journal of structural engineering, 132(4), 515-528.

[34] Schafer, B. W., & Peköz, T. (1999). Laterally braced cold-formed steel flexural members with edge stiffened flanges. Journal of Structural Engineering, 125(2), 118-127.

[35] Schafer, B. W., & Pekoz, T. (1998). Direct strength prediction of cold-formed steel members using numerical elastic buckling solutions.

[36] Schafer, B. W., (2006). CUFSM Version 5.04, Department of Civil Engineering, Johns Hopkins University.

[37] Schafer, B. W., & Peköz, T. (1998). Computational modeling of cold-formed steel: characterizing geometric imperfections and residual stresses. Journal of constructional steel research, 47(3), 193-210.

[38] Ye, J., Mojtabaei, S. M., & Hajirasouliha, I. (2018). Local-flexural interactive buckling of standard and optimised cold-formed steel columns. Journal of constructional steel research, 144, 106-118.

[39] Meza Ortiz, F. (2018). The behaviour of cold-formed steel built-up structural members (Doctoral dissertation, The University of Sheffield).

[40] ANSYS

[41] Abaqus/CAE User's Manual, version 6.23, USA, 2021.

[42] Framecad. (2018). Accelerate the construction of mid-rise buildings using cold formed steel.

[43] Chen, B., Roy, K., Fang, Z., Uzzaman, A., Chi, Y., & Lim, J. B. (2021). Web crippling capacity of fastened cold-formed steel channels with edge-stiffened web holes, un-stiffened web holes and plain webs under two-flange loading. Thin-Walled Structures, 163, 107666.

[44] Ansys. (n.d.). Introduction to Ansys mechanical APDL. https://www.ansys.com/training-center/course-catalog/structures/introduction-to-ansys-mechanical-apdl.

[45] Goengineer. (n.d.). Abaqus. https://www.goengineer.com/abaqus.

[46] American Society of Civil Engineers (ASCE). Specification for the Design of Cold-formed Stainless Steel Structural Members. Reston, Va: SEI/ASCE 8-02; 2002.

Appendix A

Table A.1 Eccentric capacity obtained from the parametric study results for CFS channel sections.

Specimen	P_{FE} (kN)								
	e_x = -50 mm	e_x = -25 mm	e_x = -10 mm	e_x = 10 mm	e_x = 25 mm	e_x = 50 mm	e_y = 50 mm	e_y = 100 mm	e_y = 200 mm
C240-L1000-T1-NH	11.73	16.82	22.90	38.16	21.76	12.07	27.25	23.05	16.94
C240-L1000-T1-UH1-0.4d	11.53	16.57	22.60	37.79	21.79	11.92	26.45	22.17	16.71
C240-L1000-T1-UH1-0.5d	11.12	15.89	21.66	34.65	21.61	11.85	25.09	22.12	16.25
C240-L1000-T1-UH1-0.5d	10.39	14.51	20.24	33.65	21.25	11.81	24.04	20.83	15.41
C240-L1000-T1-UH2-0.4d	11.54	16.53	22.36	36.95	22.08	12.04	26.96	22.95	16.56
C240-L1000-T1-UH2-0.5d	10.93	15.63	21.84	33.69	21.96	12.04	26.17	22.00	16.21
C240-L1000-T1-UH2-0.5d	10.11	14.75	20.33	33.82	21.25	12.21	24.42	20.98	15.00
C240-L1000-T1-UH3-0.4d	11.47	16.53	22.52	37.91	22.16	11.89	26.51	22.20	16.09
C240-L1000-T1-UH3-0.5d	11.29	16.23	22.15	33.74	21.94	11.81	25.68	21.43	16.18
C240-L1000-T1-UH3-0.5d	10.48	15.11	20.66	33.88	21.11	11.88	24.74	20.89	15.52

Specimen	P_{FE} (kN)								
	e_x = -50 mm	e_x = -25 mm	e_x = -10 mm	e_x = 10 mm	e_x = 25 mm	e_x = 50 mm	e_y = 50 mm	e_y = 100 mm	e_y = 200 mm
C240-L1000-T1-EH1-0.4d	11.86	17.06	23.19	38.36	21.76	12.13	27.59	23.38	17.30
C240-L1000-T1-EH1-0.5d	11.93	17.22	23.41	38.55	21.75	12.18	27.74	23.62	17.32
C240-L1000-T1-EH1-0.5d	11.95	17.32	23.66	37.85	21.72	12.20	28.06	23.67	17.28
C240-L1000-T1-EH2-0.4d	11.79	16.97	23.17	38.64	21.93	12.22	27.43	23.11	16.94
C240-L1000-T1-EH2-0.5d	11.80	17.01	23.23	38.79	21.93	12.30	27.35	23.01	16.92
C240-L1000-T1-EH2-0.5d	11.80	16.91	23.22	39.00	21.91	12.34	27.32	22.75	16.92
C240-L1000-T1-EH3-0.4d	11.86	17.14	23.18	38.17	22.00	12.12	27.96	23.52	17.31
C240-L1000-T1-EH3-0.5d	11.98	17.33	23.68	38.33	21.95	12.13	28.43	23.83	17.28
C240-L1000-T1-EH3-0.5d	12.20	17.65	24.16	37.98	21.88	12.11	28.84	24.03	17.39
C240-L2000-T1-NH	8.56	11.60	14.79	23.18	14.60	9.33	18.12	16.67	13.41
C240-L2000-T1-UH1-0.4d	8.53	11.55	14.72	22.87	14.55	9.18	18.03	16.54	13.21
C240-L2000-T1-UH1-0.5d	6.67	11.26	14.42	22.75	14.47	9.00	17.85	16.34	13.06

Specimen	P_{FE} (kN)								
	e_x = -50 mm	e_x = -25 mm	e_x = -10 mm	e_x = 10 mm	e_x = 25 mm	e_x = 50 mm	e_y = 50 mm	e_y = 100 mm	e_y = 200 mm
C240-L2000-T1-UH1-0.5d	8.08	10.82	13.93	22.33	14.33	8.73	17.31	15.72	10.49
C240-L2000-T1-UH3-0.4d	8.51	11.51	14.67	22.39	14.48	9.20	18.00	16.46	13.24
C240-L2000-T1-UH3-0.5d	6.65	11.15	14.34	22.11	14.31	9.06	17.69	16.25	13.03
C240-L2000-T1-UH3-0.5d	8.01	10.74	13.75	22.05	14.02	8.81	16.97	14.83	12.51
C240-L2000-T1-UH5-0.4d	8.49	11.45	14.61	22.32	14.46	9.20	17.91	16.35	13.14
C240-L2000-T1-UH5-0.5d	6.80	10.92	14.09	22.05	14.28	9.06	17.42	16.01	12.99
C240-L2000-T1-UH5-0.5d	7.94	10.61	13.50	22.13	13.98	8.83	16.46	15.23	12.31
C240-L2000-T1-EH1-0.4d	8.60	11.65	14.86	23.15	14.61	9.36	18.25	16.76	13.50
C240-L2000-T1-EH1-0.5d	7.05	11.62	14.90	23.12	14.61	9.37	18.33	16.83	13.55
C240-L2000-T1-EH1-0.5d	8.67	11.74	15.00	23.11	14.61	9.41	18.43	16.89	13.62
C240-L2000-T1-EH3-0.4d	8.59	11.67	14.88	23.23	14.57	9.33	18.23	16.77	13.50
C240-L2000-T1-EH3-0.5d	7.05	11.65	14.95	23.25	14.53	9.29	18.37	16.85	13.55

Specimen	P_{FE} (kN)								
	e_x = -50 mm	e_x = -25 mm	e_x = -10 mm	e_x = 10 mm	e_x = 25 mm	e_x = 50 mm	e_y = 50 mm	e_y = 100 mm	e_y = 200 mm
C240-L2000-T1-EH3-0.5d	8.70	11.80	15.06	23.36	14.45	9.25	18.45	16.97	13.63
C240-L2000-T1-EH5-0.4d	8.63	11.70	14.85	23.26	14.54	9.32	18.31	16.74	13.53
C240-L2000-T1-EH5-0.5d	7.05	11.69	15.02	23.30	14.46	9.25	18.42	16.89	13.59
C240-L2000-T1-EH5-0.5d	8.74	11.77	15.19	23.45	14.33	9.14	18.63	17.04	13.70
C240-L2500-T1-NH	7.15	9.35	11.55	17.75	12.12	8.16	13.77	12.86	10.59
C240-L2500-T1-UH1-0.4d	7.14	9.33	11.50	17.73	12.04	8.02	13.74	12.83	10.56
C240-L2500-T1-UH1-0.5d	7.05	9.26	11.39	17.70	11.93	7.88	13.67	12.76	10.50
C240-L2500-T1-UH1-0.5d	6.92	9.02	11.15	17.64	11.71	7.66	13.47	12.55	10.32
C240-L2500-T1-UH3-0.4d	7.12	9.24	11.38	17.67	12.03	8.06	13.67	12.77	10.52
C240-L2500-T1-UH3-0.5d	6.99	9.20	11.34	17.59	11.88	7.95	13.54	12.65	10.44
C240-L2500-T1-UH3-0.5d	6.79	8.93	11.02	17.39	11.58	7.76	13.25	12.38	10.21
C240-L2500-T1-UH5-0.4d	7.11	9.28	11.46	17.64	12.02	8.06	13.66	12.74	10.47

Specimen	P_{FE} (kN)								
	e_x = -50 mm	e_x = -25 mm	e_x = -10 mm	e_x = 10 mm	e_x = 25 mm	e_x = 50 mm	e_y = 50 mm	e_y = 100 mm	e_y = 200 mm
C240-L2500-T1-UH5-0.5d	6.88	9.09	11.16	17.51	11.89	7.95	13.40	12.55	10.35
C240-L2500-T1-UH5-0.5d	5.98	8.17	10.54	17.31	11.64	7.79	12.94	11.13	9.32
C240-L2500-T1-EH1-0.4d	7.20	9.46	11.69	17.75	12.15	8.18	13.91	13.00	10.70
C240-L2500-T1-EH1-0.5d	7.09	9.51	11.76	17.76	12.19	8.22	14.02	13.09	10.78
C240-L2500-T1-EH1-0.5d	7.31	9.62	11.90	17.76	12.24	8.28	14.16	13.18	10.84
C240-L2500-T1-EH3-0.4d	7.21	9.47	11.69	17.76	12.12	8.16	13.91	12.99	10.70
C240-L2500-T1-EH3-0.5d	7.16	9.52	11.78	17.78	12.13	8.17	14.04	13.10	10.79
C240-L2500-T1-EH3-0.5d	7.34	9.66	11.94	17.79	12.13	8.18	14.21	13.20	10.85
C240-L2500-T1-EH5-0.4d	7.21	9.48	11.73	17.75	12.10	8.18	13.95	13.03	10.75
C240-L2500-T1-EH5-0.5d	7.17	9.56	11.84	17.75	12.09	8.19	14.13	13.19	10.86
C240-L2500-T1-EH5-0.5d	7.21	9.68	12.07	17.71	12.02	8.16	14.33	13.32	10.93
C240-L1000-T2-NH	28.86	46.59	68.10	75.82	43.67	25.87	83.35	68.14	47.26

Specimen	P_{FE} (kN)								
	e_x = -50 mm	e_x = -25 mm	e_x = -10 mm	e_x = 10 mm	e_x = 25 mm	e_x = 50 mm	e_y = 50 mm	e_y = 100 mm	e_y = 200 mm
C240-L1000-T2-UH1-0.4d	28.33	45.07	64.60	76.42	43.66	25.82	80.73	66.41	46.63
C240-L1000-T2-UH1-0.5d	27.36	41.92	59.46	76.36	43.49	25.67	75.86	63.03	45.21
C240-L1000-T2-UH1-0.5d	25.87	38.37	53.40	76.86	43.29	25.06	67.91	55.90	40.41
C240-L1000-T2-UH2-0.4d	28.33	45.42	65.01	75.24	43.57	25.78	82.46	67.78	47.12
C240-L1000-T2-UH2-0.5d	27.05	42.19	59.82	75.85	43.41	25.65	77.80	63.99	45.90
C240-L1000-T2-UH2-0.5d	25.92	38.63	53.73	77.22	43.14	25.41	69.62	57.07	41.58
C240-L1000-T2-UH3-0.4d	28.06	44.69	64.13	75.17	43.57	25.75	79.54	65.69	46.56
C240-L1000-T2-UH3-0.5d	26.87	42.95	60.55	76.25	43.31	25.54	71.69	59.44	44.11
C240-L1000-T2-UH3-0.5d	26.02	39.68	54.91	78.09	42.91	25.16	68.07	56.46	41.36
C240-L1000-T2-EH1-0.4d	29.14	47.18	69.12	76.18	43.70	25.91	84.00	68.93	47.70
C240-L1000-T2-EH1-0.5d	29.21	47.46	69.43	76.64	43.67	25.87	84.20	68.98	47.95
C240-L1000-T2-EH1-0.5d	28.61	45.73	65.24	77.28	43.60	25.79	80.19	65.24	46.24

Specimen	P_{FE} (kN)								
	e_x = -50 mm	e_x = -25 mm	e_x = -10 mm	e_x = 10 mm	e_x = 25 mm	e_x = 50 mm	e_y = 50 mm	e_y = 100 mm	e_y = 200 mm
C240-L1000-T2-EH2-0.4d	28.94	46.65	68.11	76.44	43.54	25.79	83.14	68.35	47.64
C240-L1000-T2-EH2-0.5d	28.96	46.94	68.57	77.13	43.40	25.69	83.73	68.48	48.23
C240-L1000-T2-EH2-0.5d	28.39	45.64	65.53	78.45	43.22	25.49	81.06	66.27	47.21
C240-L1000-T2-EH3-0.4d	29.28	47.90	70.35	76.63	43.70	25.86	85.17	69.52	48.23
C240-L1000-T2-EH3-0.5d	29.29	48.43	71.04	77.71	43.61	25.78	85.40	70.13	49.47
C240-L1000-T2-EH3-0.5d	28.62	45.69	65.12	79.52	43.45	25.63	79.56	64.85	46.44
C240-L2000-T2-NH	19.46	27.80	37.64	44.99	29.71	19.57	49.17	45.44	36.94
C240-L2000-T2-UH1-0.4d	19.47	27.78	37.71	44.95	29.71	19.55	49.55	45.90	37.48
C240-L2000-T2-UH1-0.5d	16.99	27.52	36.96	44.85	29.61	19.13	48.62	44.68	36.84
C240-L2000-T2-UH1-0.5d	18.89	26.89	35.50	44.66	29.39	19.27	46.91	42.80	34.39
C240-L2000-T2-UH3-0.4d	19.41	27.71	37.52	44.99	29.62	19.48	49.17	45.51	37.12
C240-L2000-T2-UH3-0.5d	16.51	27.26	36.56	44.93	29.44	18.95	47.81	43.84	35.37

Specimen	P_{FE} (kN)								
	e_x = -50 mm	e_x = -25 mm	e_x = -10 mm	e_x = 10 mm	e_x = 25 mm	e_x = 50 mm	e_y = 50 mm	e_y = 100 mm	e_y = 200 mm
C240-L2000-T2-UH3-0.5d	18.56	26.23	34.75	44.80	29.12	19.06	44.88	40.91	32.96
C240-L2000-T2-UH5-0.4d	19.29	27.57	37.28	44.99	29.51	19.40	48.75	45.10	36.69
C240-L2000-T2-UH5-0.5d	15.97	26.44	35.59	44.93	29.25	18.65	46.71	42.79	34.64
C240-L2000-T2-UH5-0.5d	18.00	25.30	33.50	44.85	28.80	18.88	42.70	39.08	31.81
C240-L2000-T2-EH1-0.4d	19.53	27.95	37.89	44.98	29.66	19.56	49.52	45.80	37.24
C240-L2000-T2-EH1-0.5d	16.69	27.96	37.95	44.97	29.58	18.98	49.44	45.66	37.04
C240-L2000-T2-EH1-0.5d	19.34	27.63	37.43	44.90	29.42	19.41	48.09	44.06	35.58
C240-L2000-T2-EH3-0.4d	19.53	27.96	37.90	45.05	29.59	19.51	49.48	45.72	37.16
C240-L2000-T2-EH3-0.5d	16.44	27.93	37.88	45.04	29.42	18.81	49.29	45.42	36.77
C240-L2000-T2-EH3-0.5d	19.20	27.38	36.76	45.01	29.14	19.21	47.17	43.11	34.76
C240-L2000-T2-EH5-0.4d	19.53	27.97	37.91	45.06	29.51	19.46	49.47	45.69	37.12
C240-L2000-T2-EH5-0.5d	16.16	27.90	37.86	45.07	29.28	18.65	49.19	45.26	36.58

Specimen	P_{FE} (kN)								
	e_x = -50 mm	e_x = -25 mm	e_x = -10 mm	e_x = 10 mm	e_x = 25 mm	e_x = 50 mm	e_y = 50 mm	e_y = 100 mm	e_y = 200 mm
C240-L2000-T2-EH5-0.5d	19.07	27.05	35.95	45.08	28.89	19.01	46.12	42.06	33.95
C240-L2500-T2-NH	16.07	21.72	27.86	33.70	24.03	16.73	34.85	32.65	27.03
C240-L2500-T2-UH1-0.4d	16.08	21.73	27.90	33.69	24.02	16.71	35.30	33.16	27.59
C240-L2500-T2-UH1-0.5d	16.01	21.71	27.95	33.60	23.92	16.63	35.15	32.95	27.44
C240-L2500-T2-UH1-0.5d	15.83	21.45	27.56	33.41	23.73	16.47	34.67	32.44	26.96
C240-L2500-T2-UH3-0.4d	15.99	21.65	27.75	33.63	23.92	16.64	34.84	32.68	27.10
C240-L2500-T2-UH3-0.5d	15.90	21.49	27.54	33.49	23.75	16.51	34.39	32.13	26.59
C240-L2500-T2-UH3-0.5d	15.57	20.98	26.48	33.20	23.46	16.28	33.20	30.88	25.50
C240-L2500-T2-UH5-0.4d	15.93	21.56	27.63	33.56	23.83	16.57	34.51	32.32	26.73
C240-L2500-T2-UH5-0.5d	15.73	21.29	27.24	33.34	23.57	16.38	33.70	31.41	25.88
C240-L2500-T2-UH5-0.5d	15.14	20.33	25.57	32.97	23.17	16.08	31.63	29.44	24.33
C240-L2500-T2-EH1-0.4d	16.13	21.81	28.00	33.63	23.98	16.70	34.99	32.77	27.10

Specimen	P_{FE} (kN)								
	e_x = -50 mm	e_x = -25 mm	e_x = -10 mm	e_x = 10 mm	e_x = 25 mm	e_x = 50 mm	e_y = 50 mm	e_y = 100 mm	e_y = 200 mm
C240-L2500-T2-EH1-0.5d	16.11	21.81	28.03	33.54	23.89	16.66	34.88	32.63	26.94
C240-L2500-T2-EH1-0.5d	15.98	21.61	27.70	33.38	23.75	16.57	34.33	32.04	26.40
C240-L2500-T2-EH3-0.4d	16.16	21.86	28.07	33.58	23.90	16.65	35.07	32.79	27.04
C240-L2500-T2-EH3-0.5d	16.10	21.80	28.01	33.44	23.75	16.57	34.76	32.45	26.68
C240-L2500-T2-EH3-0.5d	15.91	21.44	27.43	33.21	23.49	16.40	33.67	31.30	25.71
C240-L2500-T2-EH5-0.4d	16.19	21.92	28.14	33.51	23.82	16.60	35.10	32.81	27.01
C240-L2500-T2-EH5-0.5d	16.13	21.81	28.03	33.31	23.60	16.47	34.67	32.33	26.50
C240-L2500-T2-EH5-0.5d	15.77	21.20	27.12	32.98	23.22	16.21	33.00	30.63	25.12
C240-L1000-T3-NH	43.49	74.95	119.19	107.45	62.90	38.08	154.04	118.63	76.68
C240-L1000-T3-UH1-0.4d	42.53	72.63	112.38	107.74	62.80	37.97	149.25	120.01	78.27
C240-L1000-T3-UH1-0.5d	42.08	70.70	103.38	108.03	62.64	37.86	135.52	108.81	76.05
C240-L1000-T3-UH1-0.5d	40.77	64.76	93.31	108.98	62.34	37.65	117.53	94.19	66.23

Specimen	P_{FE} (kN)								
	e_x = -50 mm	e_x = -25 mm	e_x = -10 mm	e_x = 10 mm	e_x = 25 mm	e_x = 50 mm	e_y = 50 mm	e_y = 100 mm	e_y = 200 mm
C240-L1000-T3-UH2-0.4d	42.29	72.86	114.15	108.11	62.70	37.87	150.44	120.19	77.84
C240-L1000-T3-UH2-0.5d	41.62	70.32	103.94	108.97	62.45	37.70	136.11	109.48	76.58
C240-L1000-T3-UH2-0.5d	40.30	64.81	93.50	110.32	62.05	37.41	118.32	96.27	67.82
C240-L1000-T3-UH3-0.4d	41.90	71.58	110.78	108.54	62.66	37.83	145.07	116.90	76.88
C240-L1000-T3-UH3-0.5d	41.02	68.58	102.56	109.67	62.37	37.62	131.41	106.87	74.76
C240-L1000-T3-UH3-0.5d	39.56	63.31	91.29	111.08	61.93	37.25	114.40	93.18	66.51
C240-L1000-T3-EH1-0.4d	43.72	75.93	121.01	107.99	62.77	38.06	156.93	121.09	78.23
C240-L1000-T3-EH1-0.5d	43.46	74.42	114.25	108.44	62.62	37.97	144.15	114.06	78.07
C240-L1000-T3-EH1-0.5d	42.31	68.66	101.17	109.08	62.35	37.77	124.27	99.13	69.39
C240-L1000-T3-EH2-0.4d	43.48	75.24	119.86	108.34	62.66	37.96	154.83	121.66	78.25
C240-L1000-T3-EH2-0.5d	43.14	73.82	113.74	109.13	62.43	37.80	144.57	114.99	78.40
C240-L1000-T3-EH2-0.5d	41.88	68.54	100.45	110.37	62.06	37.50	125.44	101.23	70.63

Specimen	P_{FE} (kN)								
	e_x = -50 mm	e_x = -25 mm	e_x = -10 mm	e_x = 10 mm	e_x = 25 mm	e_x = 50 mm	e_y = 50 mm	e_y = 100 mm	e_y = 200 mm
C240-L1000-T3-EH3-0.4d	43.67	75.81	120.57	108.66	62.64	37.97	157.26	123.68	78.84
C240-L1000-T3-EH3-0.5d	43.15	73.52	112.18	109.84	62.37	37.76	141.82	113.17	78.02
C240-L1000-T3-EH3-0.5d	41.54	67.41	98.70	111.38	61.95	37.40	121.75	98.10	69.52
C240-L2000-T3-NH	26.03	42.76	59.48	62.37	41.98	27.50	83.24	78.51	59.39
C240-L2000-T3-UH1-0.4d	26.15	42.68	59.86	62.29	41.85	27.43	83.88	79.36	59.94
C240-L2000-T3-UH1-0.5d	25.85	41.98	58.86	62.18	41.66	27.30	81.49	76.24	62.32
C240-L2000-T3-UH1-0.5d	25.40	40.85	56.51	61.77	41.36	27.09	76.61	69.93	55.62
C240-L2000-T3-UH3-0.4d	25.40	42.16	58.56	62.25	41.67	27.27	81.12	75.96	63.30
C240-L2000-T3-UH3-0.5d	24.56	41.08	56.67	61.78	41.33	27.01	76.95	71.37	58.19
C240-L2000-T3-UH3-0.5d	23.26	39.13	53.09	61.94	40.78	26.59	69.38	63.26	50.68
C240-L2000-T3-UH5-0.4d	24.67	41.69	58.06	61.74	41.45	27.09	79.14	73.71	60.40
C240-L2000-T3-UH5-0.5d	23.32	40.01	55.11	62.13	40.96	26.70	73.24	67.81	55.20

Specimen	P_{FE} (kN)								
	e_x = -50 mm	e_x = -25 mm	e_x = -10 mm	e_x = 10 mm	e_x = 25 mm	e_x = 50 mm	e_y = 50 mm	e_y = 100 mm	e_y = 200 mm
C240-L2000-T3-UH5-0.5d	21.51	37.66	50.73	61.86	40.18	26.08	64.72	59.11	47.75
C240-L2000-T3-EH1-0.4d	25.75	42.48	59.25	62.33	41.81	27.40	82.15	76.94	61.57
C240-L2000-T3-EH1-0.5d	25.47	42.01	58.49	62.15	41.64	27.28	80.17	74.73	61.62
C240-L2000-T3-EH1-0.5d	25.02	41.11	56.81	61.60	41.33	27.06	76.15	69.89	56.29
C240-L2000-T3-EH3-0.4d	25.34	42.32	58.93	62.18	41.65	27.25	81.31	75.62	61.99
C240-L2000-T3-EH3-0.5d	24.61	41.48	57.55	61.86	41.34	27.01	77.84	71.95	58.37
C240-L2000-T3-EH3-0.5d	23.45	40.04	54.74	62.02	40.83	26.60	71.43	65.16	52.36
C240-L2000-T3-EH5-0.4d	24.76	41.93	58.52	61.73	41.52	27.17	79.93	74.28	60.67
C240-L2000-T3-EH5-0.5d	23.62	40.86	56.52	62.13	41.06	26.80	75.25	69.52	56.45
C240-L2000-T3-EH5-0.5d	21.97	38.94	52.80	61.89	40.32	26.18	67.74	61.85	50.05
C240-L2500-T3-NH	24.16	33.25	43.57	46.85	33.84	23.99	56.29	54.89	40.57
C240-L2500-T3-UH1-0.4d	24.18	33.39	44.00	46.72	33.74	23.92	57.20	54.03	40.51

Specimen	P_{FE} (kN)								
	e_x = -50 mm	e_x = -25 mm	e_x = -10 mm	e_x = 10 mm	e_x = 25 mm	e_x = 50 mm	e_y = 50 mm	e_y = 100 mm	e_y = 200 mm
C240-L2500-T3-UH1-0.5d	23.99	33.07	43.53	46.45	33.57	23.80	56.18	52.69	40.74
C240-L2500-T3-UH1-0.5d	23.63	32.41	42.41	46.07	33.28	23.62	54.40	50.64	41.20
C240-L2500-T3-UH3-0.4d	23.98	33.05	43.32	46.37	33.57	23.80	55.56	52.02	40.88
C240-L2500-T3-UH3-0.5d	23.63	32.42	42.30	46.38	33.29	23.60	53.62	50.02	41.01
C240-L2500-T3-UH3-0.5d	23.01	31.26	40.34	45.79	32.89	23.27	50.37	46.74	38.20
C240-L2500-T3-UH5-0.4d	23.75	32.64	42.62	46.48	33.39	23.67	54.30	50.72	41.35
C240-L2500-T3-UH5-0.5d	23.23	31.72	41.09	45.92	33.02	23.36	51.59	48.06	39.38
C240-L2500-T3-UH5-0.5d	22.34	30.13	38.63	45.43	32.40	22.88	47.25	43.81	35.89
C240-L2500-T3-EH1-0.4d	24.11	33.20	43.51	46.55	33.67	23.90	55.78	52.28	40.73
C240-L2500-T3-EH1-0.5d	23.98	32.97	43.16	46.26	33.50	23.79	55.02	51.44	40.97
C240-L2500-T3-EH1-0.5d	23.69	32.43	42.31	46.20	33.26	23.62	53.50	49.83	40.83
C240-L2500-T3-EH3-0.4d	24.04	33.01	43.16	46.43	33.53	23.81	55.05	51.41	41.09

Specimen	P_{FE} (kN)								
	e_x = -50 mm	e_x = -25 mm	e_x = -10 mm	e_x = 10 mm	e_x = 25 mm	e_x = 50 mm	e_y = 50 mm	e_y = 100 mm	e_y = 200 mm
C240-L2500-T3-EH3-0.5d	23.79	32.50	42.31	46.37	33.30	23.63	53.56	49.94	40.86
C240-L2500-T3-EH3-0.5d	23.27	31.66	40.82	45.81	32.91	23.32	50.89	47.24	38.63
C240-L2500-T3-EH5-0.4d	23.96	32.83	42.82	46.48	33.41	23.70	54.49	50.83	41.55
C240-L2500-T3-EH5-0.5d	23.56	32.21	41.79	45.93	33.07	23.43	52.36	48.77	39.80
C240-L2500-T3-EH5-0.5d	22.74	30.87	39.71	45.42	32.48	22.97	48.71	45.13	36.91
C190-L1000-T1-NH	11.82	17.11	23.50	37.81	20.85	11.64	27.41	22.23	15.21
C190-L1000-T1-UH1-0.4d	11.48	16.63	23.05	37.28	20.75	11.55	26.34	21.71	14.93
C190-L1000-T1-UH1-0.5d	11.02	15.80	21.98	36.73	20.53	11.53	24.82	21.22	14.68
C190-L1000-T1-UH1-0.5d	10.17	14.66	20.17	35.37	20.13	11.57	23.60	19.21	13.42
C190-L1000-T1-UH2-0.4d	11.67	16.86	23.34	37.14	20.85	11.58	27.14	21.29	14.60
C190-L1000-T1-UH2-0.5d	11.22	16.23	22.51	36.39	20.66	11.54	25.84	20.62	14.10
C190-L1000-T1-UH2-0.5d	10.22	14.70	20.19	32.83	20.20	11.61	24.14	19.62	13.63

Specimen	P_{FE} (kN)								
	e_x = -50 mm	e_x = -25 mm	e_x = -10 mm	e_x = 10 mm	e_x = 25 mm	e_x = 50 mm	e_y = 50 mm	e_y = 100 mm	e_y = 200 mm
C190-L1000-T1-UH3-0.4d	11.45	16.53	22.87	37.35	20.80	11.50	26.37	21.43	14.96
C190-L1000-T1-UH3-0.5d	10.85	15.71	21.68	35.20	20.50	11.45	24.69	20.88	14.42
C190-L1000-T1-UH3-0.5d	10.15	14.61	20.05	32.58	19.89	11.52	23.64	18.89	13.56
C190-L1000-T1-EH1-0.4d	11.97	17.34	23.88	37.76	20.83	11.68	27.93	22.35	15.14
C190-L1000-T1-EH1-0.5d	11.96	17.34	24.05	37.88	20.78	11.71	27.90	22.27	15.33
C190-L1000-T1-EH1-0.5d	12.01	17.47	24.20	37.88	20.69	11.74	27.97	22.38	15.47
C190-L1000-T1-EH2-0.4d	11.88	17.19	23.69	37.68	20.83	11.66	27.47	22.24	15.38
C190-L1000-T1-EH2-0.5d	11.91	17.23	23.91	37.50	20.79	11.66	27.57	22.30	15.51
C190-L1000-T1-EH2-0.5d	11.97	17.33	24.09	37.46	20.72	11.62	27.73	22.12	15.32
C190-L1000-T1-EH3-0.4d	11.93	17.35	23.94	37.81	20.80	11.64	27.81	22.33	15.20
C190-L1000-T1-EH3-0.5d	11.96	17.33	24.02	37.94	20.71	11.61	27.69	22.10	15.35
C190-L1000-T1-EH3-0.5d	12.01	17.48	24.08	38.15	20.54	11.52	27.72	22.29	15.43

Specimen	P_{FE} (kN)								
	e_x = -50 mm	e_x = -25 mm	e_x = -10 mm	e_x = 10 mm	e_x = 25 mm	e_x = 50 mm	e_y = 50 mm	e_y = 100 mm	e_y = 200 mm
C190-L2000-T1-NH	7.80	11.74	15.04	21.90	14.01	9.11	18.35	16.22	12.35
C190-L2000-T1-UH1-0.4d	7.19	11.53	14.83	21.71	14.01	9.02	18.21	16.07	12.18
C190-L2000-T1-UH1-0.5d	6.72	11.30	14.56	21.61	13.99	8.90	17.96	15.80	11.96
C190-L2000-T1-UH1-0.5d	7.14	10.66	13.87	21.43	13.96	8.65	17.27	15.15	11.30
C190-L2000-T1-UH3-0.4d	7.12	11.49	14.67	21.62	13.92	9.01	18.12	16.02	12.14
C190-L2000-T1-UH3-0.5d	6.60	11.24	14.47	21.43	13.77	8.85	17.80	15.75	11.84
C190-L2000-T1-UH3-0.5d	6.91	10.57	13.67	21.30	13.51	8.57	17.00	14.98	11.22
C190-L2000-T1-UH5-0.4d	7.09	11.45	14.72	21.50	13.91	9.01	17.98	15.96	12.04
C190-L2000-T1-UH5-0.5d	6.90	11.09	14.20	21.27	13.81	8.89	17.52	15.60	11.82
C190-L2000-T1-UH5-0.5d	6.69	10.32	13.35	21.18	13.61	8.64	16.65	14.65	10.96
C190-L2000-T1-EH1-0.4d	7.20	11.74	15.25	21.87	14.06	9.17	18.61	16.47	12.57
C190-L2000-T1-EH1-0.5d	6.73	11.94	15.38	21.85	14.11	9.24	18.80	16.64	12.73

Specimen	P_{FE} (kN)								
	e_x = -50 mm	e_x = -25 mm	e_x = -10 mm	e_x = 10 mm	e_x = 25 mm	e_x = 50 mm	e_y = 50 mm	e_y = 100 mm	e_y = 200 mm
C190-L2000-T1-EH1-0.5d	7.20	12.01	15.33	21.83	14.16	9.32	18.81	16.65	12.68
C190-L2000-T1-EH3-0.4d	7.18	11.73	15.24	21.92	13.98	9.07	18.58	16.46	12.56
C190-L2000-T1-EH3-0.5d	6.71	11.94	15.14	21.95	13.97	9.06	18.81	16.66	12.75
C190-L2000-T1-EH3-0.5d	8.01	12.06	15.33	22.04	13.94	9.04	18.87	16.61	12.70
C190-L2000-T1-EH5-0.4d	7.16	11.74	14.97	21.91	14.01	9.13	18.59	16.48	12.57
C190-L2000-T1-EH5-0.5d	7.13	11.91	15.48	21.93	14.00	9.12	18.92	16.72	12.76
C190-L2000-T1-EH5-0.5d	7.13	12.20	15.43	22.02	13.93	9.07	19.04	16.73	12.70
C190-L2500-T1-NH	7.20	9.38	11.60	16.83	11.68	7.99	13.79	12.43	9.72
C190-L2500-T1-UH1-0.4d	7.19	9.40	11.63	16.83	11.65	7.90	13.80	12.44	9.71
C190-L2500-T1-UH1-0.5d	7.08	9.28	12.21	16.81	11.59	7.79	13.72	12.38	9.65
C190-L2500-T1-UH1-0.5d	6.78	8.88	11.09	16.78	11.45	7.57	13.50	12.14	9.39
C190-L2500-T1-UH3-0.4d	7.17	9.39	11.61	16.79	11.62	7.90	13.75	12.39	9.66

Specimen	P_{FE} (kN)								
	e_x = -50 mm	e_x = -25 mm	e_x = -10 mm	e_x = 10 mm	e_x = 25 mm	e_x = 50 mm	e_y = 50 mm	e_y = 100 mm	e_y = 200 mm
C190-L2500-T1-UH3-0.5d	7.05	9.26	11.46	16.72	11.52	7.80	13.62	12.29	9.57
C190-L2500-T1-UH3-0.5d	6.69	8.82	10.98	16.56	11.29	7.58	13.30	11.96	9.27
C190-L2500-T1-UH5-0.4d	7.16	9.36	11.59	16.76	11.58	7.89	13.71	12.37	9.67
C190-L2500-T1-UH5-0.5d	7.00	9.22	11.40	16.67	11.44	7.77	13.56	12.25	9.56
C190-L2500-T1-UH5-0.5d	6.71	8.75	10.86	16.49	11.15	7.55	13.14	11.83	9.15
C190-L2500-T1-EH1-0.4d	7.25	9.53	11.71	16.84	11.72	8.04	13.90	12.54	9.80
C190-L2500-T1-EH1-0.5d	7.19	9.60	11.90	16.84	11.76	8.08	14.01	12.64	9.88
C190-L2500-T1-EH1-0.5d	7.31	9.64	11.81	16.83	11.80	8.12	14.01	12.61	9.86
C190-L2500-T1-EH3-0.4d	7.26	9.55	11.83	16.84	11.69	8.01	13.95	12.57	9.81
C190-L2500-T1-EH3-0.5d	7.22	9.64	11.94	16.85	11.70	8.03	14.08	12.68	9.90
C190-L2500-T1-EH3-0.5d	7.34	9.69	11.89	16.82	11.85	8.02	14.06	12.64	9.85
C190-L2500-T1-EH5-0.4d	7.26	9.55	11.74	16.81	11.63	7.96	13.96	12.58	9.84

Specimen	P_{FE} (kN)								
	e_x = -50 mm	e_x = -25 mm	e_x = -10 mm	e_x = 10 mm	e_x = 25 mm	e_x = 50 mm	e_y = 50 mm	e_y = 100 mm	e_y = 200 mm
C190-L2500-T1-EH5-0.5d	7.23	9.65	12.00	16.79	11.60	7.95	14.13	12.73	9.94
C190-L2500-T1-EH5-0.5d	7.38	9.76	11.96	16.71	11.50	8.13	14.14	12.68	9.87
C190-L1000-T2-NH	29.35	47.07	68.54	71.77	41.67	25.14	81.85	61.94	39.15
C190-L1000-T2-UH1-0.4d	28.89	44.93	63.88	71.99	41.61	25.04	77.88	61.00	39.40
C190-L1000-T2-UH1-0.5d	27.28	41.19	58.25	71.48	41.31	24.91	72.15	56.44	38.49
C190-L1000-T2-UH1-0.5d	25.27	37.82	52.99	71.51	41.34	24.67	64.82	50.34	34.55
C190-L1000-T2-UH2-0.4d	28.81	45.15	64.50	71.45	41.55	25.06	75.65	59.47	39.40
C190-L1000-T2-UH2-0.5d	27.56	41.84	59.29	71.85	41.39	24.90	71.14	58.17	39.16
C190-L1000-T2-UH2-0.5d	25.76	38.52	54.35	72.69	40.63	24.67	65.80	51.25	35.05
C190-L1000-T2-UH3-0.4d	28.65	44.65	63.56	71.75	41.46	24.94	77.83	60.85	38.81
C190-L1000-T2-UH3-0.5d	26.97	41.10	58.00	72.25	41.40	24.76	71.98	56.50	38.15
C190-L1000-T2-UH3-0.5d	25.29	37.67	52.27	73.26	40.95	24.40	63.83	50.83	34.97

Specimen	P_{FE} (kN)								
	e_x = -50 mm	e_x = -25 mm	e_x = -10 mm	e_x = 10 mm	e_x = 25 mm	e_x = 50 mm	e_y = 50 mm	e_y = 100 mm	e_y = 200 mm
C190-L1000-T2-EH1-0.4d	29.53	48.03	70.38	71.59	41.68	25.16	82.42	61.96	39.13
C190-L1000-T2-EH1-0.5d	29.14	47.15	68.09	71.81	41.64	25.16	80.81	60.88	39.03
C190-L1000-T2-EH1-0.5d	27.70	43.40	61.29	72.07	41.58	25.09	70.60	54.47	36.66
C190-L1000-T2-EH2-0.4d	29.86	48.30	70.25	72.39	41.51	24.97	83.69	62.69	39.41
C190-L1000-T2-EH2-0.5d	29.81	47.71	68.72	72.90	41.37	24.83	80.91	61.73	39.44
C190-L1000-T2-EH2-0.5d	27.99	43.77	61.88	73.70	41.18	24.61	72.61	56.03	37.42
C190-L1000-T2-EH3-0.4d	29.56	48.54	71.15	72.19	41.59	25.07	83.25	63.15	39.67
C190-L1000-T2-EH3-0.5d	29.02	47.14	67.88	72.90	41.51	24.96	80.60	62.02	39.83
C190-L1000-T2-EH3-0.5d	27.33	42.57	59.85	74.21	41.35	24.80	70.23	54.56	37.13
C190-L2000-T2-NH	16.54	27.98	37.89	42.51	28.54	18.16	49.08	43.90	32.91
C190-L2000-T2-UH1-0.4d	16.86	28.03	38.06	42.45	28.48	18.73	49.65	44.54	33.27
C190-L2000-T2-UH1-0.5d	16.80	27.75	37.45	42.32	28.36	18.64	48.91	43.53	33.21

Specimen	P_{FE} (kN)								
	e_x = -50 mm	e_x = -25 mm	e_x = -10 mm	e_x = 10 mm	e_x = 25 mm	e_x = 50 mm	e_y = 50 mm	e_y = 100 mm	e_y = 200 mm
C190-L2000-T2-UH1-0.5d	16.64	26.82	35.61	42.17	28.15	18.50	46.61	40.52	30.14
C190-L2000-T2-UH3-0.4d	16.59	27.90	37.77	42.45	28.38	17.99	48.95	43.77	32.97
C190-L2000-T2-UH3-0.5d	16.24	27.52	37.04	42.35	28.18	17.81	47.42	42.03	32.13
C190-L2000-T2-UH3-0.5d	15.59	25.87	34.48	42.18	27.83	17.53	43.77	38.08	28.68
C190-L2000-T2-UH5-0.4d	16.27	27.71	37.37	42.42	28.27	17.87	48.30	43.11	32.60
C190-L2000-T2-UH5-0.5d	15.66	26.96	36.01	42.29	27.99	17.58	45.91	40.60	31.04
C190-L2000-T2-UH5-0.5d	14.58	25.12	33.02	42.10	27.50	17.16	41.02	35.85	27.30
C190-L2000-T2-EH1-0.4d	16.50	28.11	38.19	42.50	28.46	18.09	49.29	43.92	32.60
C190-L2000-T2-EH1-0.5d	16.37	27.86	37.80	42.42	28.35	18.01	48.47	43.09	32.42
C190-L2000-T2-EH1-0.5d	16.15	27.17	36.64	42.35	28.20	17.88	46.07	40.33	30.50
C190-L2000-T2-EH3-0.4d	16.35	28.06	38.13	42.48	28.36	17.99	49.16	43.72	32.76
C190-L2000-T2-EH3-0.5d	16.02	27.67	37.48	42.44	28.18	17.81	47.85	42.41	31.95

Specimen	P_{FE} (kN)								
	e_x = -50 mm	e_x = -25 mm	e_x = -10 mm	e_x = 10 mm	e_x = 25 mm	e_x = 50 mm	e_y = 50 mm	e_y = 100 mm	e_y = 200 mm
C190-L2000-T2-EH3-0.5d	15.44	26.71	35.67	42.35	27.87	17.53	44.45	38.91	29.54
C190-L2000-T2-EH5-0.4d	16.20	28.07	38.23	42.47	28.28	17.86	49.05	43.43	32.18
C190-L2000-T2-EH5-0.5d	15.68	27.58	37.47	42.43	28.06	17.61	47.25	41.60	31.24
C190-L2000-T2-EH5-0.5d	14.76	26.08	34.83	42.30	27.66	17.21	42.73	37.31	28.40
C190-L2500-T2-NH	16.08	21.76	28.00	31.95	23.10	16.30	34.45	31.16	24.30
C190-L2500-T2-UH1-0.4d	16.16	21.95	28.38	31.92	23.07	16.27	35.27	31.93	24.91
C190-L2500-T2-UH1-0.5d	16.10	21.83	28.20	31.81	22.96	16.19	35.05	31.65	24.63
C190-L2500-T2-UH1-0.5d	15.86	21.47	27.53	31.62	22.78	16.02	34.33	30.78	23.77
C190-L2500-T2-UH3-0.4d	16.09	21.82	28.12	31.83	22.97	16.20	34.70	31.37	24.41
C190-L2500-T2-UH3-0.5d	15.94	21.59	27.75	31.67	22.79	16.07	34.03	30.63	23.81
C190-L2500-T2-UH3-0.5d	15.55	20.88	26.70	31.39	22.50	15.83	32.44	29.00	22.43
C190-L2500-T2-UH5-0.4d	16.08	21.79	28.06	31.74	22.86	16.12	34.51	31.11	24.12

Specimen	P_{FE} (kN)								
	e_x = -50 mm	e_x = -25 mm	e_x = -10 mm	e_x = 10 mm	e_x = 25 mm	e_x = 50 mm	e_y = 50 mm	e_y = 100 mm	e_y = 200 mm
C190-L2500-T2-UH5-0.5d	15.80	21.37	27.38	31.48	22.61	15.93	33.30	29.87	23.18
C190-L2500-T2-UH5-0.5d	15.21	20.36	25.73	31.10	22.20	15.63	30.83	27.51	21.35
C190-L2500-T2-EH1-0.4d	16.10	21.81	28.08	31.85	23.00	16.25	34.46	31.13	24.20
C190-L2500-T2-EH1-0.5d	16.02	21.73	27.95	31.75	22.90	16.18	34.21	30.85	23.94
C190-L2500-T2-EH1-0.5d	15.85	21.41	27.48	31.58	22.75	16.08	33.39	29.96	23.24
C190-L2500-T2-EH3-0.4d	16.11	21.79	28.06	31.79	22.92	16.19	34.35	30.96	23.99
C190-L2500-T2-EH3-0.5d	15.93	21.59	27.73	31.63	22.76	16.08	33.79	30.39	23.50
C190-L2500-T2-EH3-0.5d	15.68	21.06	26.92	31.38	22.50	15.89	32.32	28.94	22.45
C190-L2500-T2-EH5-0.4d	16.08	21.75	27.97	31.71	22.84	16.12	34.19	30.80	23.81
C190-L2500-T2-EH5-0.5d	15.85	21.52	27.55	31.47	22.59	15.96	33.45	30.02	23.16
C190-L2500-T2-EH5-0.5d	15.48	20.65	26.30	31.10	22.21	15.68	31.41	28.05	21.76
C190-L1000-T3-NH	44.41	77.51	121.63	100.85	59.95	36.98	138.07	96.58	60.31

Specimen	P_{FE} (kN)								
	e_x = -50 mm	e_x = -25 mm	e_x = -10 mm	e_x = 10 mm	e_x = 25 mm	e_x = 50 mm	e_y = 50 mm	e_y = 100 mm	e_y = 200 mm
C190-L1000-T3-UH1-0.4d	43.48	74.56	112.99	101.07	59.78	36.85	135.18	98.41	61.02
C190-L1000-T3-UH1-0.5d	42.04	68.26	100.05	101.47	59.60	36.71	118.61	89.57	58.86
C190-L1000-T3-UH1-0.5d	38.78	60.75	87.31	102.05	59.30	36.47	101.37	77.74	52.09
C190-L1000-T3-UH2-0.4d	43.44	72.70	108.22	101.47	59.68	36.76	133.09	98.33	61.50
C190-L1000-T3-UH2-0.5d	42.10	67.98	99.53	102.13	59.42	36.53	119.44	90.22	59.03
C190-L1000-T3-UH2-0.5d	38.63	60.60	86.37	103.08	59.02	36.20	102.86	79.71	53.07
C190-L1000-T3-UH3-0.4d	42.82	72.96	109.91	101.84	59.58	36.66	133.30	97.59	60.78
C190-L1000-T3-UH3-0.5d	41.06	66.34	96.63	102.63	59.26	36.39	116.24	88.84	58.63
C190-L1000-T3-UH3-0.5d	37.62	58.48	83.09	103.78	58.79	35.98	99.02	77.07	52.08
C190-L1000-T3-EH1-0.4d	43.89	75.99	116.97	101.13	59.77	36.89	140.02	98.72	61.44
C190-L1000-T3-EH1-0.5d	43.04	71.04	105.51	101.54	59.62	36.76	124.32	93.20	60.62
C190-L1000-T3-EH1-0.5d	40.39	64.16	92.82	102.10	59.36	36.52	107.35	81.75	54.69

Specimen	P_{FE} (kN)								
	e_x = -50 mm	e_x = -25 mm	e_x = -10 mm	e_x = 10 mm	e_x = 25 mm	e_x = 50 mm	e_y = 50 mm	e_y = 100 mm	e_y = 200 mm
C190-L1000-T3-EH2-0.4d	44.51	76.78	116.33	101.57	59.64	36.72	137.71	98.15	60.76
C190-L1000-T3-EH2-0.5d	43.48	71.41	105.28	102.18	59.41	36.52	124.50	93.22	60.52
C190-L1000-T3-EH2-0.5d	40.42	64.03	92.09	102.98	59.06	36.24	108.83	83.33	55.42
C190-L1000-T3-EH3-0.4d	43.54	75.35	115.88	101.82	59.63	36.76	139.45	100.08	62.07
C190-L1000-T3-EH3-0.5d	42.36	69.86	102.71	102.60	59.34	36.53	122.62	92.87	60.60
C190-L1000-T3-EH3-0.5d	39.47	62.25	89.05	103.73	58.89	36.10	105.46	81.33	54.84
C190-L2000-T3-NH	25.38	42.73	60.09	58.81	40.04	27.20	83.40	71.00	48.95
C190-L2000-T3-UH1-0.4d	25.41	42.64	59.91	58.55	39.90	26.06	83.26	71.69	48.52
C190-L2000-T3-UH1-0.5d	25.11	41.82	57.74	58.21	39.73	25.93	79.40	70.81	50.21
C190-L2000-T3-UH1-0.5d	24.58	39.58	54.28	58.11	39.45	25.72	72.33	62.02	45.63
C190-L2000-T3-UH3-0.4d	24.65	41.92	58.74	58.38	39.74	25.88	79.36	70.84	48.37
C190-L2000-T3-UH3-0.5d	23.83	40.71	56.12	58.52	39.45	25.61	73.52	64.65	47.58

Specimen	P_{FE} (kN)								
	e_x = -50 mm	e_x = -25 mm	e_x = -10 mm	e_x = 10 mm	e_x = 25 mm	e_x = 50 mm	e_y = 50 mm	e_y = 100 mm	e_y = 200 mm
C190-L2000-T3-UH3-0.5d	22.56	38.02	51.06	58.07	38.98	25.19	65.10	56.33	42.24
C190-L2000-T3-UH5-0.4d	23.94	41.34	57.46	58.58	39.55	25.69	76.45	67.91	49.82
C190-L2000-T3-UH5-0.5d	22.68	39.63	53.98	58.30	39.10	25.27	69.30	60.96	46.38
C190-L2000-T3-UH5-0.5d	20.89	36.36	48.22	57.99	38.41	24.64	60.09	52.38	39.83
C190-L2000-T3-EH1-0.4d	25.09	42.42	59.61	58.41	39.87	26.00	81.37	73.34	49.31
C190-L2000-T3-EH1-0.5d	24.83	41.85	58.42	58.19	39.71	25.88	78.67	70.04	48.64
C190-L2000-T3-EH1-0.5d	24.38	40.46	55.27	58.23	39.45	25.68	73.24	63.73	47.59
C190-L2000-T3-EH3-0.4d	24.56	42.10	58.88	58.41	39.73	25.85	79.23	70.50	48.83
C190-L2000-T3-EH3-0.5d	23.85	41.20	56.98	58.54	39.46	25.60	74.66	65.92	47.84
C190-L2000-T3-EH3-0.5d	22.76	39.24	53.13	58.17	39.02	25.21	67.51	58.78	44.35
C190-L2000-T3-EH5-0.4d	24.03	41.79	58.16	58.57	39.56	25.69	77.45	68.56	49.81
C190-L2000-T3-EH5-0.5d	22.92	40.46	55.42	58.40	39.16	25.31	71.49	62.94	47.16

Specimen	P_{FE} (kN)								
	e_x = -50 mm	e_x = -25 mm	e_x = -10 mm	e_x = 10 mm	e_x = 25 mm	e_x = 50 mm	e_y = 50 mm	e_y = 100 mm	e_y = 200 mm
C190-L2000-T3-EH5-0.5d	21.32	37.85	50.72	58.12	38.52	24.72	63.25	55.25	42.07
C190-L2500-T3-NH	23.96	32.88	43.22	44.22	32.39	23.11	54.76	47.23	34.00
C190-L2500-T3-UH1-0.4d	23.92	32.97	43.26	44.12	32.28	23.03	54.90	47.22	34.04
C190-L2500-T3-UH1-0.5d	23.67	32.52	42.45	43.98	32.12	22.92	53.72	47.55	34.16
C190-L2500-T3-UH1-0.5d	23.09	31.48	40.98	43.72	31.88	22.75	51.56	45.95	34.43
C190-L2500-T3-UH3-0.4d	23.72	32.51	42.64	44.06	32.13	22.91	53.32	47.76	34.25
C190-L2500-T3-UH3-0.5d	23.31	31.83	41.40	43.65	31.86	22.72	51.20	45.79	35.20
C190-L2500-T3-UH3-0.5d	22.47	30.36	38.96	43.30	31.44	22.41	47.66	42.42	32.69
C190-L2500-T3-UH5-0.4d	23.49	32.19	42.02	43.82	31.96	22.79	52.11	46.68	34.48
C190-L2500-T3-UH5-0.5d	22.84	31.13	40.22	43.45	31.55	22.49	49.11	43.93	33.85
C190-L2500-T3-UH5-0.5d	21.64	29.15	37.11	42.81	30.92	22.04	44.57	39.74	30.80
C190-L2500-T3-EH1-0.4d	23.83	32.67	42.90	44.12	32.22	23.00	53.88	47.50	34.13

Specimen	P_{FE} (kN)								
	e_x = -50 mm	e_x = -25 mm	e_x = -10 mm	e_x = 10 mm	e_x = 25 mm	e_x = 50 mm	e_y = 50 mm	e_y = 100 mm	e_y = 200 mm
C190-L2500-T3-EH1-0.5d	23.64	32.34	42.34	43.97	32.08	22.89	52.97	47.48	34.25
C190-L2500-T3-EH1-0.5d	23.23	31.62	41.02	43.67	31.84	22.73	51.23	45.77	34.69
C190-L2500-T3-EH3-0.4d	23.69	32.47	42.47	44.02	32.10	22.90	52.92	47.45	34.36
C190-L2500-T3-EH3-0.5d	23.36	31.93	41.52	43.63	31.85	22.72	51.26	45.90	35.25
C190-L2500-T3-EH3-0.5d	22.72	30.85	39.73	43.33	31.45	22.44	48.37	43.16	33.31
C190-L2500-T3-EH5-0.4d	23.53	32.26	42.06	43.80	31.95	22.79	52.14	46.73	34.60
C190-L2500-T3-EH5-0.5d	23.03	31.44	40.68	43.47	31.58	22.53	49.80	44.57	34.25
C190-L2500-T3-EH5-0.5d	22.08	29.94	38.24	42.86	30.99	22.10	45.95	41.03	31.80